

**EVAPORATION FROM A SUBARCTIC WILLOW-BIRCH FOREST**

**VEGETATION CONTROLS ON EVAPORATION  
FROM A SUBARCTIC WILLOW-BIRCH FOREST**

**By**

**PETER DAVID BLANKEN, B.Sc.**

**A Thesis**

**Submitted to the School of Graduate Studies**

**in Partial Fulfilment of the Requirements**

**for the Degree**

**Master of Science**

**McMaster University**

**November 1992**

**© Copyright by Peter David Blanken 1992**

**MASTER OF SCIENCE (1992)  
(Geography)**

**McMASTER UNIVERSITY  
Hamilton, Ontario**

**TITLE: Vegetation Controls on Evaporation from a Subarctic Willow-Birch Forest**

**AUTHOR: Peter David Blanken, B.Sc. (McMaster University)**

**SUPERVISOR: Professor W. R. Rouse**

**NUMBER OF PAGES: xv, 171**

## ABSTRACT

Continuous measurements of the energy and radiation balance were made during the 1991 growing season over a dwarf willow-birch forest located near Churchill, Manitoba. The ecological setting is described in terms of both the nature of the substrate and the morphology and distribution of the plant species. Intensive measurements of stomatal conductance and xylem pressure potential for several species were taken on three fair weather days. These represented a wide range of air temperatures and leaf-to-air vapour pressure deficits and allowed the quantification of the surface-atmosphere interactions. The very dynamic and important role of the vegetation in the evaporative process is illustrated.

The willow-birch forest consists of six main species which have colonized the recently emerged coastline. There is a wide range in the plant height, rooting networks, and above-to-below ground plant mass. A mature leaf area index of  $0.81 \text{ m}^2 \text{ m}^{-2}$  was reached within 15 days after the onset of growth. The substrate consists of a 20 cm moderately saline organic layer situated on top of sand. Soil moisture was high, with at least some of the roots of all plants residing within the saturated zone throughout the growing season.

The influence of the vegetation on both the radiation and energy balance is illustrated by partitioning the growing season into growth, mature and senescence periods. A strong relationship between surface albedo and vegetation growth indicates that the canopy is more effective in reflecting than in trapping radiation. As the canopy matures, the addition of transpiration to the

overall evaporation dramatically increases the magnitude of the latent heat flux at the expense of the sensible heat flux.

A sensitivity analysis indicates that evaporation is highly sensitive to the canopy resistance. The sensitivity of evaporation to canopy resistance, in turn, is a function of the ratio of canopy-to-aerodynamic resistance. Strong seasonal and diurnal trends are shown in the sensitivity of evaporation to net radiation, canopy resistance, and aerodynamic resistance.

Diurnal stomatal conductance measurements indicate that some species show a pronounced midday stomatal closure. A conceptual model is developed which attributes this behaviour to differences in the sensitivities to the leaf-to-air vapour pressure deficit. A non-linear boundary line analysis of stomatal conductance indicates species-specific responses to irradiance, air temperature, leaf-to-air vapour pressure deficit, and xylem pressure potential.

The results of the boundary line analysis are coupled with a modified version of the Penman-Monteith combination model. The model predicts evaporation accurately when the canopy is mature, and indicates that 80% of the evaporation originates from the plants (transpiration). The model is used to examine the potential effects of species composition and climate change on evaporation. This illustrates the important and variable role that vegetation can play in determining responses to climate change.

## ACKNOWLEDGEMENTS

The people that have influenced myself and this thesis over the past two years are far too many to list here. I will, however, acknowledge a few of them and apologize to the many that I have missed.

I would like to thank my advisor Dr. Wayne R. Rouse for many things. Foremost for introducing me to The North during the 1989 geography field course and giving me the opportunity to return there over the past years. Summers (I mean growing seasons) will never be the same unless they are spent in Churchill. Also for the humorous comments on the drafts of this manuscript, which I think could be made into a book. Finally, for being supportive throughout the time I have known him.

I would be in serious trouble if I didn't mention the boys in GS 413. Dale Boudreau is the only person I know who can make me spend days discussing the positioning of a negative sign or the derivation of some equation I don't even understand. When we're finished, neither of us knows why we started. I would also like to apologize to Dale for placing that caesar salad behind his desk (where it remained for 3 months) and for the many crashes of his computer I caused by trying to make sounds that it really shouldn't. Derek Carlson helped tremendously in the field and taught me a great deal about data analysis. Dave Wessel turned many, many hours under adverse conditions in the field into comedy sessions. Even though I laughed at the time, I did feel bad about the ping-pong/filing cabinet collision and the sliding glass door incident. I

pass some of the blame (credit) to Dave for those computer crashes described above.

Now to the professionals. Dr. Peter M. Lafleur provided valuable tips in the field and over the phone, and his thesis was very helpful in many aspects. Dr. John A. Davies was very helpful with the theoretical aspects, and generously loaned his laser printer for the printing of this thesis. I've always enjoyed the long hours discussing computers with him. Peter A. Scott helped identify all the plant species and the visits in the field were always enlightening. Dr. Karen L. Johnson also assisted in identifying the willow species. I would also like to thank the people associated with the Churchill Northern Studies Centre for the logistical support over the past years.

Finally, I wish to thank my family for being supportive throughout my education. Everyone has encouraged me to continue with school and endured my sometimes erratic behaviour. Finally, you can see what I've been doing these past two years. I would also like to thank Michèle for her tremendous support both in and out of the field. This thesis would be worth less without her.

The Natural Science and Engineering Research Council of Canada and northern student training grants provided by the Department of Indian and Northern Affairs provided the monetary support required to make this thesis possible.

## TABLE OF CONTENTS

<b>DESCRIPTIVE NOTE</b> .....	ii
<b>ABSTRACT</b> .....	iii
<b>ACKNOWLEDGEMENTS</b> .....	v
<b>TABLE OF CONTENTS</b> .....	vii
<b>LIST OF FIGURES</b> .....	xi
<b>LIST OF TABLES</b> .....	xiv
<b>CHAPTER 1: INTRODUCTION</b> .....	1
<b>CHAPTER 2: ECOLOGICAL SETTING</b> .....	5
<b>A. INTRODUCTION</b> .....	5
<b>B. EXPERIMENTAL PROCEDURE</b> .....	7
B.1. Air Temperature, Precipitation, and the Water Table .....	7
B.2. Coastal Emergence .....	8
B.3. Soil Structure and Soil Moisture .....	8
B.4. Salinity .....	9
B.5. Permafrost .....	9
B.6. Plant Identification and Coverage .....	10
B.7. Plant Height and Root Network .....	10
B.8. Plant Mass and Moisture Storage .....	11
B.9. Leaf Area Index .....	11
<b>C. RESULTS AND DISCUSSION</b> .....	13
C.1. Air Temperature, Precipitation, and the Water Table .....	13
C.2. Coastal Emergence .....	15
C.3. Soil Structure and Soil Moisture .....	16
C.4. Salinity .....	18
C.5. Permafrost .....	19
C.6. Plant Identification and Coverage .....	19
C.7. Plant Height and Root Network .....	22

C.8. Plant Mass and Moisture Storage .....	24
C.9. Leaf Area Index .....	24
D. CONCLUSIONS .....	27
<b>CHAPTER 3: RADIATION AND ENERGY BALANCE .....</b>	<b>28</b>
A. INTRODUCTION .....	28
B. THEORY .....	28
B.1. Radiation Balance .....	28
B.2. Bowen Ratio Energy Balance (BREB) .....	29
B.3. The Aerodynamic Approach .....	31
C. EXPERIMENTAL PROCEDURE .....	34
C.1. Radiation Balance .....	34
C.2. Energy Balance .....	34
C.2.1. Humidity and Air Temperature .....	34
C.2.2. Ground Heat Flux and Temperature .....	36
C.2.3. Wind Speed, Roughness Length, and Zero Plane Displacement .....	37
C.3. Data Storage and Manipulation .....	38
D. RESULTS AND DISCUSSION .....	39
D.1. Radiation Balance .....	39
D.2. Energy Balance .....	45
E. CONCLUSIONS .....	47
<b>CHAPTER 4: SENSITIVITY ANALYSIS .....</b>	<b>49</b>
A. INTRODUCTION .....	49
B. THEORY .....	49
B.1. The Penman-Monteith Combination Model .....	49
B.2. Sensitivity Analysis .....	51
C. EXPERIMENTAL PROCEDURE .....	52
D. RESULTS AND DISCUSSION .....	54
D.1. Sensitivity to $Q^*$ .....	54
D.2. Sensitivity to $r_a$ .....	60
D.3. Sensitivity to $r_c$ .....	61
E. CONCLUSIONS .....	62

<b>CHAPTER 5: STOMATAL CONDUCTANCE</b> .....	63
A. INTRODUCTION .....	63
B. PHYSIOLOGY OF PLANT WATER TRANSPORT .....	63
B.1. Role of Stomata in Photosynthesis and Transpiration .....	63
B.2. Internal Transport of Water .....	65
C. EXPERIMENTAL PROCEDURE .....	66
C.1. Stomatal Conductance .....	66
C.2. Xylem Pressure Potential .....	67
D. RESULTS AND DISCUSSION .....	68
D.1. Ambient Conditions .....	68
D.2. Stomatal Distribution .....	72
D.3. Maximum Stomatal Conductance .....	76
D.4. Diurnal Patterns of Stomatal Conductance .....	78
D.5. Diurnal Patterns of Xylem Pressure Potential .....	85
D.6. Root Resistance .....	90
D.7. Environmental Controls on Stomatal Conductance .....	93
<i>D.7.1. Introduction</i> .....	93
<i>D.7.2. Irradiance</i> .....	95
<i>D.7.3. Leaf-to-air Vapour Pressure Deficit</i> .....	99
<i>D.7.4. Threshold Values of the Leaf-to-air Vapour</i> <i>Pressure Deficit</i> .....	105
<i>D.7.5. Air Temperature</i> .....	110
<i>D.7.6. Soil Temperature</i> .....	114
<i>D.7.7. Xylem Pressure Potential</i> .....	115
D.8. Modelling Stomatal Conductance .....	119
E. CONCLUSIONS .....	132
 <b>CHAPTER 6: MODELLING EVAPORATION</b> .....	 134
A. INTRODUCTION .....	134
B. EXPERIMENTAL PROCEDURE .....	134
C. RESULTS AND DISCUSSION .....	137
C.1. Model Performance .....	137
C.2. The Role of Transpiration .....	137
C.3. Climate Change Scenarios .....	143
D. CONCLUSIONS .....	146
 <b>CHAPTER 7: CONCLUSIONS</b> .....	 148

<b>APPENDIX A: CALCULATING STOMATAL CONDUCTANCE AND TRANSPIRATION</b> .....	150
<b>APPENDIX B: SYMBOLS</b> .....	158
<b>REFERENCES</b> .....	163

## LIST OF FIGURES

Figure 1.1.	North American locations of several shrub species . . . . .	2
Figure 2.1.	General location of the study site . . . . .	6
Figure 2.2.	Seasonal course of air temperature, precipitation, and depth of the water table below the surface. . . . .	14
Figure 2.3.	Seasonal course of leaf area index . . . . .	26
Figure 3.1.	Diurnal course of the radiation balance . . . . .	41
Figure 3.2.	Diurnal course of air temperature, surface temperature, and apparent emissivity . . . . .	42
Figure 3.3.	Seasonal course of the surface albedo . . . . .	44
Figure 4.1.	Seasonal course of the relative sensitivity of evaporation to net radiation, aerodynamic resistance, and canopy resistance . . . . .	55
Figure 4.2.	Diurnal course of the relative sensitivity of evaporation to net radiation, aerodynamic resistance, and canopy resistance . . . . .	56
Figure 4.3.	Relationships between the relative sensitivity of evaporation to net radiation and the ratio of canopy-to-aerodynamic resistance, relative sensitivity of evaporation to aerodynamic resistance and the ratio of evaporation-to-net radiation and, relative sensitivity of evaporation to canopy resistance and the ratio of canopy-to- aerodynamic resistance . . . . .	58
Figure 5.1.	Diurnal course of solar irradiance . . . . .	69
Figure 5.2.	Diurnal course of temperature and vapour pressure deficit measured at 1.7 m above the ground and at the leaf surface . . . . .	71
Figure 5.3.	Diurnal course of ground temperatures . . . . .	73
Figure 5.4a.	Diurnal course of stomatal conductance . . . . .	81

Figure 5.4b.	Diurnal course of stomatal conductance . . . . .	82
Figure 5.5a.	Diurnal course of xylem pressure potential . . . . .	88
Figure 5.5b.	Diurnal course of xylem pressure potential . . . . .	89
Figure 5.6.	Relationship between canopy xylem pressure potential and canopy transpiration . . . . .	92
Figure 5.7a.	Scatter diagram of stomatal conductance and irradiance . . . . .	97
Figure 5.7b.	Scatter diagram of stomatal conductance and irradiance . . . . .	98
Figure 5.8a.	Scatter diagram of stomatal conductance and the leaf-to-air vapour pressure deficit . . . . .	103
Figure 5.8b.	Scatter diagram of stomatal conductance and the leaf-to-air vapour pressure deficit . . . . .	104
Figure 5.9.	Theoretical relationship between stomatal conductance and the leaf-to-air vapour pressure deficit . . . . .	106
Figure 5.10.	Theoretical diurnal course for the relative sensitivity of stomatal conductance to the leaf-to-air vapour pressure deficit during a cool, damp day and a hot, dry day . . . . .	109
Figure 5.11a.	Scatter diagram of stomatal conductance and air temperature . . . . .	111
Figure 5.11b.	Scatter diagram of stomatal conductance and air temperature . . . . .	112
Figure 5.12a.	Scatter diagram of stomatal conductance and xylem pressure potential . . . . .	116
Figure 5.12b.	Scatter diagram of stomatal conductance and xylem pressure potential . . . . .	117
Figure 5.13a.	Diurnal course of the stomatal conductance of <i>S. planifolia</i> plotted with the best boundary line non-linear modelling estimate . . . . .	125
Figure 5.13b.	Diurnal course of the stomatal conductance of <i>S. candida</i> plotted with the best boundary line non-linear modelling estimate . . . . .	126

Figure 5.13c.	Diurnal course of the stomatal conductance of <i>S. reticulata</i> plotted with the best boundary line non-linear modelling estimate .	127
Figure 5.13d.	Diurnal course of the stomatal conductance of <i>C. aquatilis</i> plotted with the best boundary line non-linear modelling estimate .	128
Figure 5.13e.	Diurnal course of the stomatal conductance of <i>B. glandulosa</i> plotted with the best boundary line non-linear modelling estimate .	129
Figure 5.13f.	Diurnal course of the stomatal conductance of <i>M. gale</i> plotted with the best boundary line non-linear modelling estimate .	130
Figure 6.1.	Seasonal course of measured $Q_E$ and modelled $Q_E$ . . . . .	138
Figure 6.2.	Relationship between measured $Q_E$ and modelled $Q_E$ . . . . .	140
Figure 6.3.	Seasonal course of the relative role of transpiration in the overall evaporation . . . . .	141
Figure 6.4.	Seasonal course of the overall evaporation, transpiration, and pond evaporation . . . . .	142

## LIST OF TABLES

Table 2.1.	Variation of volumetric soil moisture with depth and distance inland	17
Table 2.2.	Surface cover at different distances from the coast . . . . .	21
Table 2.3.	Plant height, depth of tap root, and extent of lateral roots . . . . .	23
Table 2.4.	Plant mass and moisture content above and below ground . . . . .	25
Table 3.1a.	Daily averages of radiation balance components . . . . .	40
Table 3.1b.	Morning and afternoon averages of the radiation balance components, air temperature, surface temperature, surface albedo, and apparent emissivity . . . . .	40
Table 3.2.	Daily averages of the energy balance (and related terms) divided into growth, mature, and senescence periods . . . . .	46
Table 4.1a.	Summary of the relative sensitivities of $Q_E$ to $Q^*$ , $r_a$ , and $r_c$ based on the seasonal trends . . . . .	57
Table 4.1b.	Summary of the relative sensitivities of $Q_E$ to $Q^*$ , $r_a$ , and $r_c$ based on the diurnal trends . . . . .	57
Table 4.2.	Equations used to fit the curves shown in Figures 4.3a through 4.3c . . . . .	59
Table 5.1.	Ambient conditions during the three days when intensive stomatal conductance measurements were taken . . . . .	70
Table 5.2.	Percentage of the total leaf stomatal conductance occurring on the adaxial and abaxial leaf surfaces . . . . .	75
Table 5.3a.	Maximum stomatal conductance for each species . . . . .	77
Table 5.3b.	Maximum stomatal conductance for various species . . . . .	77

Table 5.4.	Average stomatal conductance for each species . . . . .	83
Table 5.5.	Average xylem pressure potential for each species . . . . .	87
Table 5.6.	Parameters used to model stomatal conductance using boundary line analysis . . . . .	96
Table 5.7.	Sensitivity of $g$ to $\Delta W$ for different stomatal behaviour patterns . . .	107
Table 5.8.	Optimum air temperatures for maximum stomatal conductance and the range of air temperatures for stomatal conductance for each species . . . . .	113
Table 5.9a.	Results of boundary line analysis with individual species responding to solar irradiance, leaf-to-air vapour pressure deficit, air temperature, and xylem pressure potential . . . . .	122
Table 5.9b.	Results of boundary line analysis with individual species responding to solar irradiance, leaf-to-air vapour pressure deficit, air temperature, and xylem pressure potential . . . . .	123
Table 6.1.	Comparison of measured $Q_E$ to modelled $Q_E$ for the fully developed canopy . . . . .	139
Table 6.2.	Changes in $Q_E$ from the present $Q_E$ expressed as a percentage . . .	145

# CHAPTER 1

## INTRODUCTION

The purpose of this study is to investigate the surface-atmosphere interaction over a dwarf willow-birch Subarctic forest in the Hudson Bay Lowland. This study focuses on the dynamic role the vegetation plays in the evaporative water loss to the atmosphere.

A dwarf willow-birch Subarctic forest was selected for this study for three main reasons. First, this surface (comprised of several willow, birch, and sedge species not exceeding 2 m in height growing in a wet environment) is common in Arctic and Subarctic regions. Of the vegetated regions in the High Arctic, shrub vegetation covers 1.51 million km<sup>2</sup>, which is equivalent to 44% of the region (Chapin and Shaver, 1985). On a continental scale, shrub species can be found throughout the treeline regions of North America (Porsild and Cody, 1980). In general, shrub species are found juxtaposed with the treeline (Figure 1.1), with some species concentrated north of the treeline (e.g. *Salix reticulata*) while others are concentrated slightly south of the treeline (e.g. *Salix planifolia*). Within the Hudson Bay Lowland, the sedge *Carex aquatilis* has a widespread distribution pattern with abundant frequency (Riley, 1990).

The second reason is that the Arctic and Subarctic regions where the shrub vegetation assemblage is found are especially sensitive to climatic change. The main

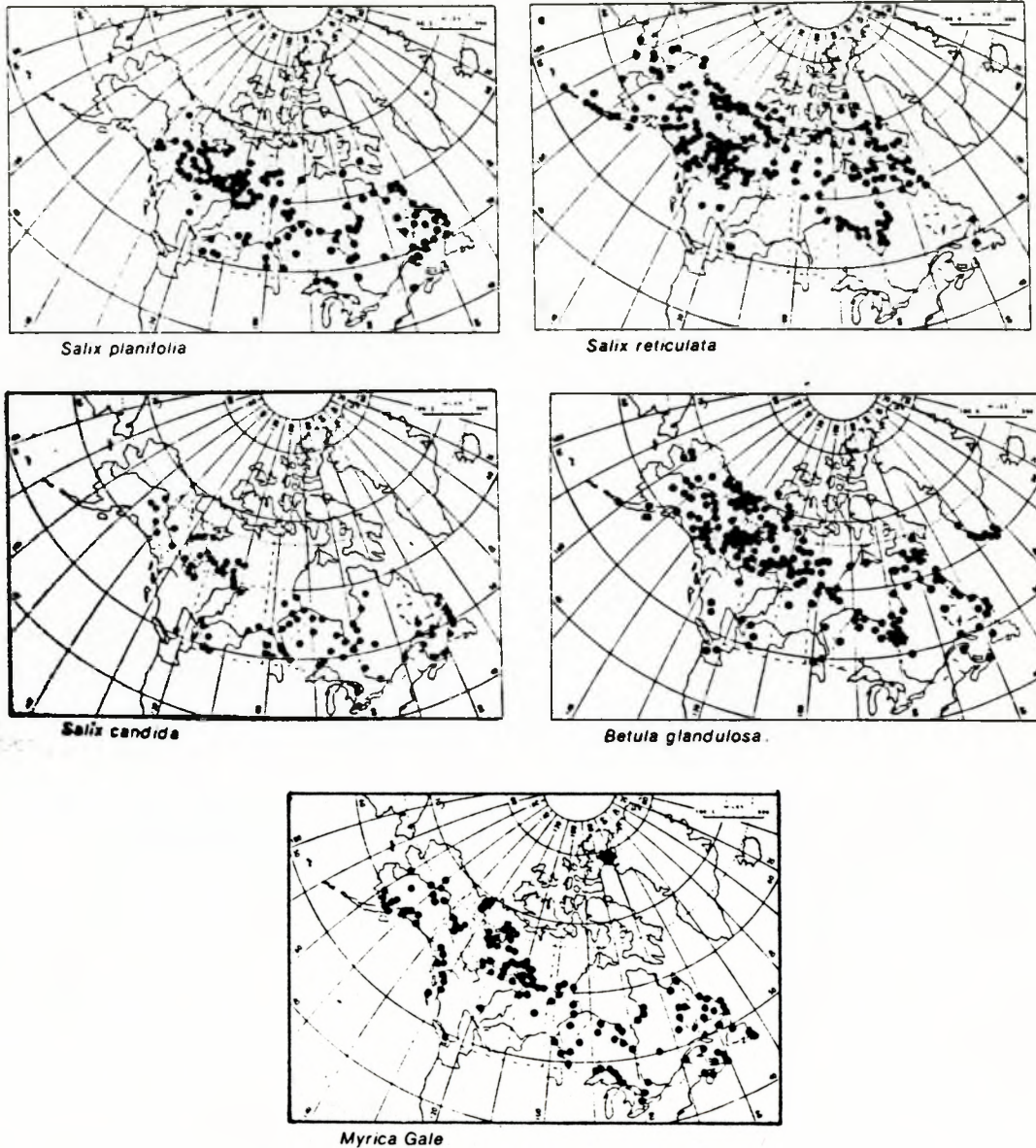


Figure 1.1. North American locations of several shrub species (after Porsild and Cody, 1980).

mechanism for this is the temperature-albedo feedback. Given an increase in air temperature in a CO<sub>2</sub> enhanced atmosphere, the highly reflective snow and sea ice would melt earlier in the spring and form later in the fall. The resulting reduction in surface albedo would, in turn, increase available energy at the surface which would then promote more melting and further heat the surface (see, for example, Wetherald and Manabe, 1981; Ingram et al., 1989; Roots, 1989; Rizzo and Wiken, 1992). The Hudson Bay Lowland may be especially sensitive to climate change, since the cooling effect from winds originating over Hudson Bay would be reduced if the sea ice cover is diminished (Rouse, 1991).

The third reason is that until recently, advanced Global Climate Models have failed to treat vegetated surfaces as a dynamic component of the Earth's energy balance. Land surfaces were considered to be bare soil with no canopy resistance. These bucket models were unrealistic since they allowed completely dry soil to evaporate near potential conditions (Dickinson et al., 1991). Recently, however, global climate models have attempted to include submodels of the vegetation-atmosphere interaction in order to make the models more physically realistic (see, for example, Sellers et al., 1986; Dickinson et al., 1991; Xue et al., 1991). The addition of a vegetation submodel improves on the bucket model since groundwater, that plant roots have access to, is now available for evaporation, and an active canopy resistance through the plants' regulation of stomatal conductance is introduced. In order, however, to include a vegetation submodel, a detailed knowledge of how the vegetation responds to the atmosphere is required. The goal of this

study is to obtain such knowledge.

The presentation in this thesis is separated into seven main chapters. This introduction (Chapter 1) is followed by a detailed description of the ecological setting (Chapter 2). Chapter 3 describes the radiation and energy balance and emphasizes the importance of evaporation. A sensitivity analysis of evaporation to surface and atmospheric controls is presented in Chapter 4. This is followed by an investigation into the physiological control by the tree canopy on evaporation through the mechanism of stomatal conductance (Chapter 5). Chapter 6 details the accuracy of modelling evaporation and examines the effect of possible climate change on evaporation. Overall conclusions from this thesis are provided in Chapter 7.

## CHAPTER 2

### ECOLOGICAL SETTING

#### A. INTRODUCTION

A knowledge of the background ecological conditions is required in order to set the context of the dwarf willow-birch shrub environment and to aid in the interpretation of the surface-atmosphere interactions. This chapter, therefore, focuses on the present state (condition) of the plants and the environment in which they exist. Throughout this study, the term "growing season" refers to the period when the daily mean air temperature exceeds 5 °C (Energy, Mines, and Resources, 1981).

The study site is located near Churchill, Manitoba, on the west coast of Hudson Bay (Figure 2.1). Physiographically, the area lies within the Hudson Bay Lowland which covers approximately 474,000 km<sup>2</sup> of Canada (5% of Canada's land surface). The area is an extensive wetland, and is classified as a High Subarctic wetland region (Wetland Working Group, 1981). Based on distinctive ecological responses to climate, the Churchill area lies within the High Subarctic ecoclimatic region of Canada (Ecoregions Working Group, 1989).

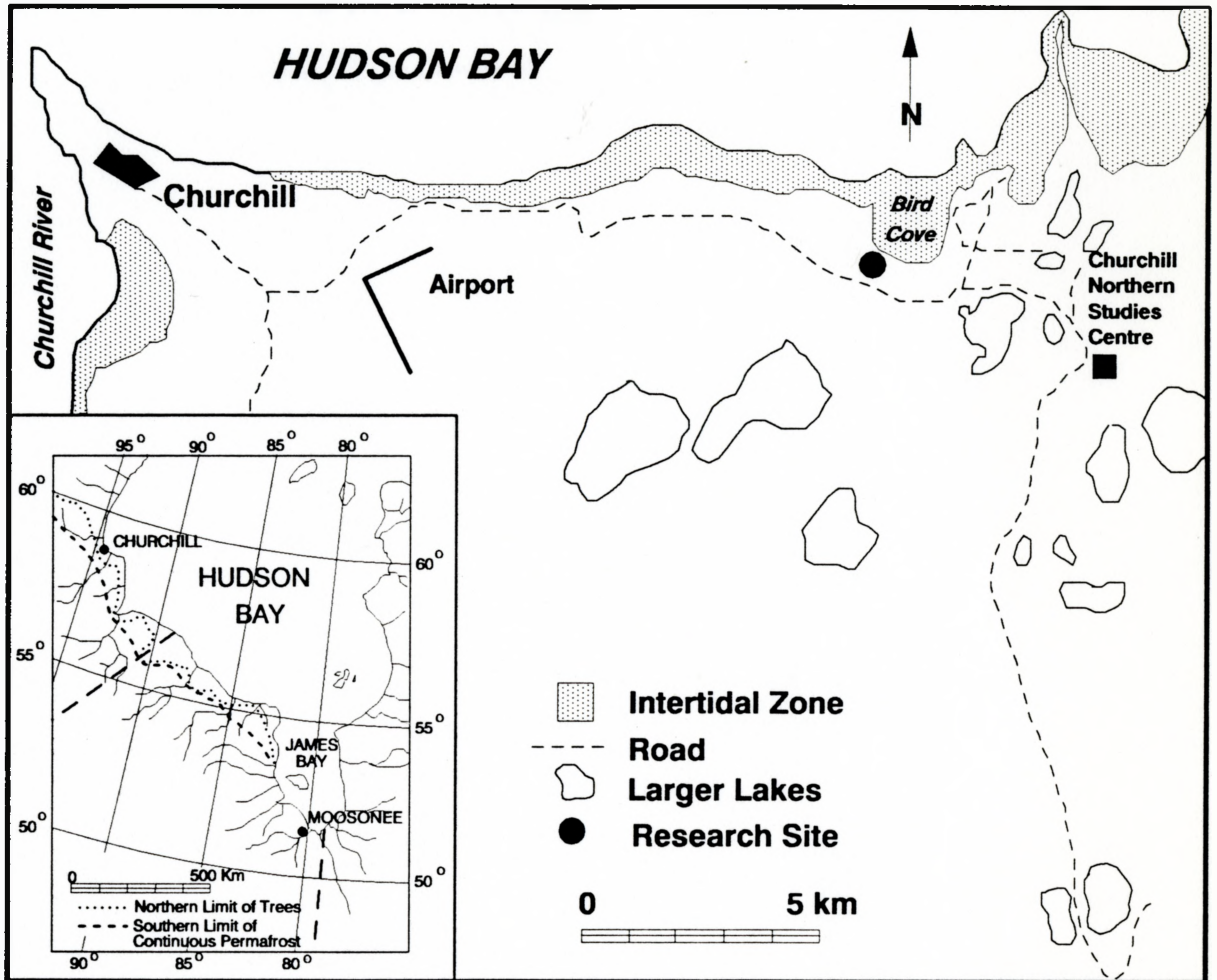


Figure 2.1. General location of the study site.

## B. EXPERIMENTAL PROCEDURE

### B.1. Air Temperature, Precipitation, and the Water Table

To compare the air temperature ( $T_a$ ) recorded at the site to the 30 year long term record (hereafter referred to as the normal), the dry bulb temperature measured at a height of 1.7 m above the ground was used (see Chapter 3, Section C.2.1 for more details). The 30 year record for  $T_a$  spanning the period from 1951 to 1980 was recorded by the official Atmospheric Environment Service weather station at the Churchill Airport, 14 km east of the site (Phillips, 1990). Since only monthly averages are reported for the normal temperatures, a third order polynomial of the form

$$T_a(JD) = -33.08 - (8.40 \times 10^{-3})(JD) + (3.05 \times 10^{-3})(JD^2) - (9.45 \times 10^{-6})(JD^3) \quad (2.1)$$

was fitted to the months of May through September ( $JD$  refers to the Julian Day). Equation 2.1 was then used to calculate normal temperatures on a daily basis for comparison with the measurement period.

Precipitation was measured using a tipping bucket rain gauge (Weathertronics Model 6010, Sacramento, California, U.S.A.) with a sensitivity of one tip per 0.25 mm and an accuracy of 0.5% at a precipitation rate of 12.7 mm per hour. Again, the normal precipitation amounts recorded at the Churchill Airport are expressed as monthly averages (Phillips, 1990). To match the precipitation amounts recorded over the measurement period with the monthly normal precipitation amounts, the monthly normal precipitation

amounts were divided by the number of days in each month.

The depth of the water table below the surface was determined using a 65 mm diameter PVC pipe placed approximately 0.5 m below the ground and 0.301 m above the surface. 10 mm holes along the pipe's entire length allowed infiltration of groundwater. The distance from the top of the well to the water table was subtracted from the height of the well above the surface to obtain the depth of the water table below the surface. Measurements were made daily, with the times of measurement being converted to a time series.

## B.2. Coastal Emergence

On a north to south transect through the willow-birch forest, ground elevations above the mean high water mark were determined using basic surveying equipment. Using elevation and an estimated isostatic rebound rate, the time of emergence from the coast could be determined.

At the north edge, middle, and south edge of the site, cross sections of the largest tree trunks were cut for ring counting under a microscope (the largest trees were selected to represent the oldest trees).

## B.3. Soil Structure and Soil Moisture

The soil horizons were determined by excavating two 3 x 3 m soil pits approximately 0.50 m deep at distances of 50 and 150 m from the coast. Two sites were

selected to check for any inhomogeneity in the substrate composition.

Soil moisture was measured volumetrically at weekly intervals throughout the growing season. Samples were taken at depths of 3.5, 10.5, 17.5, and 24.5 cm near each soil pit. Samples were taken at slightly different locations each time to maintain an accurate sample (exposure of open soil pits drained soil moisture from the upper horizons). The volume of each soil tin was found by weighing each tin when completely filled with water. Samples were immediately weighed to an accuracy of 0.1 g, oven dried at 100 °C for 24 hours, and then re-weighed. Weights were recorded using an electronic scale (Ohaus, Model 65081) accurate to 0.1 g.

#### B.4. Salinity

Salinity measurements were taken using a hand-held portable salinity meter (Hanna Instruments, Italy). The instrument was calibrated against a known concentration of NaCl before each measurement. The meter had a limited range of 6 to 59 g l<sup>-1</sup>. Salinity measurements of water were taken at the following locations: 1) groundwater at each soil pit; 2) standing surface water and; 3) sea water in the intertidal zone. After a 10 day period without rain, leaves were collected and rinsed with distilled water to detect any possible salt that may have precipitated on the leaf surfaces.

#### B.5. Permafrost

The depth to permafrost was determined by driving a 1.12 m steel probe into the

ground until ice was detected. Measurements were made at four sites in a north-south transect through the site. Each determination consisted of the average of several probings, since rocks were often encountered.

#### B.6. Plant Identification and Coverage

Plant identification was determined early in the growing season when catkins on the willows were well-developed. This made identification of the closely related *Salix* species much easier. Species were identified using keys found in Johnson (1987), and Porsild and Cody (1980) with the aid of Scott (1991).

Plant coverage was determined by measuring a 10 x 10 m plot at the north edge (coast), middle, and south edge of the site. Each plot was then partitioned into one hundred 1 by 1 m sections. Starting at the northwest corner, the sections were numbered consecutively from 1 to 100. Using a random number generator, 10 numbers for each plot were chosen. The random numbers determined which 10 sections in each plot were to be used to estimate coverage by visual inspection. Plant coverage in each plot was determined by averaging coverage in each of the 10 sections. Plant coverage for the site was determined by averaging coverage in each of the 3 plots.

#### B.7. Plant Height and Root Network

Due to the change in species coverage with distance from the coast, plant heights were determined by recording the occurrence and height of each species along a north-

south transect perpendicular to the coast. This involved a total of 18,352 individual plants. The depth and the lateral extent of the roots were determined by carefully removing an entire plant from the ground. The roots were then cleaned and measured with the lateral root measurement referring to the total horizontal root extent. Due to the difficulty of this procedure, only one and sometimes two plants of each species were sampled.

#### B.8. Plant Mass and Moisture Storage

Plants that were removed for root measurements were also separated into above and below ground portions immediately after collection. The weights of each portion were recorded accurate to 0.1g (Ohaus, Model 65081) to give the above and below ground mass. Each portion was then oven dried at 90 °C for 24 hrs to allow determination of the above and below ground moisture contents.

#### B.9. Leaf Area Index

Leaf area index (*LAI*) was determined in a non-destructive manner using an LAI-2000 Plant Canopy Analyzer (LI-COR Inc, Lincoln, Nebraska, U.S.A). This instrument computes an estimate of *LAI* from measurements of light interception through the canopy made at five incident angles simultaneously. Two optical sensors were used, with one being placed above the canopy on a 2 m tripod, while the other was mounted on a small tripod beneath the canopy 5 cm above the ground. Based on the relative fraction of diffuse beam radiation reaching the lower sensor, *LAI* was computed using a simple model

of radiation transfer (LI-COR, 1992).

Since the LAI-2000 is a radiation based instrument, it (as all radiation based instruments) cannot distinguish live from dead vegetation or branches and stems from leaves (Norman and Wells, 1991). The *LAI* as determined by the LAI-2000 is in reality a measure of foliage area index (*FAI*), since the LAI-2000's estimate is a composite of all foliage elements that block radiation. A correction, therefore, must be made to account for the wood or branch area index (*WAI*) and the dead area index (*DAI*) to arrive at the true *LAI* (*LAI* refers exclusively to the living portion of the canopy that is capable of transpiration). For this study, it is assumed that the dead leaves would quickly drop off the branches, thereby making the *DAI* insignificant. To determine the *WAI*, the LAI-2000 was used early in the growing season before any leaf emergence. At this time *LAI* determined by the instrument was equal to *WAI*. Assuming that any branch growth during a single growing season is insignificant, the *WAI* was taken to be constant throughout the season. The LAI-2000's estimate of *LAI* was corrected for *WAI* by subtracting the *WAI* from each LAI-2000 measurement.

Monitoring of *LAI* was performed six times during the 1991 growing season, beginning on June 24 and ending on August 8. Measurements were made only under completely diffuse radiation conditions (a requirement for proper instrument function). In an attempt to incorporate the heterogenous nature of the canopy cover, three 10 x 10 m plots, each representing various degrees of vegetation cover, were marked at the beginning of the growing season. Within each plot, six equidistant locations were selected.

Measurements were made throughout the season at these locations. The *LAI* for each plot was calculated as the average of the six readings, while the *LAI* for the site was calculated as the average of all three plots.

## C.RESULTS AND DISCUSSION

### C.1. Air Temperature, Precipitation, and the Water Table

The average  $T_a$  of 14.2°C recorded during the 1991 growing season was significantly higher than the normal  $T_a$  of 10.7°C and only slightly higher than the 14.0°C temperature recorded at the Churchill airport (Figure 2.2a). The standard deviation was large (5.6°C) due to the large range in daily averages (2.7 to 27.1°C).

Using equation 2.1 and the definition of the growing season (days with the mean  $T_a > 5$  °C), the growing season spanned the period between June 10 and September 16 (inclusive). Since the measurement period started on June 16 and ended on August 23, 70% of the growing season was represented by the measurement period.

Total precipitation at the site at 189 mm was significantly higher than the 30 year normal of 109 mm and significantly lower than the 217 mm recorded at the airport (Figure 2.2b). All precipitation was in the form of rain. Discrepancies between the study site and the airport are attributed to localized convective storms. Rainfall intensity showed large variation throughout the growing season. Of the 25 precipitation events recorded (a precipitation event is defined as a period of continuous precipitation), intensity

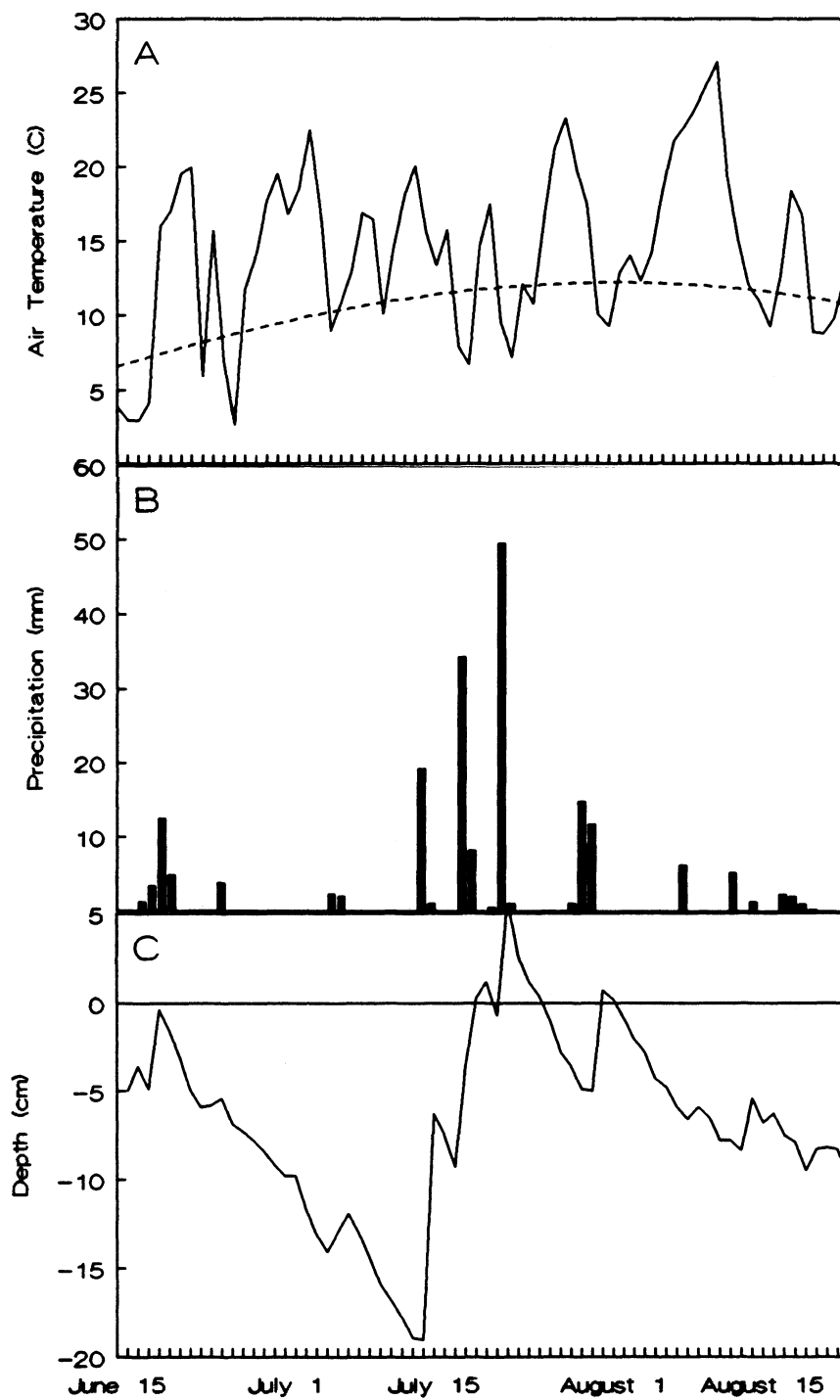


Figure 2.2. Seasonal course of air temperature (A), precipitation (B), and depth of the water table below the surface (C). Dashed line in (A) is the 30 year mean air temperature.

ranged from 0.5 to 16 mm h<sup>-1</sup> with an average of 1.7 mm h<sup>-1</sup>.

The depth of the water table below the surface averaged 6.5 cm with a range from 5.7 cm above to 19.0 cm below the surface (Figure 2.2c). The maximum draw-down was reached after a 24 day period which experienced only 8 mm of rain. The water table quickly rose above the surface in response to the large mid-season rain storms and then gradually fell below the surface towards the end of the season.

## C.2. Coastal Emergence

The study site has a nearly flat topography, with a total rise of 2.5 m over a distance of 173 m giving an average slope 0.8°. Given an estimated isostatic rebound rate of 1 m per century (Clarke et al., 1982), the south edge of the site (longest exposure) has been emerged for approximately 250 years.

Tree rings at the seaward edge of the site revealed that *Salix planifolia* with a 33 mm basal diameter and *Salix candida* with a 43 mm basal diameter had ages of 15 and 19 years, respectively. At the middle of the site (approximate emergence of 100 years), a 30 and 40 mm basal diameter *S. planifolia* were aged at 32 and 44 years, respectively. At the inland edge of the site (approximate emergence of 250 years), a 22 mm basal diameter *S. planifolia* and a 23 mm basal diameter *Betula glandulosa* were aged at 43 and 41 years, respectively. Although the age of the trees is far less than the time of coastal emergence, it should be noted that many of the species are likely to be at least second or third generation.

### C.3. Soil Structure and Soil Moisture

The soil pit located approximately 50 m inland from the coast, SP(*shore*) revealed a poorly-developed surface organic layer 17 cm deep consisting entirely of dense roots and partially decomposed plant litter. The development of this relatively thick organic horizon has been aided by the thick mats of kelp deposited during tidal surges. For example, a tidal surge caused by a severe storm during October 1990 resulted in kelp deposits 20 cm thick over areas as large as 2 x 10 m at a distance of 50 m inland from the mean high tide mark. Beneath the organic layer was a 6 cm thick limestone shelf. These frost-shattered stones averaged 5 x 5 cm with some being as large as 20 x 27 cm. The stone shelf occurs locally and does not appear to extend beneath the entire area. Under the stone shelf (23 cm from the surface) was very fine sand with occasional inclusions of well-rounded stones and shells. This sand layer appears to extend deep below the surface.

The second soil pit located approximately 150 m from the coast SP(*inland*) revealed a similar poorly-developed organic layer 20 cm deep with extensive roots and considerable plant litter. A 7 cm layer of well rounded small stones occurred beneath the organic layer. Some very fine roots were found extending beyond the small stones into fine sand to a maximum depth of 30 cm. Fine sand and occasional large stones (15 x 30 cm) were found at depths below 30 cm.

Soil moisture varies both with depth and distance from the coast (Table 2.1). At both soil pits, soil moisture is highest in the organic horizon and sharply decreases in the

Table 2.1. Variation of volumetric soil moisture (%) with depth and distance inland. Values in parenthesis refer to the observed range.

Depth (cm)	Distance from Coast (m)	
	50	150
3.5	67 (61 - 80)	58 (43 - 80)
10.5	53 (43 - 69)	62 (26 - 88)
17.5	40 (38 - 43)	55 (34 - 74)
24.5	35 (30 - 40)	38 (33 - 46)

sand. Maximum soil moisture is reached further below the surface at *SP(inland)* than *SP(coast)*. This occurs because the slightly higher elevation of *SP(inland)* causes the water table to extend further below the surface. Also, the organic horizon extends deeper at *SP(inland)* since the area has been vegetated longer.

#### C.4. Salinity

The salt concentration in the groundwater and standing surface water was  $< 6 \text{ g l}^{-1}$  throughout the growing season. This is of similar magnitude to the  $1\text{-}2 \text{ g l}^{-1}$  near-surface concentration measured in southern James Bay (Price et al., 1992). This low salt concentration is due to the flushing of salts by meteoric water and spring snowmelt. A salt concentration of  $< 6 \text{ g l}^{-1}$  was also detected on the leaf surfaces after a prolonged dry period.

At a depth of 3.5 cm, the groundwater salt concentration is equivalent to 0.35% by soil weight. At 10.5 cm, it decreases to 0.22% (these values represent the extreme upper limit, since the salinity meter's resolution did not extend below  $6 \text{ g l}^{-1}$ ). These salinity values are within the range of 0.15 to 0.35% given for moderately saline soils (FitzPatrick, 1986) and indicate a small salt deposition from the nearby sea.

Hudson Bay water at high tide revealed increasing salinity with distance from shore. A salinity of  $13 \text{ g l}^{-1}$  50 m from shore gradually increased to  $17 \text{ g l}^{-1}$  100 m from shore. This low salinity is due to the large freshwater input of the nearby Churchill River which is carried past the study site by the counter-clockwise circulation of Hudson Bay

waters.

### C.5. Permafrost

The depth of the active layer decreased from 1.10 m in the intertidal zone to 0.84 m at the inland edge of the willows in early July. By early August, the depth to permafrost exceeded 1.12 m at all locations. A similar pattern was found beneath a willow-birch forest located near the Churchill River (Hansell et al., 1983; Dyke, 1988).

The presence of the forest near the coast appears to retard the development of permafrost. As the coastline emerges, colonization by the willows traps snow which serves to insulate the ground and raise the soil temperature. Thus, in the spring, less heat is required to raise the soil temperature above 0°C and more heat is available for the phase change from ice to water. As the willows become taller and trap more snow, the process continues until eventual, isostatic rebound raises the rooting network above the water table causing the willows to die. The thinning forest loses the ability to trap snow, thus eliminating the insulating blanket and allowing a lowering of soil temperatures and the development of permafrost.

### C.6. Plant Identification and Coverage

Willow species at the site consisted of *Salix arctophila* Cockerell, *Salix brachycarpa* Nutt. ssp. *brachycarpa*, *Salix candida* Flugge, *Salix glauca* L. s.lat, *Salix planifolia* Pursh ssp. *planifolia*, and *Salix reticulata* L.. The low shrubs *Betula glandulosa*

Michx. and *Myrica gale* L. were also identified. Sedges consisted of *Carex aquatilis* Wahlenb. var. *aquatilis* and *Carex saxatilis* L.. Also present were *Arctostaphylos rubra* Fern. (Bear Berry) which closely resembles *S. reticulata*, *Vaccinium uliginosum* L. (Blue Berry), *Potentilla palustris* L. (Marsh Cinquefoil), and *Aulacomnium turgidum* Wahlenb. (moss).

In general, distinct bands of plant coverage can be identified in progression from the coast inland (Table 2.2). Near the coast, *S. candida* is dominant with large spacing between individual plants. These spaces are often covered with standing water due to tidal inundation. The understory vegetation comprises *C. aquatilis*, *P. palustris* and *A. turgidum*. Half way between the coast and the inland edge, the coverage of *S. planifolia* and *B. glandulosa* increases, while that of *S. candida* and *C. aquatilis* decreases. *M. gale* is found only in this zone. Near the inland edge band where the overall coverage again becomes sparse, *S. planifolia* and *B. glandulosa* achieve their maximum coverage. The large open areas between *S. planifolia* and *B. glandulosa* are covered by well-developed patches of *S. reticulata*, *V. uliginosum* and *A. rubra*. At the inland margin, the sedge cover has changed from a dense cover of *C. aquatilis* to a sparse cover of *C. saxatilis*. Standing and running water can be found throughout the site, but is most pronounced near the coast and middle of the willow band.

Over the entire site, there is no domination by a particular species, but rather smaller cover by many species. *S. planifolia* exhibits the largest coverage (32%). Together *S. planifolia*, *C. aquatilis*, *S. candida*, and water cover 70% of the surface. The inclusion

Table 2.2. Surface cover (%) at different distances from the coast.

Species	Distance from Coast			Average (%)
	10 m	80 m	160 m	
<i>S. planifolia</i>	4	34	57	31.7
<i>C. aquatilis</i>	37	21	8	22.0
<i>S. candida</i>	34	11	1	15.3
Water	5	10	3	6.0
<i>S. reticulata</i>	0	0	17	5.7
<i>M. gale</i>	0	16	0	5.3
<i>B. glandulosa</i>	0	7	8	5.0
<i>P. potentilla</i>	8	0	0	2.7
<i>A. turgidum</i>	2	2	0	1.3
<i>V. uliginosum</i>	0	0	3	1.0
<i>A. rubra</i>	0	0	3	1.0
<i>C. saxatilis</i>	0	0	1	0.3

of *S. reticulata*, *M. gale*, and *B. glandulosa* increases the coverage to 90%. The other species cover the remaining 10%.

### C.7. Plant Height and Root Network

Above ground heights and tap root depths are shown in Table 2.3. As noted previously, the sample size (and thus confidence) for the plant heights is much greater than that for the root network. Canopy height is highly variable, with a range from 3 to 77 cm and average of 43 cm.

Tap root depths are shallow, ranging from 5 to 25 cm with an average of 11 cm. Roots rarely penetrated beyond the organic horizon. Since the water table was never less than 20 cm from the surface and often never less than 10 cm, some of the roots of all plants resided within the saturation zone throughout the growing season. The extent of lateral rooting far exceeded the rooting depth for all species.

Variation between species was high, ranging from 29 to 126 cm with an average lateral root length of 60 cm. There was no clear relation between plant height and lateral root length. For example, *M. gale* was the second shortest species yet had the second largest lateral root extent. In all species, the lateral rooting concentration in the organic layer is promoted by the warmer ground temperatures and the inhibiting effects of the drier, less penetrable and nutrient-poor sands below the organic layer.

Table 2.3. Plant height, depth of tap root, and extent of lateral roots.

Species	Plant Height (cm)	Depth of Tap Root (cm)	Extent of Lateral Roots (cm)
<i>S. candida</i>	77	9	54
<i>S. glauca</i>	63	12	126
<i>S. planifolia</i>	54	8	68
<i>B. glandulosa</i>	47	25	55
<i>S. brachycarpa</i>	42	10	41
<i>M. gale</i>	34	15	75
<i>C. aquatilis</i>	27	7	29
<i>S. reticulata</i>	3	5	30

### C.8. Plant Mass and Moisture Storage

All species have a substantial below-ground root mass. In general, there is a trend towards increasing below ground mass with decreasing plant height. The three tallest species (*S. glauca*, *S. planifolia*, and *S. candida*) have 60% or more of their total mass above the ground (Table 2.4). *C. aquatilis* has a near equal proportion of mass above and below the surface while *B. glandulosa* has over 60% of its total mass below ground. The shorter species all have over 70% of their total mass below ground.

The proportion of plant moisture storage above and below ground (Table 2.4) is almost identical to the above and below ground proportion of mass. This suggests that the ratio of plant mass to water content is uniform throughout the plant.

### C.9. Leaf Area Index

During the 1990 season, the wood area index (*WAI*) was found to average  $0.66 \text{ m}^2 \text{ m}^{-2}$ . In 1991 a *WAI* of  $0.73 \text{ m}^2 \text{ m}^{-2}$  was determined from more intensive measurements. Although visual inspection of the shrubs revealed an extensive branch network, the *WAI* appeared to be high relative to woody species growing in more temperate climates. For example, *WAI* values of 0.7, 0.5, 0.6, and  $0.48 \text{ m}^2 \text{ m}^{-2}$  have been reported for Douglas Fir (Chen et al., 1991), Aspen/Red Maple (Neumann et al., 1989), Oak/Hickory (Hutchinson et al., 1986), and Oak forests (Rauner, 1976), respectively.

The seasonal development of *LAI* is shown by Figure 2.3. A quadratic equation of the form

Table 2.4. Plant mass and moisture content above and below ground.

Species	Plant Mass		Plant Moisture Content	
	Above (%)	Below (%)	Above (%)	Below (%)
<i>S. glauca</i>	66	34	60	40
<i>S. planifolia</i>	64	36	57	43
<i>S. candida</i>	60	40	55	45
<i>C. aquatilis</i>	47	53	44	56
<i>B. glandulosa</i>	38	62	38	62
<i>S. reticulata</i>	28	73	29	71
<i>M. gale</i>	25	75	25	75
<i>S. brachycarpa</i>	22	78	15	85

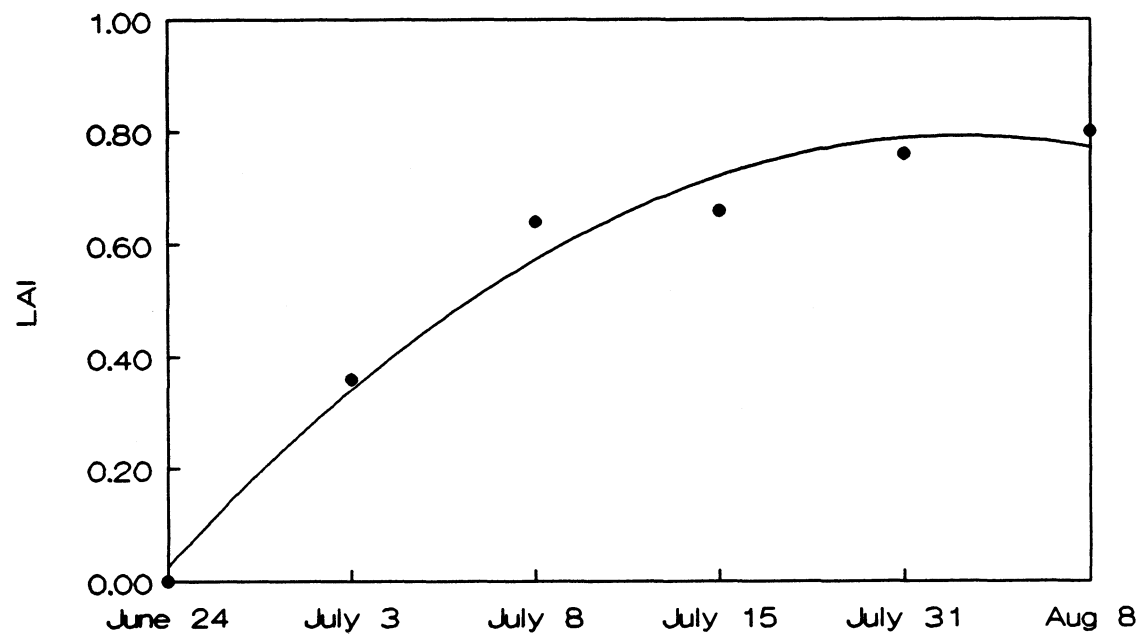


Figure 2.3. Seasonal course of leaf area index.

$$LAI_f(JD) = -28.2 + 0.276(JD) - (6.59 \times 10^{-4})(JD^2) \quad (2.2)$$

was fitted to the data points ( $r^2=0.96$ ). Most the leaf development occurred during a 15 day period, with canopy maturity being reached by approximately July 8. Taking the derivative of equation 2.2 and setting it equal to zero revealed that a maximum *LAI* of 0.81 was reached on July 29. Solving for the roots of equation 2.2 indicated that *LAI* would be equal to zero on June 24 and September 2.

#### D. CONCLUSIONS

Plants of the dwarf willow-birch forest are subject to harsh and variable conditions. However, despite the cool air temperatures, variable precipitation, and wet, cool and saline soil conditions, the shrub species are the first to colonize the emerging coastline. A variety of species with various morphologies and rooting networks have created a relatively stable ecosystem which has developed during the last 250 years and which appears to have one of the largest biomasses of this Subarctic maritime region.

## CHAPTER 3

### RADIATION AND ENERGY BALANCE

#### A. INTRODUCTION

This chapter describes the basic radiation and energy balance of the dwarf willow-birch forest. The influence of the vegetation on these two balances is investigated by partitioning the growing season into growth, mature, and senescence periods.

#### B. THEORY

##### B.1. Radiation Balance

The radiation balance at the surface ( $Q^*$ ) can be expressed as

$$Q^* = K^* + L^* \quad (3.1)$$

where  $K^*$  and  $L^*$  are the net shortwave and longwave radiation, respectively.  $K^*$  is given by

$$K^* = K\downarrow - K\uparrow = K\downarrow(1 - \alpha) \quad (3.2)$$

where  $\alpha$  is the surface albedo ( $\alpha = K\uparrow/K\downarrow$ ). Similarly,  $L^*$  is given by

$$L^* = L\downarrow - L\uparrow \quad (3.3)$$

The outgoing longwave radiation  $L\uparrow$  is a function of the surface temperature ( $T_o$  in °K) and is described by the Stefan-Boltzmann Law

$$L\uparrow = \epsilon\sigma(T_o)^4 \quad (3.4)$$

where  $\epsilon$  is the surface emissivity and  $\sigma$  is the Stefan-Boltzmann constant. Leaves behave approximately as black bodies (Jones, 1983) with  $\epsilon$  typically between 0.94 and 0.99 (Idso et al., 1969). For this study  $\epsilon$  was set equal to 0.97 which is within the range given for forests (Oke, 1987). If all terms in equation 3.1 are known, then  $L\downarrow$  can be determined by residual.

## B.2. Bowen Ratio Energy Balance Approach (BREB)

The vertical flux densities for heat ( $Q_H$ ), water vapour ( $Q_E$ ), and momentum ( $\tau$ ) through the turbulent boundary layer can be expressed as

$$Q_H = -\rho C_p K_H \frac{\partial T_a}{\partial z} \quad (3.5)$$

$$Q_E = -\frac{\rho C_p}{\gamma} K_w \frac{\partial e}{\partial z} \quad (3.6)$$

$$\tau = \rho K_M \frac{\partial u}{\partial z} \quad (3.7)$$

where  $K_H$ ,  $K_w$  and  $K_M$  are the turbulent transfer coefficients for heat, water vapour, and momentum, respectively,  $\rho$  is the density of air,  $C_p$  is the specific heat of air at constant

pressure, and  $\gamma$  is the psychrometer constant.  $\gamma$  can be evaluated as

$$\gamma = \frac{C_p P}{L_v \epsilon} \quad (3.8)$$

where  $P$  is the atmospheric pressure,  $L_v$  is the latent heat of vaporization, and  $\epsilon$  is the ratio of the molecular weights of water and dry air (0.62).

Assuming there is negligible storage or advection,  $\partial T_a$  and  $\partial e$  remain constant with height (partial derivatives can be replaced with a finite difference), and assuming  $K_H = K_w$ , equations 3.5 and 3.6 can be combined using the definition of the Bowen ratio,  $\beta$  as

$$\beta = \frac{Q_H}{Q_E} = \gamma \frac{\partial T}{\partial e} = \gamma \frac{\Delta T}{\Delta e} \quad (3.9)$$

The basic energy balance equation for an extensive homogeneous surface can be written as

$$Q^* - Q_G = Q_H + Q_E \quad (3.10)$$

where  $Q_G$  is the ground heat flux density. While  $Q^*$  and  $Q_G$  can be measured directly, substitution of equation 3.9 in equation 3.10 yields

$$Q_E = \frac{Q^* - Q_G}{(\beta + 1)} \quad (3.11)$$

$Q_H$  can then be calculated as  $Q_H = \beta Q_E$ .

### B.3. The Aerodynamic Approach

The plot of wind speed  $u(z)$  against the natural logarithm of height  $\ln(z)$  is linear under neutral atmospheric stability. Assuming that the slope is constant and equal to  $u^*/k$ , the equation describing this relationship is written as

$$u(z) = \frac{u^*}{k} \ln\left(\frac{z}{z_0}\right) \quad (3.12)$$

where  $u^*$  is the friction velocity and  $k$  is von Karman's constant. The y-intercept is, by definition, the roughness length  $z_0$  given by

$$z_0 = e^{\ln(\bar{z}) - \left(\frac{\ln(z_2) - \ln(z_1)}{u_2 - u_1}\right) (u(\bar{z}))} \quad (3.13)$$

where  $\bar{z}$  is the geometric mean height.

Over a vegetated surface, the relationship between wind speed and height departs from the linear form. Linearity returns, however, if the surface is displaced to an apparent height some distance above the actual surface. This zero plane displacement ( $d$ ) is a function of vegetation height. For wind profile measurements taken over vegetation,  $z$  must be replaced by  $(z-d)$  in equations 3.12 and 3.13.

Equation 3.12 when solved for  $u^*$  and substituted into the relationship between  $\tau$  and  $u^*$  ( $\tau = u^{*2} \rho$ ) gives

$$\tau = k^2 \rho \left( \frac{\partial u}{\partial \ln z} \right)^2 \quad (3.14)$$

Combining equations 3.7 and 3.14 and solving for  $K_m$  yields

$$K_M = k^2 \frac{\partial u}{\partial \ln z} \quad (3.15)$$

Assuming that the turbulent transfer coefficients are equal ( $K_H = K_W = K_M$ ), substitution of equation 3.15 in equations 3.5, 3.6, and 3.7 gives

$$Q_H = -\rho C_p k^2 \left( \frac{\partial u}{\partial \ln z} \right) \left( \frac{\partial T}{\partial \ln z} \right) \quad (3.16)$$

$$Q_E = -\frac{\rho C_p}{\gamma} k^2 \left( \frac{\partial u}{\partial \ln z} \right) \left( \frac{\partial e}{\partial \ln z} \right) \quad (3.17)$$

$$\tau = \rho k^2 \left( \frac{\partial u}{\partial \ln z} \right)^2 \quad (3.18)$$

which are valid only under conditions of neutral atmospheric stability.

The atmospheric stability can be categorized by means of the Richardson Number ( $Ri$ ) given as

$$Ri = \frac{G}{\bar{T}} z \frac{(\partial \bar{T} / \partial \ln z)}{(\partial u / \partial \ln z)^2} \quad (3.19)$$

where  $G$  is the acceleration due to gravity. If  $Ri > 0.2$ , then the atmosphere is strongly stable. If  $0.0 \leq Ri \leq 0.2$ , then an unstable atmosphere is indicated. Finally,  $Ri < 0.0$  is

indicative of an unstable atmosphere (Thom, 1975). Since equations 3.16 through 3.18 apply only to conditions of neutral stability, the following stability functions must be applied (Dyer, 1974; Halliwell and Rouse, 1989). For an stable atmosphere

$$\Phi_H = \Phi_W = \Phi_M = (1 - 5Ri)^{-1} \quad (3.20)$$

and for an unstable atmosphere

$$\Phi_H = \Phi_W = (1 - 16Ri)^{-0.5} \quad (3.21)$$

$$\Phi_M = (1 - 16Ri)^{-0.25} \quad (3.22)$$

where  $\Phi_H$ ,  $\Phi_W$ , and  $\Phi_M$  are the dimensionless stability functions for heat, water vapour, and momentum, respectively. Equations 3.16 through 3.18 may now be rewritten to include the stability functions, such that

$$Q_H = -\rho C_p k^2 \left( \frac{\partial u}{\partial \ln z} \right) \left( \frac{\partial T}{\partial \ln z} \right) (\Phi_H \Phi_M)^{-1} \quad (3.23)$$

$$Q_E = -\frac{\rho C_p}{\gamma} k^2 \left( \frac{\partial u}{\partial \ln z} \right) \left( \frac{\partial e}{\partial \ln z} \right) (\Phi_W \Phi_M)^{-1} \quad (3.24)$$

$$\tau = \rho k^2 \left( \frac{\partial u}{\partial \ln z} \right)^2 (\Phi_M \Phi_M)^{-1} \quad (3.25)$$

## C. EXPERIMENTAL PROCEDURE

### C.1 Radiation Balance

$Q^*$  was measured with a Middleton CN-1 pyrrometer (Melbourne, Australia) mounted 3 m above the surface on a climatological tower. The polyethylene domes were inflated with desiccated air supplied by an inner tube. Shortwave radiation was measured with Eppley black and white pyranometers (Model 8-48, Newport, Rhode Island, U.S.A.).  $K\downarrow$  was measured by an upfacing pyranometer mounted on a horizontal surface above the canopy.  $K\uparrow$  was measured with a downfacing pyranometer mounted at a height of 3 m on the climatological tower. Surface temperature used to calculate  $L\uparrow$  was obtained from the extrapolation of the  $T_e$  profile to the zero plane displacement.  $L\downarrow$  was calculated as a residual of equation 3.1.

### C.2. Energy Balance

#### *C.2.1. Humidity and Air Temperature*

The gradients of temperature and vapour pressure were determined by a six level wet and dry bulb aspirated psychrometer system. The psychrometers were located on the climatological tower at heights of 1.0, 1.25, 1.5, 1.7, 2.1, and 2.5 m above the ground. The sensors were shielded in styrofoam and covered with reflective tape to prevent artificial solar heating. Ventilation was provided by 12 volt fans powered by a marine battery charged by a solar panel (MSX 53, Solarex, Rockville, Maryland, U.S.A.). Wet

and dry bulb temperatures were measured by copper-constantan thermocouples housed in stainless steel tubing sealed with epoxy resin. The wet bulb thermocouples were enclosed with a cotton wick continuously supplied with distilled water through reservoirs. Water levels in the reservoirs were inspected daily and filled when required. The cotton wicks were changed twice during the measurement period due to yellowing and pollen build up. To determine the wet bulb depression at each level, each wet bulb was referenced to the corresponding dry bulb. The dry bulbs were referenced to a ground temperature plug which, in turn, was referenced to the panel temperature of the data logger. This was required to eliminate any temperature differences across the input cards in the data logger.

Vapour pressure was calculated using the psychrometer equation

$$e_a = e_s(T_w) - \gamma(T_a - T_w) \quad (3.26)$$

where  $e_a$  is the ambient vapour pressure,  $e_s(T_w)$  is the saturation vapour pressure evaluated at the wet bulb temperature ( $T_w$ ), and  $\gamma$  is the psychrometer constant.  $e_s(T_w)$  was calculated as

$$e_s(T_w) = ae^{\left(\frac{bT_w}{T_w+c}\right)} \quad (3.27)$$

where  $a$ ,  $b$ , and  $c$  are coefficients optimized for a temperature range from 0 to 50 °C ( $a=0.61121$ ,  $b=17.368$ ,  $c=238.88$ ) (Buck, 1981). The atmospheric vapour pressure deficit,  $D$  was calculated as

$$D = e_s(T_a) - e_a \quad (3.28)$$

where  $e_s(T_a)$  is calculated using equation 3.27 with  $T_a$  substituted for  $T_w$ .

### *C.2.2. Ground Heat Flux and Temperature*

$Q_G$  was measured by two Middleton CN-3 soil heat flow transducers (Melbourne, Australia) buried approximately 1 cm beneath the surface. A single value was taken as the average of the two transducers. It has been found that  $Q_G$  is underestimated by these transducers possibly due to poor thermal contact with the highly porous soil or due to the different thermal conductivities of the soil and the plates (Rouse, 1984a).

To correct this underestimation, Halliwell and Rouse (1987) suggest that the calorimetric method, which requires a knowledge of the ground temperature gradient, also be used to calculate  $Q_G$ . Due to the irregular behaviour of  $Q_G$  inherent with the calorimetric method, the daily cumulative value of  $Q_G$  using the calorimetric method was divided by the daily cumulative value of  $Q_G$  as measured by the transducers. This ratio (correction factor) was then averaged over the entire growing season. The values of  $Q_G$  given by the transducers were then multiplied by this correction factor.

The correction factor of 2.53 indicates a serious underestimation by the transducers. This is likely the result of the highly porous nature of organic soil which causes poor thermal contact with the transducers. Although the correction factor is large, it is similar to that calculated during the 1990 growing season (2.73) and to the 2.22 and 1.72 factors calculated near Churchill during the 1984 and 1985 growing seasons, respectively (Halliwell, 1989).

Ground temperatures were measured at depths of 1, 4, 7, 10, 15, 20, 30 and, 40 cm using copper-constantan thermocouples. Since the average rooting depth of the plants is 11 cm (Chapter 2, Section C.7), the temperature of the rooting zone was calculated as the average temperature of the 1, 4, 7, and 10 cm thermocouples.

### *C.2.3. Wind Speed, Roughness Length, and Zero Plane Displacement*

Wind speed was measured at heights of 1.25, 1.5, 2.1, and 2.5 m above the surface with Young 3-cup anemometers (Model 12102-3, Traverse City, Michigan., U.S.A.). The anemometers had a threshold wind speed of approximately  $0.4 \text{ m s}^{-1}$  and produced analogue output directly proportional to wind speed. Wind direction was measured with a Young wind vane (Model 05103) mounted on top of the climatological tower, approximately 3.5 m above the surface.

The zero plane displacement ( $d$ ) was calculated using Lettau's (1957) method where an iterative procedure is used until a  $d$  is found that minimizes the mean square error of the neutral wind profile (equation 3.12) (Tanner, 1963). The roughness length was then calculated as the y-intercept of the straight line (equation 3.13). Since the height of the vegetation did not change during the growing season, and since there was no significant difference in  $d$  as the leaves matured,  $d$  was set equal to the daily average value of 44 cm.

### C.3. Data Storage and Manipulation

Signals from all of the above instruments were recorded by an electronic data logger set at a scan rate of 10 s (Model CR7, Campbell Scientific, Logan, Utah, U.S.A.). Signals were averaged over half hour periods and downloaded to cassette tape in the field. The site was visited daily to ensure all instruments were in proper working order. The tapes were collected weekly and transfer to a personal computer using a Campbell C20 Cassette Tape Interface.

Energy balance data were analyzed using a graphical program which calculates the turbulent fluxes using both the BREB and aerodynamic approaches. Visual inspection of the individual data points allows the removal of erroneous data due to, for example, a dry wet bulb. The program is described fully by Halliwell and Rouse (1989). Fluxes were calculated using the BREB method except when this method failed (for example, during sunrise and sunset when  $\beta \rightarrow \infty$ ). Following the criteria given by Ohmura (1982), BREB calculations were substituted with aerodynamic calculations when  $-1.4 \leq \beta \leq -0.7$ . Instead of a direct substitution of both fluxes, the aerodynamic  $Q_H$  was substituted for the BREB  $Q_H$ , and  $Q_E$  was calculated as  $Q_E = Q_H / \beta$ . This method was preferred over direct substitution since  $Q_E$  determined from both methods relies on the vapour pressure gradient which is often the reason for failed BREB calculations. The aerodynamic  $Q_H$ , however, relies only on the wind and temperature gradients. Substitutions were seldom necessary and the BREB calculations encompassed the majority of the calculations.

## D. RESULTS AND DISCUSSION

### D.1. Radiation Balance

The daily average values of the radiation balance components are given in Table 3.1a. The relatively small  $\alpha$  together with the long daylength periods (average daylength during the growing season is 16 hrs) resulted in high values of  $K^*$  and  $K^*/K\downarrow$ . Overall, the radiation efficiency of the surface ( $Q^*/K\downarrow$ ) at 60% is similar to the 55 and 61% for a tundra and open spruce-lichen forest site, respectively, located approximately 5 km east of the willow site (Rouse, 1984b).

The diurnal patterns of the radiation balance components are given in Figure 3.1. Morning and afternoon averages are given in Table 3.1b.  $K\downarrow$  is smaller in the PM than AM and displays a less symmetrical afternoon pattern. The decrease in  $K^*$ , however, is offset by an increase in  $L^*$  in the afternoon.

The asymmetrical behaviour is due to greater afternoon cloudiness which decreases  $K\downarrow$  and increase  $L\downarrow$ , the latter the result of higher temperatures and greater apparent emissivity, ( $\epsilon'$ ) as calculated from

$$L\downarrow = \epsilon' \sigma (T_a)^4 \quad (3.29)$$

Figure 3.2 shows that  $\epsilon'$  increases dramatically approaching 0.90 with the presence of afternoon clouds. The early morning increase in  $\epsilon'$  is likely the result of an increase in atmospheric water vapour because of the large stomatal conductance measured at this time

Table 3.1a. Daily averages of radiation balance components. Values are expressed in  $\text{W m}^{-2}$  (except  $K^*/K\downarrow$ ,  $Q^*/K\downarrow$ , and  $\alpha$  which are dimensionless).

$Q^*$	$K^*$	$L^*$	$K^*/K\downarrow$	$Q^*/K\downarrow$
138	194	-55	0.84	0.60
$K\downarrow$	$K\uparrow$	$\alpha$	$L\downarrow$	$L\uparrow$
231	37	0.16	321	376

Table 3.1b. Morning (AM) and afternoon (PM) averages of the radiation balance components  $Q^*$ ,  $K\downarrow$ ,  $K\uparrow$ ,  $L\downarrow$ , and  $L\uparrow$  ( $\text{W m}^{-2}$ ), air temperature  $T_a$  ( $^{\circ}\text{C}$ ), surface temperature  $T_s$  ( $^{\circ}\text{C}$ ), surface albedo  $\alpha$  (dimensionless) and apparent emissivity,  $\epsilon'$  (dimensionless).

	AM	PM
$Q^*$	138	138
$K\downarrow$	235	227
$K\uparrow$	39	36
$\alpha$	0.17	0.16
$L\downarrow$	313	329
$L\uparrow$	370	381
$T_a$	13	15
$T_s$	13	15
$\epsilon'$	0.81	0.85

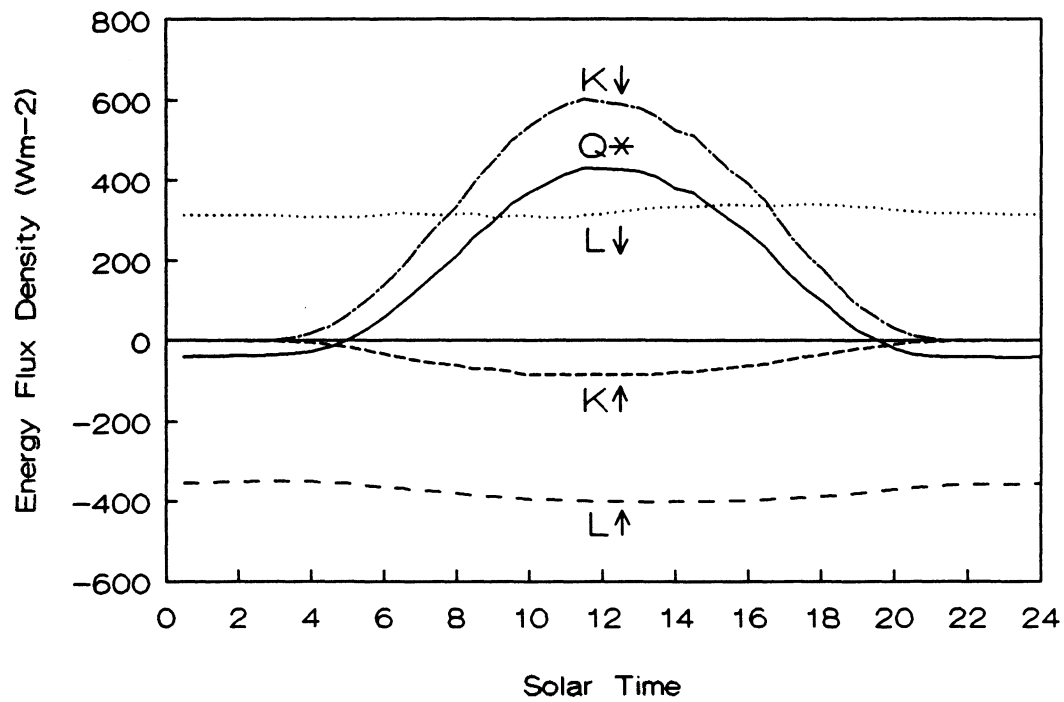


Figure 3.1. Diurnal course of the radiation balance. To aid interpretation,  $K\uparrow$  and  $L\uparrow$  are plotted as negatives.

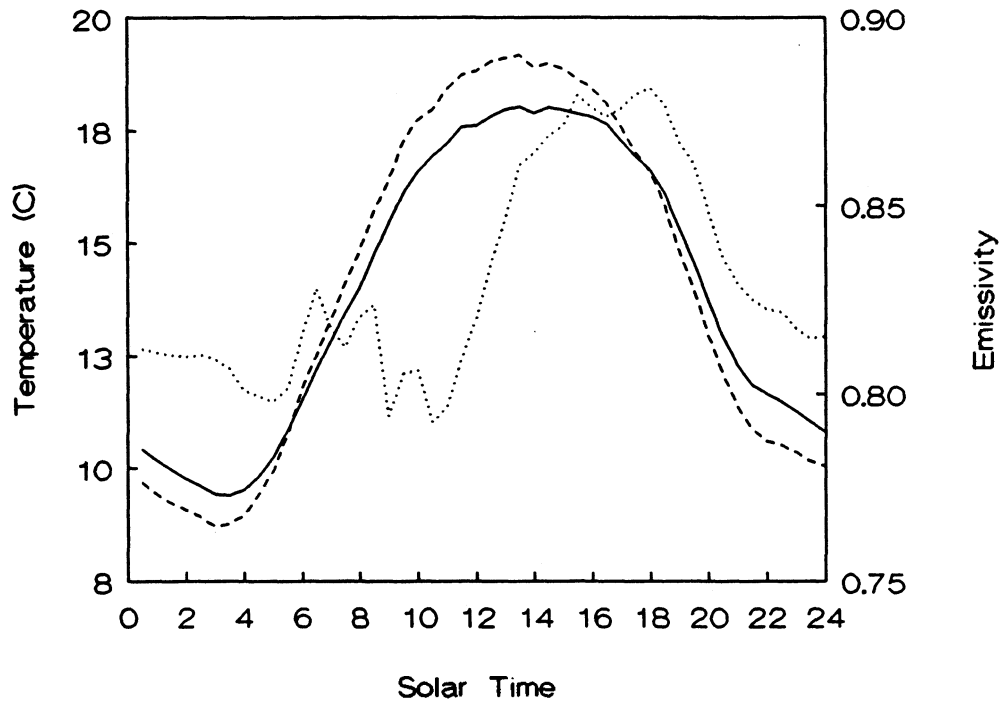


Figure 3.2. Diurnal course of air temperature (solid), surface temperature (dashed), and apparent atmospheric emissivity (dotted).

(Chapter 5, Section E.4).

Surface albedo showed a strong seasonal trend (Figure 3.3). An initial  $\alpha$  of 0.11 increased to 0.16 during the first 15 days of the growing season, which corresponds to the period of rapid vegetation growth (Figure 2.3). There is a strong linear relationship between  $\alpha$  and  $LAI$  ( $r^2=0.90$ ) during this period (June 19 to July 9), suggesting that the canopy is more effective in reflecting than in trapping  $K\downarrow$ . Besides changing the reflectivity of the surface, canopy absorption by the developing leaves also prevented radiation from reaching the wet soil beneath.

The variability about the trend shown in Figure 3.3 can be explained by the extent of standing water at the surface. A sharp decrease in  $\alpha$  coincides with periods when heavy rain caused the water table to rise above the surface (e.g. July 18 and 31). When the surface dried,  $\alpha$  increased back to the seasonal daily average of 0.16. Periods of light rain were insufficient to raise the water table above the surface, and therefore did not decrease  $\alpha$ .

Overall, the seasonal daily average  $\alpha$  of 0.16 compares closely to the 0.168 value reported over a *B. glandulosa* surface, yet is slightly lower than the 0.214 value reported over a *Salix* surface, both of which were found in the Boreal forest near Schefferville, Quebec (Petzold and Rencz, 1975). The seasonal daily average  $\alpha$  exceeded the 0.12 and 0.13 values found over nearby open spruce-lichen forest and tundra, respectively (Lafleur et al., 1992).  $\alpha$  falls within the lower part of the 0.15-0.25 range typical of deciduous forest (Brutsaert, 1982).

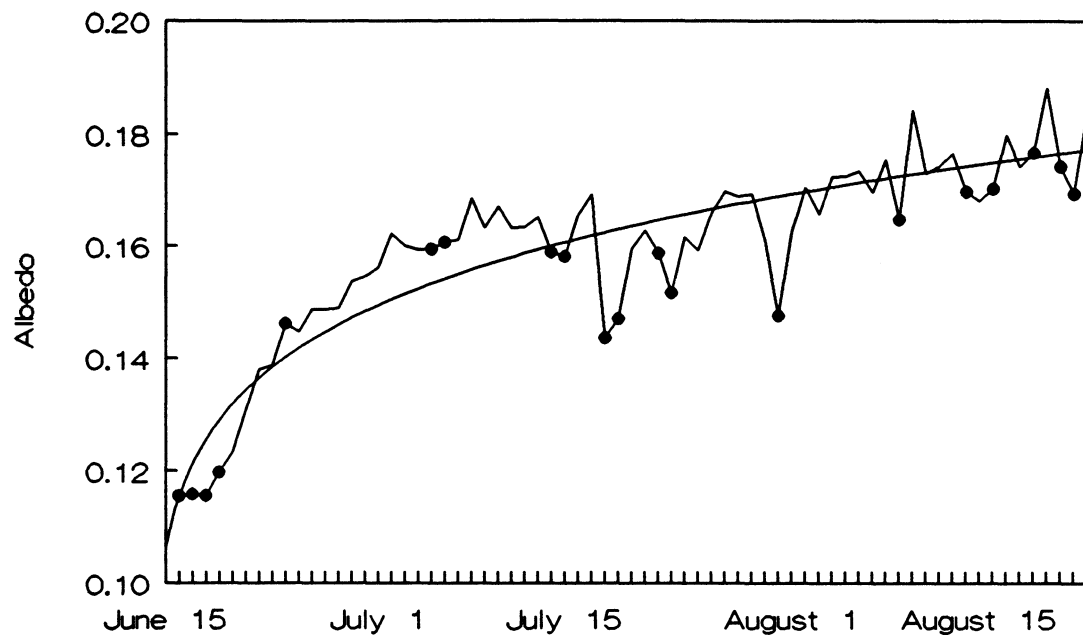


Figure 3.3. Seasonal course of the surface albedo. Dots mark days with precipitation.

## D.2. Energy Balance

To aid in the interpretation of the role vegetation plays in the energy balance, the growing season has been divided into three parts. The *growth* division represents the period of rapid vegetation growth from June 16 to July 12, when  $LAI < 0.60$ . The period of leaf maturity from July 13 to August 14 when  $LAI > 0.60$  is referred to as the *mature* period. The interval from August 15 to August 23 when leaves began to yellow and  $LAI < 0.60$  is referred to as the *senescence* period. The daily averages calculated over each of the three vegetation stages are summarized by Table 3.2.

The *growth* period is characterized by the large amount of available energy. The large  $Q^*$  is mainly the result of the large  $K\downarrow$  during the long days near the summer solstice. The small  $\alpha$  over the immature canopy and the cold  $T_o$  assist in maintaining a large  $Q^*$ . Small transpiration from the immature canopy plus cold air temperatures restricts  $Q_E$  to utilizing only 55% of  $Q^*$  and large vertical temperature gradients enhance  $Q_H$  (32% of  $Q^*$ ). A relatively large portion of  $Q^*$  (12%) is used as  $Q_G$ , due to the large thermal conductivity of the wet soil and the large subsurface temperature gradient.

The maturation of the canopy results in major changes in the energy balance.  $Q^*$  decreases because of smaller  $K\downarrow$  and larger  $\alpha$ . The addition of the transpiration is reflected by the large increase in the ratio of  $Q_E/Q^*$  from 55 to 74% and equally large decrease in the ratio of  $Q_H/Q^*$  from 32 to 10%. During this period, air temperatures have risen sufficiently to decrease the large temperature gradient which drove the large  $Q_H$  earlier in the season.  $Q_G/Q^*$  increases slightly, probably due to an increase in thermal

Table 3.2. Daily averages of the energy balance (and related terms) divided into *growth* ( $LAI < 0.60$ ), *mature* ( $LAI > 0.60$ ), and *senescence* ( $LAI < 0.60$ ) periods. Energy balance terms are given in  $W\ m^{-2}$ .  $\beta$  is dimensionless.

	<i>Growth</i>	<i>Mature</i>	<i>Senescence</i>
$Q^*$	167	125	104
$Q_E$	92	93	56
$Q_H$	54	13	34
$Q_G$	20	20	11
$Q_E/Q^*$	0.55	0.74	0.54
$Q_H/Q^*$	0.32	0.10	0.33
$Q_G/Q^*$	0.12	0.16	0.11
$\beta$	0.82	0.24	0.69

conductivity of the near-saturated soil caused by the heavy rains experienced during this period.

With the decrease in  $LAI$  and stomatal conductance, the energy balance during the *senescence* period returns to a similar pattern displayed during the *growth* period. Shorter days result in a decrease in  $K\downarrow$  and  $Q^*$ . The ratio of the energy balance components to  $Q^*$  is almost identical to the *growth* period. The decrease in transpiration results in a decrease in the ratio of  $Q_E/Q^*$  to pre-leaf levels. The decrease in  $Q_E$  together with colder air temperatures increases the ratio of  $Q_H/Q^*$  to pre-leaf levels.  $Q_G/Q^*$  also returns to pre-leaf levels.

## E. CONCLUSIONS

This chapter has shown that both the radiation and energy balance are affected by the presence of vegetation. Transpiration results in an increase in apparent atmospheric emissivity shortly after sunrise and in the mid-afternoon. The diurnal pattern of the apparent atmospheric emissivity is similar to the bimodal pattern of stomatal conductance discussed in Chapter 5, suggesting that transpiration results in a substantial increase in water vapour in the lower atmosphere. There is a strong relationship between increasing  $\alpha$  and  $LAI$  during the vegetation *growth* period, indicating that the canopy is more effective in reflecting rather than trapping radiation. While the partitioning of the energy balance components is almost identical during the *growth* and *senescence* periods, the

ratio of  $Q_E/Q^*$  increases dramatically during the *mature* period. This increase is due to the addition of transpiration to the overall evaporation.

## **CHAPTER 4**

### **SENSITIVITY ANALYSIS**

#### **A.INTRODUCTION**

The process of evaporation is better understood when the sensitivity to variables which drive and control the evaporative process is investigated. In order to perform such a task, it is first necessary to express evaporation in a format that explicitly states these variables in a physically based manner. The format that will be used in this sensitivity analysis is the well known Penman-Monteith combination model. Evaluation of the sensitivity of evaporation to net radiation, aerodynamic resistance and canopy resistance is accomplished by taking the first derivative of the Penman-Monteith combination model with respect to the preceding three variables. This is done on both a seasonal and diurnal bases.

#### **B.THEORY**

##### **B.1.The Penman-Monteith Combination Model**

The Penman-Monteith combination model combines both energy balance and

aerodynamic theory. The Penman model (Penman, 1948) describes evaporation from open water or short green vegetation with an ample supply of water (Thom, 1975). Therefore, there was no need for any surface or physiological resistance. The Penman model takes the form

$$Q_E = \frac{S}{S+\gamma}(Q^* - Q_G) + \frac{\gamma}{S+\gamma}E_A \quad (4.1)$$

where  $E_A$  is given by

$$E_A = f(u)(e_s(T_a) - e_a) \quad (4.2)$$

and describes the drying power of the atmosphere (Brutsaert, 1982). The wind function,  $f(u)$  is empirically derived from measurements of wind speed and has received considerable debate as to its proper expression. An important assumption in equation 4.1 is that the surface is saturated, so that  $e_s = e_s(T_a)$ .

Dry surfaces and surfaces with vegetation that can regulate water loss through stomatal conductance cannot be described by the original Penman equation. To overcome this limitation, Monteith (1965) amended equation 4.1 to include aerodynamic and surface resistances to evaporation. This is referred to as the Penman-Monteith combination model, and is given as

$$Q_E = \frac{S(Q^* - Q_G) + \rho c_p D / r_a}{S + \gamma(1 + r_d / r_a)} \quad (4.3)$$

where  $r_a$  is the aerodynamic resistance given as

$$r_a = \frac{[\ln((z-d)/z_o)]^2}{k^2 u} \quad (4.4)$$

The main advantages of equation 4.3 are that it is physically based and has been applied to many surfaces with good success. Its main disadvantage is that  $r_c$  is rarely known and cannot easily be predicted (Chapter 5, Section D.8). This has resulted in equation 4.3 most often being used in a diagnostic capacity as opposed to a predictive capacity. If  $Q_E$  has been determined by some other means, then  $r_c$  in equation 4.3 can be solved by residual and used to characterize the surface. In order to minimize any errors in predicting  $r_c$  from the model of stomatal resistance developed in the next Chapter,  $r_c$  in equation 4.3 has been calculated as a residual for this sensitivity analysis.

## B.2. Sensitivity Analysis

The sensitivity of variable  $X$  is a function of the input variables  $v_i$ , such that

$$X = f(v_1, v_2, v_3, \dots, v_n) \quad (4.5)$$

where  $n$  is the number of input variables. Assuming that the input variables are independent of  $X$ , then

$$X + \Delta X = f(v_1 + \Delta v_1, v_2 + \Delta v_2, \dots, v_n + \Delta v_n) \quad (4.6)$$

Expanding equation 4.6 in a Taylor series while ignoring second order terms gives

$$\Delta X = \frac{\partial X}{\partial v_1} \Delta v_1 + \frac{\partial X}{\partial v_2} \Delta v_2 + \dots + \frac{\partial X}{\partial v_n} \Delta v_n \quad (4.7)$$

The partial derivatives in equation 4.7 are, by definition, the sensitivities of variable  $X$  to each input variable  $v_n$ , as they indicate the change in  $X$  per unit change in  $v_n$  (McCuen, 1974; Beven, 1979; Jacobs and De Bruin, 1992). Since the sensitivities may themselves be sensitive to the relative magnitude of  $X$  and  $v_n$ , they may be divided by the ratio  $X/v_i$  which leads to a non-dimensional relative sensitivity defined as

$$RS(v_i) = \frac{\partial X}{\partial v_i} \frac{v_i}{X} \quad (4.8)$$

(Beven, 1979; Jacobs and De Bruin, 1992).  $RS(v_i)$  varies between -1 and +1 where negative values indicate that as  $v_i$  increases,  $X$  decreases. Positive values indicate that as  $v_i$  increases,  $X$  also increases. The magnitude of  $RS(v_i)$  may be interpreted as follows:  $RS(v_i) = 0.50$  indicates a 10% increase in  $v_i$  would result in a 5% increase in  $X$  or;  $RS(v_i) = -0.25$  indicates a 10% increase in  $v_i$  would result in a 2.5% decrease in  $X$ .

### C. EXPERIMENTAL PROCEDURE

The experimental procedure used here is taken directly from Jacobs and De Bruin (1992). First, since  $Q^*$  is the driving force behind  $Q_E$ , the Penman-Monteith combination model (equation 4.3) is scaled in terms of  $Q^*$  giving

$$\frac{Q_E}{Q^*} = \frac{\frac{S(Q^* - Q_G)}{Q^*} + \frac{\rho C_p D}{Q^* r_a}}{S + \gamma \left(1 + \frac{r_c}{r_a}\right)} \quad (4.9)$$

Following equation 4.8, the relative sensitivity of  $Q_E$  to  $Q^*$ ,  $r_a$ , and  $r_c$  are given as follows:

$$RS(Q^*) = \frac{\partial Q_E}{\partial Q^*} \frac{Q^*}{Q_E} = \left(1 + \frac{\rho C_p D}{S(Q^* - Q_G) r_a}\right)^{-1} \quad (4.10)$$

$$RS(r_a) = \frac{\partial(Q_E/Q^*)}{\partial r_a} \frac{r_a}{(Q_E/Q^*)} = \frac{\frac{S}{(S+\gamma)} \frac{(Q^* - Q_G)/Q^*}{(Q_E/Q^*)} - 1}{1 + \frac{\gamma}{(S+\gamma)} \frac{r_c}{r_a}} \quad (4.11)$$

$$RS(r_c) = \frac{\partial(Q_E/Q^*)}{\partial r_c} \frac{r_c}{(Q_E/Q^*)} = - \left(1 + \left(1 + \frac{S}{\gamma}\right) \frac{r_a}{r_c}\right)^{-1} \quad (4.12)$$

The procedures used to calculate the variables used in equations 4.10 through 4.12 have been described previously (Chapter 3, Section C).  $r_a$  was calculated using equation 4.4 employing wind speed obtained at a height of 1.7 m above the surface.  $r_c$  was calculated as a residual of equation 4.3, given as

$$r_c = \frac{r_a [S(Q^* - Q_G - Q_E) - \gamma Q_E] + \rho C_p D}{\gamma Q_E} \quad (4.13)$$

## D. RESULTS AND DISCUSSION

### D.1. Sensitivity to $Q^*$

The seasonal and diurnal trends of  $RS(Q^*)$  are shown in Figures 4.1a and 4.2a, respectively, and summarized in Tables 4.1a and 4.1b.  $RS(Q^*)$  is always positive, indicating that an increase in  $Q^*$  always results in an increase in  $Q_E$ . Seasonally,  $RS(Q^*)$  decreases as the growing season progresses. Temporal variation is large, with  $RS(Q^*)$  varying from 0.13 to 0.78 about a mean of 0.37. Diurnally,  $RS(Q^*)$  decreases from a nighttime value of approximately 0.25 to near zero at sunrise and sunset. A maximum sensitivity of 0.45 is reached during the midday hours. In order to understand the seasonal and diurnal behaviour of  $RS(Q^*)$ ,  $RS(Q^*)$  was plotted against variables given in equation 4.3. Large scatter occurs with each plot, but the least is observed when  $RS(Q^*)$  is plotted against the ratio of  $r_c/r_a$  (Figure 4.3a)

Although the correlation is modest (Table 4.2),  $RS(Q^*)$  decreases as  $r_c/r_a$  increases. When  $r_c$  is small relative to  $r_a$ , the canopy plays a small role in controlling  $Q_E$ . This represents the situation when there is plenty of water available for  $Q_E$  and there are either no leaves or if there are leaves, the stomata are fully open. Hence,  $Q_E$  is largely under the influence of  $Q^*$  and to some extent of  $r_a$ . This represents the situation early in

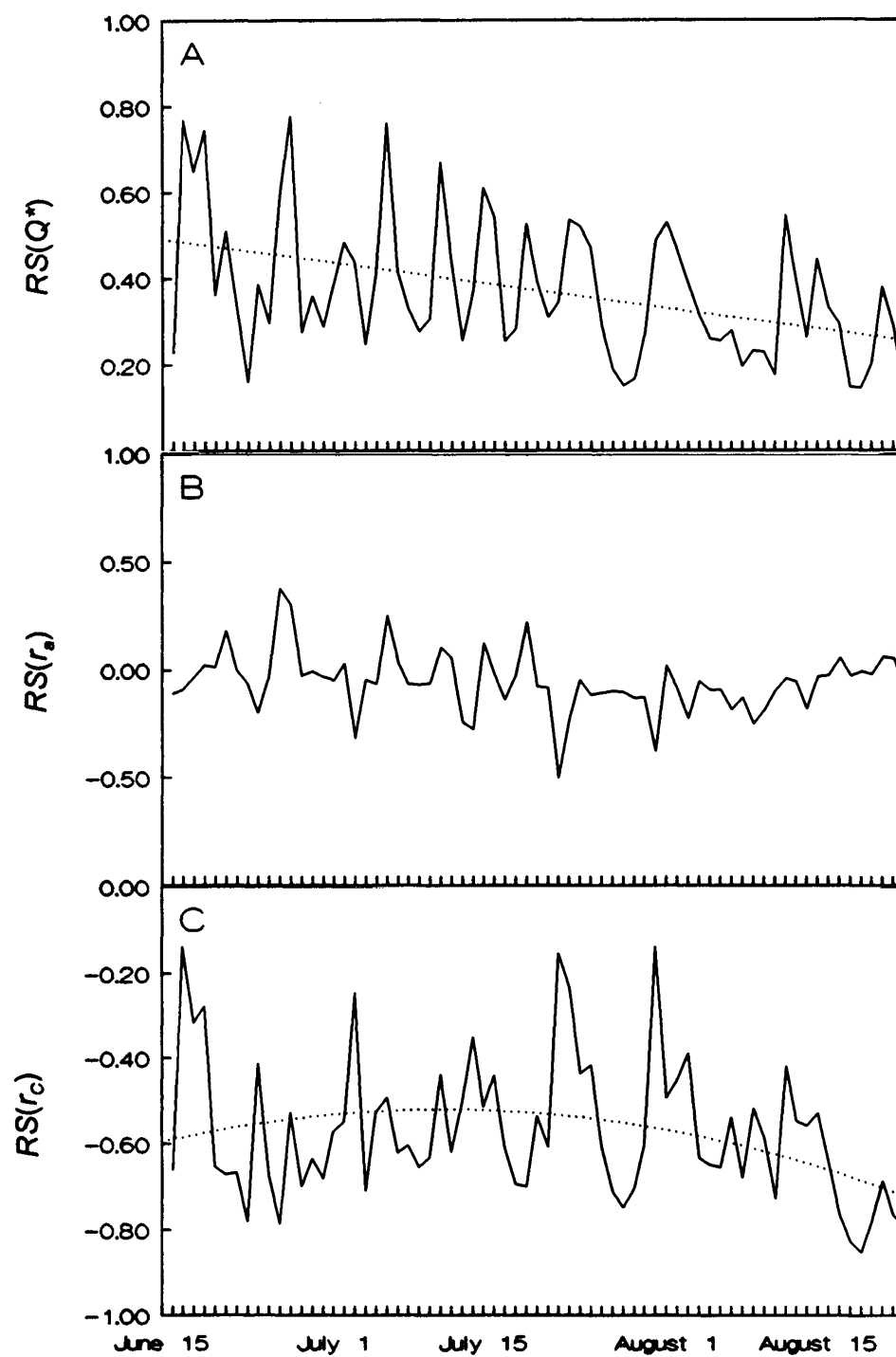


Figure 4.1. Seasonal course of the relative sensitivity of evaporation to net radiation (A), aerodynamic resistance (B), and canopy resistance (C). Dotted lines show the seasonal trends.

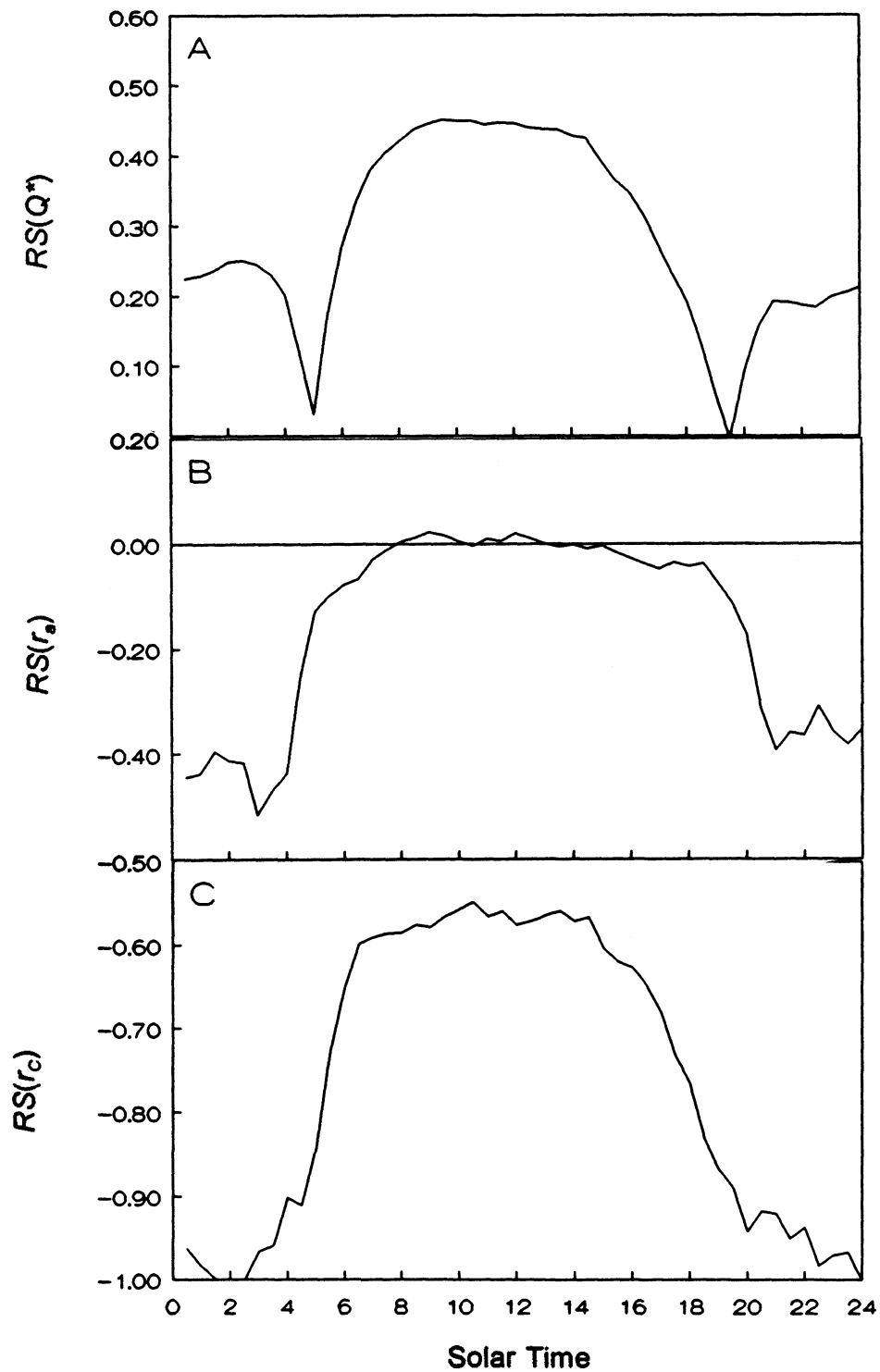


Figure 4.2. Diurnal course of the relative sensitivity of evaporation to net radiation (A), aerodynamic resistance (B), and canopy resistance (C).

Table 4.1a. Summary of the relative sensitivities of  $Q_E$  to  $Q^*$ ,  $r_a$ , and  $r_c$  based on the seasonal trends shown in Figures 4.1a through 4.1c.

	$RS(Q^*)$	$RS(r_a)$	$RS(r_c)$
Seasonal	0.37	-0.06	-0.57
Std. Deviation	0.16	0.14	0.16
Std. Error	0.02	0.02	0.02
Maximum	0.78	0.37	-0.14
Minimum	0.13	-0.50	-0.85

Table 4.1b. Relative sensitivities of  $Q_E$  to  $Q^*$ ,  $r_a$ , and  $r_c$  based on the diurnal trends shown in Figures 4.2a through 4.2c.

	$RS(Q^*)$	$RS(r_a)$	$RS(r_c)$
Average	0.28	-0.16	-0.76
Std. Deviation	0.13	0.18	0.18
Std. Error	0.02	0.02	0.02
Maximum	0.45	0.02	-0.55
Minimum	0.00	-0.52	-1.09

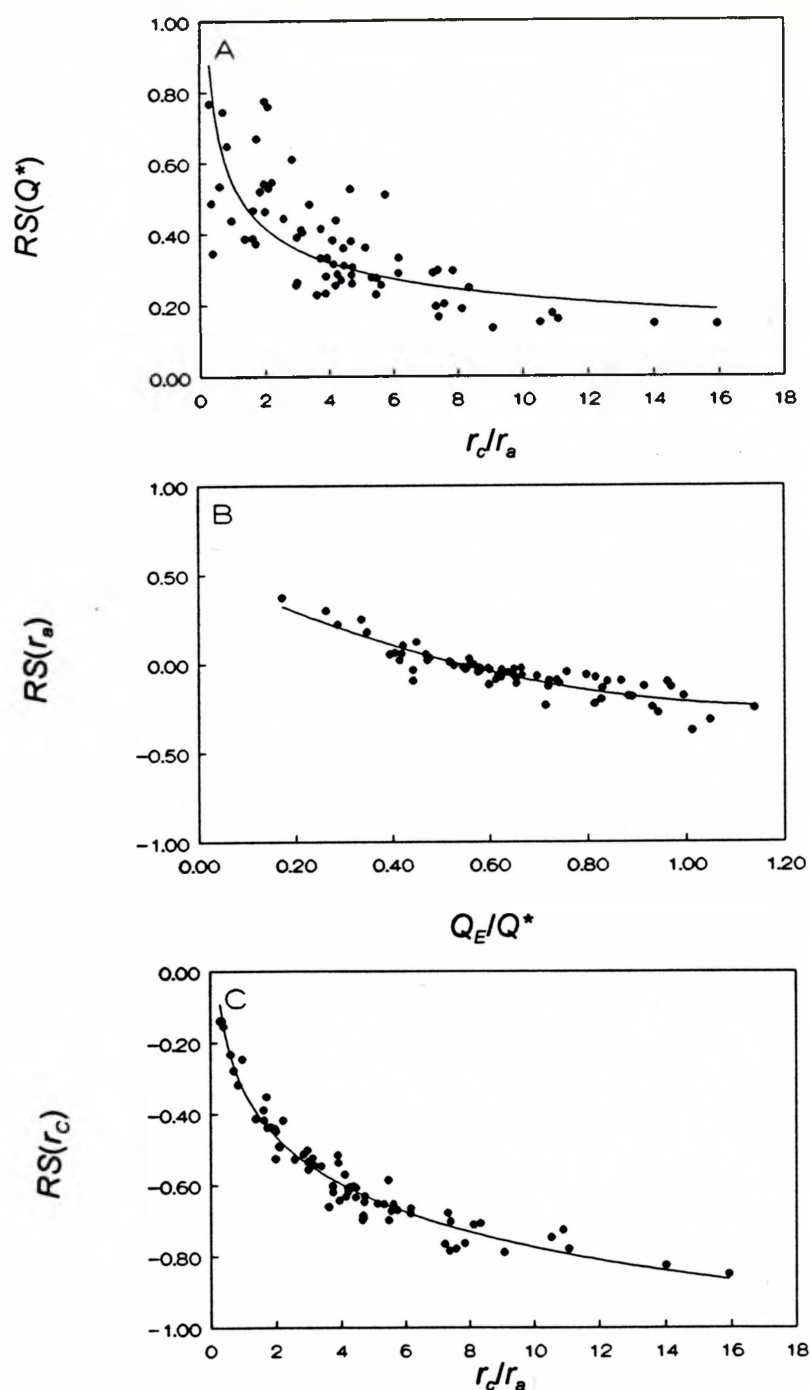


Figure 4.3. Relationships between the relative sensitivity of evaporation to net radiation and the ratio of canopy-to-aerodynamic resistance (A), relative sensitivity of evaporation to aerodynamic resistance and the ratio of evaporation-to-net radiation (B) and, relative sensitivity of evaporation to canopy resistance and the ratio of canopy-to-aerodynamic resistance (C).

Table 4.2. Equations used to fit the curves shown in Figures 4.3a through 4.3c.

Figure	Equation	n	$r^2$
$RS(Q^*)$ vs $r_c/r_a$	$y=0.55x^{-0.39}$	69	0.55
$RS(r_d)$ vs $Q_E/Q^*$	$y=0.52-1.25x+0.51x^2$	69	0.82
$RS(r_d)$ vs $r_c/r_a$	$y=-0.33-0.19 \ln(x)$	69	0.95

the growing season when the leaves are immature causing the canopy to have little influence on  $Q_E$ . This also represents the average midday situation when  $r_c$  around midday decreases due to an increased transpiration stream through the open stomata.

$RS(Q^*)$  also responds to the magnitude of  $Q^*$  itself. Although the relationship between  $RS(Q^*)$  and  $Q^*$  is very weak (not shown),  $Q_E$  is least sensitive to  $Q^*$  when  $Q^*$  approaches zero. This can be seen in Figure 4.2a where the sensitivity of  $Q_E$  to  $Q^*$  at sunrise and sunset approaches zero as  $Q^*$  approaches zero. The seasonal trend in  $RS(Q^*)$  can also be partially explained by the fact that  $Q^*$  gradually decreases as the growing season progresses. Also, it has been found that  $RS(Q^*)$  shows a slight temperature dependence (Rowntree, 1991). The compounding influence of  $r_c/r_a$ ,  $Q^*$ , and  $T_a$  promotes the relatively large scatter shown in Figure 4.3a.

## D.2. Sensitivity to $r_a$

The seasonal (Figure 4.1b, Table 4.1a) and diurnal (Figure 4.2b, Table 4.1b) trends of  $RS(r_a)$  show that an increase in  $r_a$  usually serves to decrease  $Q_E$ . There are, however, occasions when an increase in  $r_a$  increases  $Q_E$ . These instances when  $r_a$  works in a reverse manner occur at periods when  $r_a$  has absolutely no effect on  $Q_E$ . This occurs during midday periods when the sensitivities of  $Q_E$  to  $Q^*$  and  $r_c$  totally override the minor sensitivity to  $r_a$ . Seasonally, there is no apparent trend in  $RS(r_a)$ . Diurnally, the largest  $RS(r_a)$  occurs during the night, while (as mentioned above)  $Q_E$  is insensitive to  $r_a$  during daylight hours.

Plots of the variables given in equation 4.3 against  $RS(r_a)$  reveal that  $RS(r_a)$  is a function of the ratio of  $Q_E$  to  $Q^*$  (Figure 4.3b, Table 4.2).  $Q_E/Q^*$  approaches unity when  $Q_H$  and/or  $Q_G$  are very small (a common nighttime occurrence). During these periods, the small  $Q^*$  reduces any  $Q_E$  from open water. Also,  $r_c$  is large since all stomata have closed due to low light levels, thus eliminating any transpirational water loss. Therefore, any  $Q_E$  (albeit small) must be driven by aerodynamic processes alone. This is confirmed by Figures 4.1b through 4.3b.  $Q_E$  is most sensitive to  $r_a$  during the night when aerodynamic processes control  $Q_E$ , and  $RS(r_a)$  is near zero during the day when  $Q_E$  is driven by radiation processes. Seasonally,  $RS(r_a)$  is strongest on days when radiation inputs are low (for example, July 3 and July 22) and aerodynamic processes dominant, and  $Q_E$  is least sensitive to  $r_a$  when radiation processes control  $Q_E$  (for example, June 27 and July 20).

### D.3. Sensitivity to $r_c$

The sensitivity of  $Q_E$  to  $r_c$  is consistently negative both seasonally (Figure 4.1c, Table 4.1a) and diurnally (Figure 4.2c, Table 4.1b) indicating that an increase in  $r_c$  always results in a decrease in  $Q_E$ . A weak seasonal pattern in sensitivity exists, with  $RS(r_c)$  being smallest near the middle of the growing season. Diurnally,  $Q_E$  is least sensitive to  $r_c$  during the midday periods.

Scatter plots of  $RS(r_c)$  against the variables in equation 4.3 reveal a very strong relationship with the ratio  $r_c/r_a$  (Figure 4.3c, Table 4.2). A small  $r_c/r_a$  would prevail when

there is sufficient energy to trigger and drive transpiration. The addition of transpiration decreases the sensitivity of  $Q_E$  to  $r_c$  and therefore reduces  $RS(r_c)$ . Diurnally, the sensitivity of  $Q_E$  to  $r_c$  is greatest during nighttime periods when stomatal closure increases  $r_c$  to a maximum. During daytime periods when the majority of  $Q_E$  occurs,  $r_c$  decreases thus decreasing  $r_c/r_a$  and  $RS(r_c)$ .  $r_c$ , however, does not fall to zero. The canopy is always exerting some resistance due to stomatal functioning, resulting in a relatively consistent midday  $RS(r_c)$  value of -0.60.

The seasonal trend of  $RS(r_c)$ , being greatest near the beginning and end of the growing season, can also be explained. Early in the season, the canopy is underdeveloped, the transpiration stream is negligible, and  $r_c$  is large. As the canopy matures, the additional transpiration reduces  $r_c$  and as a consequence, reduces  $RS(r_c)$ . During senescence transpiration is decreased and  $Q_E$  becomes less sensitive to  $r_c$  as the ratio  $r_c/r_a$  decreases.

## E. CONCLUSIONS

The sensitivity of evaporation to net radiation, aerodynamic resistance, and canopy resistance displays both seasonal and diurnal trends. Overall, evaporation is highly sensitive to the canopy resistance, indicating the importance of vegetation in the evaporative process. Both the seasonal and diurnal trends in the sensitivity to canopy resistance can be explained by the ratio of canopy to aerodynamic resistances.

## CHAPTER 5

### STOMATAL CONDUCTANCE

#### A. INTRODUCTION

Because vegetation plays a major role in evaporation from the willow-birch forest, this chapter provides a detailed description of the species-specific physiology of water movement through the plants. The relationships between stomatal conductance, transpiration, and the environmental controls which influence these processes are stressed.

#### B. PHYSIOLOGY OF PLANT WATER TRANSPORT

##### B.1 Role of Stomata in Photosynthesis and Transpiration

Photosynthesis is the process whereby light energy trapped by the green pigment chlorophyll is used to chemically convert water (H<sub>2</sub>O) and carbon dioxide (CO<sub>2</sub>) into organic molecules (CH<sub>2</sub>O) and oxygen (O<sub>2</sub>) (equation 5.1).



Plants found at the study site, as do most plants, incorporate CO<sub>2</sub> into organic molecules by means of the C<sub>3</sub> or Calvin Cycle. In C<sub>3</sub> plants, a CO<sub>2</sub> and 5-carbon molecule react to form two 3-carbon molecules. This cycle is completed six times to form one 6-carbon

glucose molecule (hexose sugars) (Arms and Camp, 1982).

The basic  $C_3$  photosynthesis pathway has been modified by some plants in dry environments. Plants using the  $C_4$  or Hatch-Slack pathway have the ability to add an additional  $CO_2$  molecule to the 3-carbon molecule. The net effect is to increase to photosynthetic rate (and therefore growth) at the expense of a less efficient use of energy. Such plants exist in dry, tropical climates where light energy is abundant, air temperatures are high, and water stress often occurs (Arms and Camp, 1982; Nobel, 1991). Despite the high temperatures and low precipitation sometimes experienced in Arctic and Subarctic regions, there are no  $C_4$  Arctic plants (Chapin and Shaver, 1985).

Both the upper (adaxial) and lower (abaxial) surfaces of leaves are covered by a layer of epidermis cells which secrete a protective waterproof cuticle. The cuticle inhibits water loss through the leaf to the atmosphere yet also prevents  $CO_2$  (the source of carbon for photosynthesis) from entering the plant. Plants have evolved openings in the cuticle called stomata surrounded by two guard cells which serve to regulated gas exchange in the plant. The opening of the stomata allows  $CO_2$  (and  $O_2$  for respiration) to enter the plant at the expense of water loss from the plant (transpiration). Thus, a measure of the plant's ability to conduct water vapour through the stomatal opening is referred to as the stomatal conductance.

The guard cells have the ability to control stomatal aperture through their shape and turgor. Thicker cell walls next to the stomatal opening maintain a closed stoma when turgor pressure is low, while swelling of the cells causes the stoma to open when turgor

pressure is high (Arms and Camp, 1982).

The opening and closing of the stomata is a response to changes in the concentration of CO<sub>2</sub> and H<sub>2</sub>O. Opening occurs when CO<sub>2</sub> uptake due to photosynthesis results in decrease in the CO<sub>2</sub> concentration in the guard cells. The low CO<sub>2</sub> concentration triggers the active transport of potassium into the guard cells, thus lowering the osmotic potential allowing water to enter and increase the turgor. Closure occurs when transpirational water loss exceeds the plant's ability to deliver water. When the water potential becomes too low, the hormone abscisic acid is released causing the guard cells to lose turgor and close the stomata (Arms and Camp, 1982).

## B.2. Internal Transport of Water

All species of plants found at the study site (except *Aulacomnium turgidum*) are vascular. The *Carex* species are monocotyledons (Scott, 1991), with the phloem and xylem being scattered throughout the stem (Raven et al., 1981). The *Salix* species, *B. glandulosa*, and *M. gale* are dicotyledons (Scott, 1991), with the xylem arranged in concentric rings surrounded by the phloem (Arms and Camp, 1982). Since only the xylem conducts water, the role of the phloem will be ignored in this thesis.

Water enters the plant at the root tips by a lowering of the water potential within the roots. This is accomplished by active transport of ions into the root cells from the surrounding soil, which requires a sufficient supply of O<sub>2</sub> to supply the high respiratory demand of the cells. The resulting root pressure, however, is not capable of pushing water

to the stomata in all but very short plants. An additional pull is created by the transpirational losses at the stomata. The lowering of the water potential at the leaf surface draws water from adjacent cells, thus creating a continual pull on the column of water through the plant from the leaf to the root tips (Rost et al., 1979).

Since the continuous internal water column experiences a negative pressure at the leaf and a slight positive pressure at the roots, the water in the xylem is under considerable tension. The measure of this internal tension gives an indication of the overall water status of the plant, since the tension is both a function of transpiration and soil moisture availability.

## C. EXPERIMENTAL PROCEDURE

### C.1. Stomatal Conductance

Stomatal conductance ( $g$ ) was measured on both leaf surfaces of the major species found at the study site, namely *S. planifolia*, *C. aquatilis*, *S. candida*, *S. reticulata*, *B. glandulosa* and *M. gale*. The theory behind calculating  $g$  and transpiration ( $T_r$ ) can be found in Appendix A. Measurements were taken at hourly intervals from before sunrise to after sunset on June 28, July 16, and July 28, 1991. These days were selected because they were fair weather days. The LI-1600M porometer was calibrated by the factory prior to field use, and the desiccant was thoroughly dried before each measurement session. Care was taken to ensure that the leaf thermocouple made proper contact with the leaf

surface.

Leaf temperature was measured with a chromel-constantan thermocouple (0.051 mm diameter) attached to the porometer. The abaxial and adaxial temperatures were averaged to obtain the leaf temperature for each species, while all leaf temperatures were averaged to obtain the canopy temperature ( $T_c$ ).

The leaf-to-air vapour pressure deficit ( $\Delta W$ ) was calculated as the difference between the saturation vapour pressure evaluated at  $T_c$  and the vapour pressure measured at 1.7 m above the ground surface.

## C.2. Xylem Pressure Potential

Xylem pressure potential ( $\Psi$ ) was measured with a Scholander-type pressure chamber (Model 1000, PMS Instruments, Corvallis, Oregon, U.S.A.) (Scholander, 1964). A small sample was cut from each plant and immediately placed inside the pressure chamber after the phloem was peeled back. Measurements were not made on *C. aquatilis*, since it being a monocotyledon, any measurements would be an inseparable composite of both water and glucose. Since the leaf stems were too small and delicate to insert into the pressure chamber, the pressure potential of the xylem was recorded.  $\Psi$  is closely related, but not always equal to leaf water potential (Ritchie and Hinckley, 1975), and is often reported erroneously as leaf water potential. Use of  $\Psi$  as a direct measure of leaf water potential requires calibration of  $\Psi$  with leaf water potential using stem psychometers. Such calibration was not performed in this study. Compressed nitrogen gas

was used to pressurize the chamber, and the pressure at which xylem sap (water) appeared at the cut end of the xylem was recorded (a magnifying lens was used to determine the presence of sap). Measurements were taken concurrently with  $g$  measurements.

## D. RESULTS AND DISCUSSION

### D.1. Ambient Conditions

Diurnal measurements of  $g$  were taken on mainly clear days (Figure 5.1; Table 5.1). Although it is recognized that measurements taken only on clear days may bias results, the behaviour of the plants would be easiest to detect under such conditions since stomatal opening would be severely limited under poor light conditions. Moreover, measurements made in fluctuating light conditions would confuse the results, since the opening and closing time of stomata varies between species, and in some species may be as long as 40 minutes (Turner, 1991).

Average air and canopy temperatures for the three days are shown in Figure 5.2 and Table 5.1. During the day,  $T_c$  exceeded  $T_a$ , because the net radiation received at the leaf exceeded the heat loss from evaporative cooling. At sunrise and sunset,  $T_c$  fell below  $T_a$  due to radiation loss exceeding any heat release from evaporative cooling (Oke, 1987). The effect of evaporative cooling of the leaf surface was illustrated on each day. The greatest difference between  $T_c$  and  $T_a$  was experienced on June 29 when canopy transpiration was small. In contrast, the difference between  $T_c$  and  $T_a$  was smallest on July

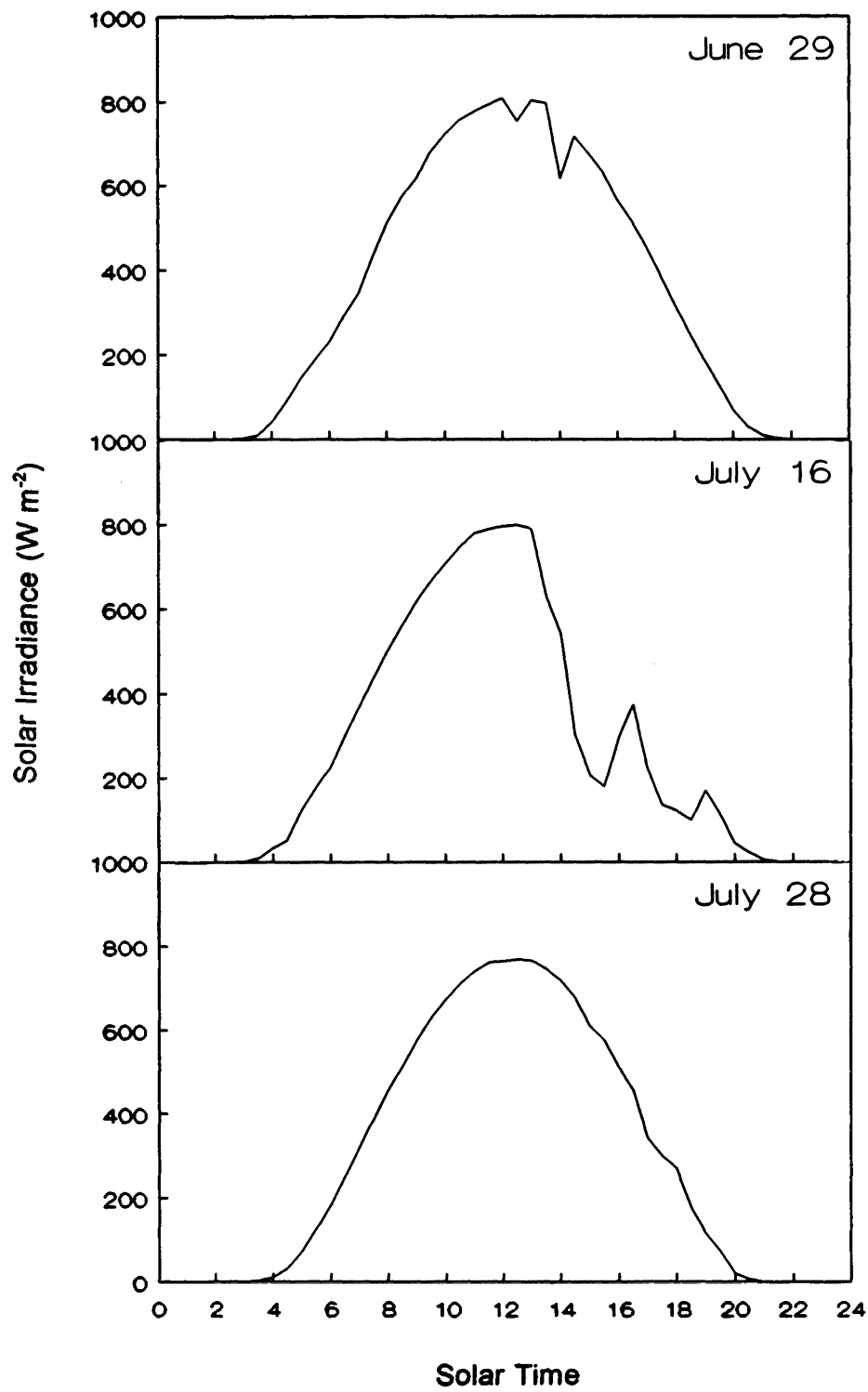


Figure 5.1. Diurnal course of solar irradiance.

Table 5.1. Ambient conditions during the three days when intensive stomatal conductance measurements were taken.

	June 29	July 16	July 28
$K\downarrow$ Average ( $W\ m^{-2}$ )	397	340	398
$K\downarrow$ Maximum ( $W\ m^{-2}$ )	807	797	767
Sunrise	0251	0312	0336
Sunset	0910	0853	0828
$T_a$ Average ( $^{\circ}C$ )	15.5	14.5	24.6
$T_c$ Average ( $^{\circ}C$ )	17.8	15.9	25.8
$D$ (kPa)	0.7707	0.4461	1.7931
$\Delta W$ (kPa)	1.0647	0.6034	2.2827
$T_{root}$ Maximum ( $^{\circ}C$ )	13.4 @1600	13.6 @1600	17.0 @1600
$T_{root}$ Minimum ( $^{\circ}C$ )	5.7 @400	8.4 @800	11.1 @800
$T_{root}$ Average ( $^{\circ}C$ )	9.3	10.8	13.9

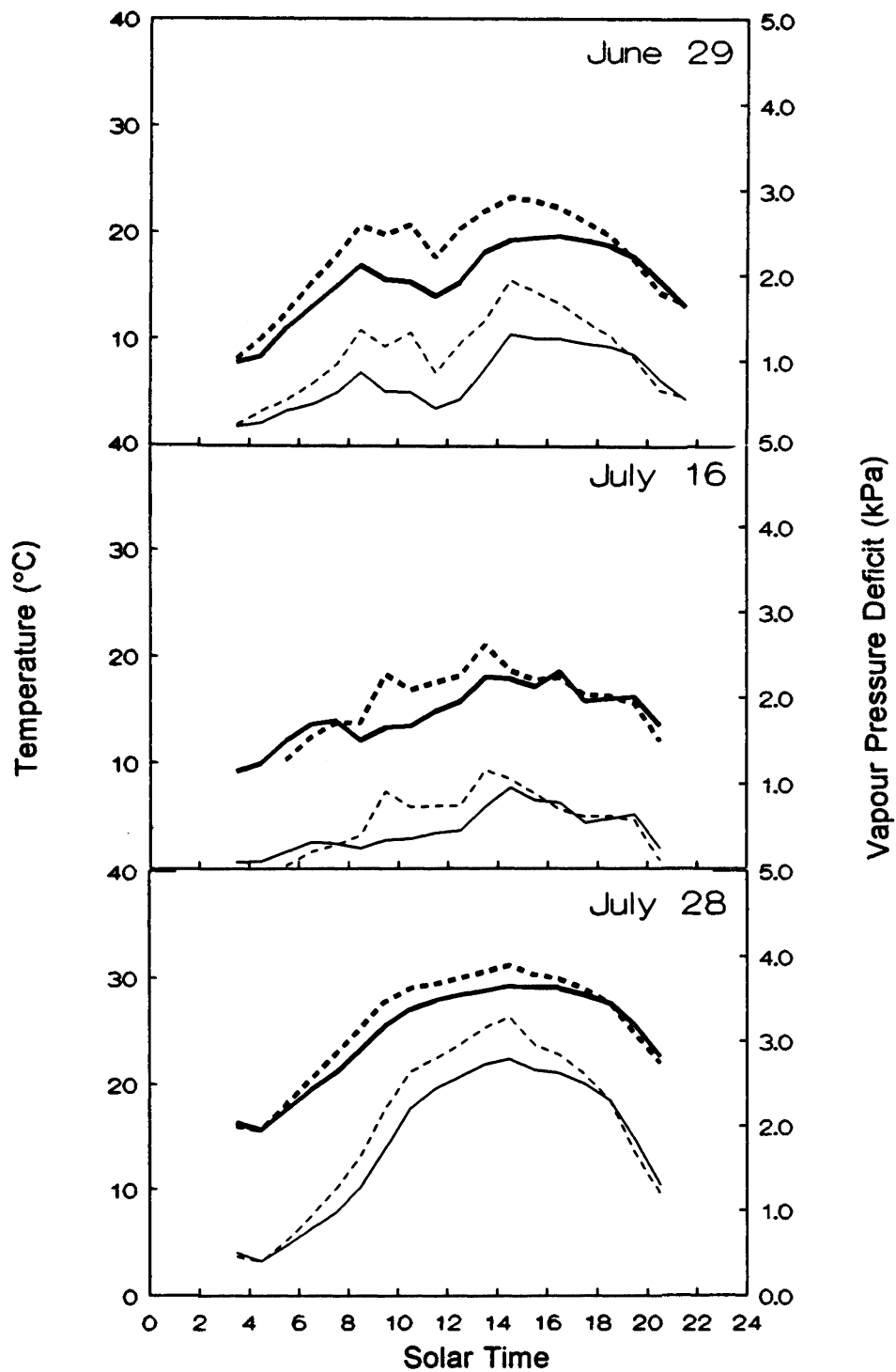


Figure 5.2. Diurnal course of temperature (heavy lines) and vapour pressure deficit (thin lines). Solid line represents measurements made 1.7 m above the ground. Dashed lines represent measurements made at the leaf surfaces.

28, when transpiration was large.

The difference between  $T_c$  and  $T_a$  resulted in a difference between  $\Delta W$  and  $D$  (Figure 5.2, Table 5.1). Due to the exponential relationship between temperature and vapour pressure, the difference between  $\Delta W$  and  $D$  was greatest on July 28 when both  $T_c$  and  $T_a$  were high. Even when temperatures are moderate (June 29 and July 16), the differences between  $T_c$  and  $T_a$  can create a substantial difference between  $\Delta W$  and  $D$ . Thus, assuming that  $T_c = T_a$  would lead to an underestimation of  $\Delta W$ , which would then lead to an underestimation of transpiration.

Soil temperature within the rooting zone ( $T_{root}$ ) increased as the growing season progressed (Figure 5.3). The maximum was reached at 1600 on all days, while the minimum was reached at 0400 on June 29 and at 0800 on July 16 and 28. The largest range in  $T_{root}$  was experienced within the upper 0.20 m of soil, which corresponds to the organic soil horizon (Chapter 2, Section C.3).

## D.2. Stomatal Distribution

Within the genus *Salix*, there is considerable variation in the stomatal distribution on the two leaf surfaces. Goudley et al. (1985) found stomata on both leaf surfaces of *S. interior*. Frequency ranged from 26 to 28 stomata per mm<sup>2</sup> with stomata being 10% more abundant on the adaxial surface. Larsson (1981) found stomata only on the abaxial surface of *S. capera* and *S. viminalis*. Binns et al. (1980) examination of 19 *Salix* species and 12 hybrids found that most species in the subgenus *Salix* had stomata on both leaf surfaces.

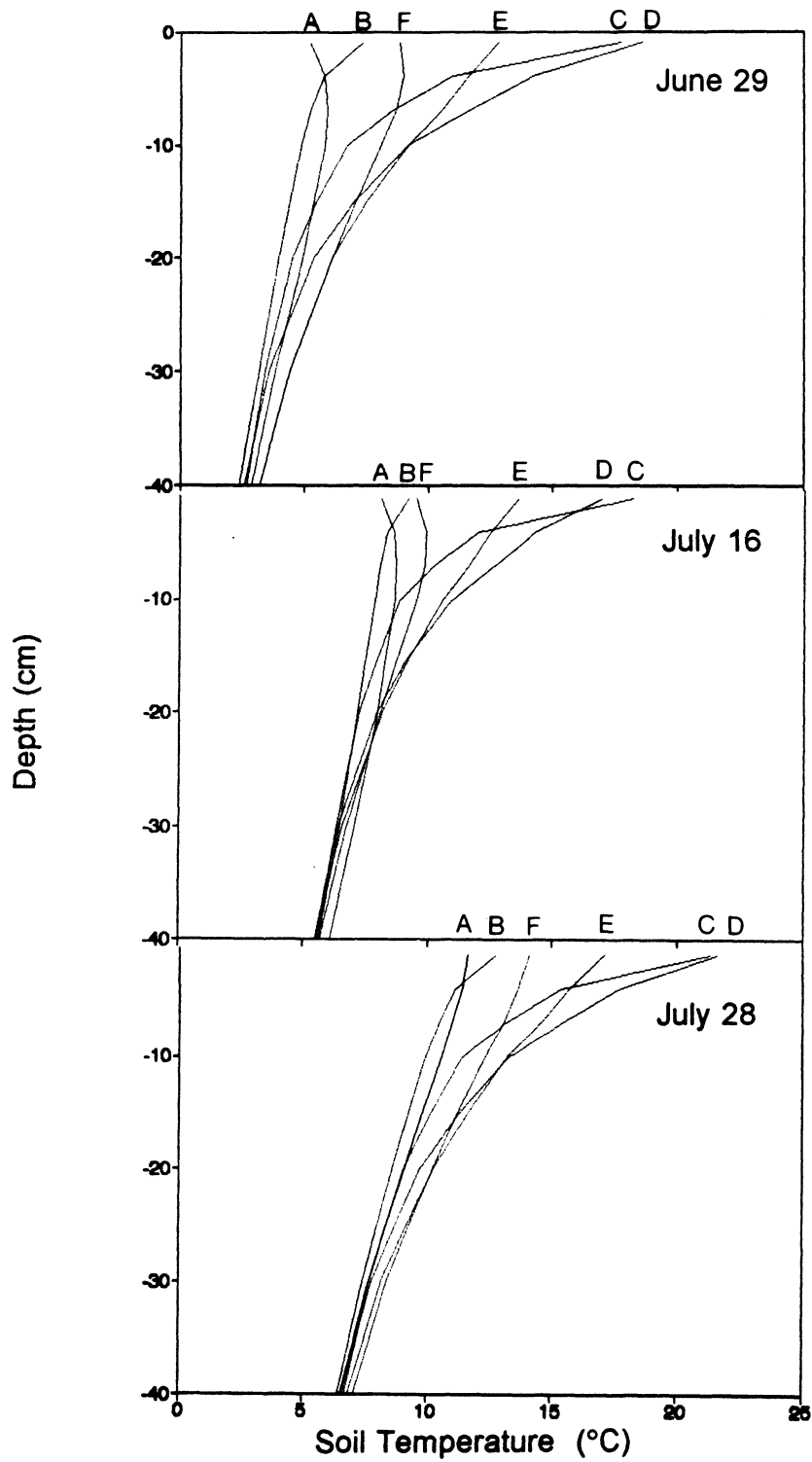


Figure 5.3. Diurnal course of ground temperatures. Letters refer to profiles taken at the following times: A=0400; B=0800; C=1200; D=1600; E=2000 and; F=2400.

The subgenus *caprisalix* had abaxial stomata only (with a few exceptions), while the subgenus *chaemetia* (dwarf, alpine willows) had some species with stomata on both leaf surfaces (e.g. *S. herbacea*) while some had abaxial stomata only (e.g. *S. reticulata*).

Variation on the stomatal distribution within the genus *Carex* also exists. Standley (1986) found that *C. aquatilis* var *dives* had stomata on the adaxial surface only while *C. aquatilis* var *aquatilis* was amphistomatous. There was also considerable intraspecies variation, with differences possibly being due to the environmental conditions.

Although correct measurements of stomatal distribution involve visual examination under a very high powered microscope, measurements of stomatal distribution can be inferred from measurements of *g*. This method assumes that the cuticle conductance is similar on both leaf surfaces, and that there is no difference in microclimate between the leaf surfaces.

The percentage of the total leaf *g* occurring from each leaf surface is shown in Table 5.2. All of the dicotyledon species were amphistomatous, with the majority of *g* originating from the abaxial surface. Values ranged from a maximum of 90% abaxial conductance (*S. candida*; June 28 and July 29) to a minimum of 61% (*M. gale*; July 16). The ratio of adaxial to abaxial conductances appears to be independent of the different climatological conditions experienced on the three days. The monocotyledon species *C. aquatilis* was also amphistomatous, with no clear dominance by either leaf surface.

The amphistomatous leaf conductances found in all species in this Subarctic environment might, as Standley (1986) suggests, be an adaptation of the plant to the

Table 5.2. Percentage of the total leaf stomatal conductance occurring on the adaxial (Ad) and abaxial (Ab) leaf surfaces.

Species	June 29		July 16		July 28		Average	
	Ad	Ab	Ad	Ab	Ad	Ab	Ad	Ab
<i>S. planifolia</i>	20	80	17	83	16	84	18	82
<i>S. candida</i>	10	90	24	76	10	90	15	85
<i>S. reticulata</i>	34	66	26	74	28	72	29	71
<i>C. aquatilis</i>	60	40	46	54	46	54	51	49
<i>B. glandulosa</i>	16	84	31	69	19	81	22	78
<i>M. gale</i>	34	66	39	61	23	77	32	68

harsh environment. The short growing season demands that growth and reproduction occur quickly. For plants growing in a wet environment, the extra CO<sub>2</sub> intake possible with the additional stomata may offset the additional transpirational water loss.

Whatever the reason for the amphistomatous leaves, it is important that the  $g$  be measured on both leaf surfaces of all the species found in this environment, since  $g$  (and transpiration) would be seriously underestimated if hypostomatous leaves were assumed.

### D.3. Maximum Stomatal Conductance

Maximum stomatal conductance ( $g_{max}$ ) is useful for comparative purposes since it represents the upper limit to stomatal conductance when, in theory, all factors limiting stomatal conductance are minimal. Thus,  $g_{max}$  represents the potential for stomatal conductance and is limited by the plant itself, not the surrounding environment.

The  $g_{max}$  values found in this study for each species are shown in Table 5.3a. *S. planifolia* had the largest average  $g_{max}$ . *B. glandulosa*, *C. aquatilis*, and *S. reticulata* all had similar  $g_{max}$  values, while *S. candida* and *M. gale* had the lowest values. All species experienced  $g_{max}$  early in the morning when efficient photosynthesis could occur without a high transpirational loss ( $\Delta W$  is low at this time).

In general, all  $g_{max}$  values were very high compared to those reported in the literature (Table 5.3b). Literature on the stomatal conductance for Arctic and Subarctic wetland species are very few. Also, as noted by Turner (1991), early reports of  $g$  may be erroneous due to calibration, temperature, and methodological errors. Therefore, it is not

Table 5.3a. Maximum stomatal conductance ( $\text{mmol m}^{-2} \text{s}^{-1}$ ) for each species.

Species	June 29	July 16	July 28	Average
<i>S. planifolia</i>	786	1020	1305	1037
<i>C. aquatilis</i>	488	1030	1088	869
<i>B. glandulosa</i>	652	901	981	845
<i>S. reticulata</i>	878	811	801	830
<i>M. gale</i>	977	804	687	823
<i>S. candida</i>	659	894	504	686

Table 5.3b. Maximum stomatal conductance ( $\text{mmol m}^{-2} \text{s}^{-1}$ ) for various species. + indicates that values were read from graphs and tables. \* indicates that values were originally expressed as velocity units and were converted to molar units for comparative purposes.

Species	$g_{max}$	Reference
<i>S. arctica</i> (Arctic)	125	Dawson and Bliss (1989) <sup>+</sup>
<i>S. arctica</i> (Alpine)	175	"
<i>S. bebbiana</i>	424	Lafleur (1987) <sup>*</sup>
<i>S. discolor</i>	436	"
<i>C. paleacea</i>	461	"
woody plants	42-208	Körner et al. (1979) <sup>+</sup> *
aquatic plants	291-416	"

exactly clear if large stomatal conductances measured at this study site are abnormally high.

#### D.4. Diurnal Patterns of Stomatal Conductance

The diurnal pattern of stomatal conductance has been documented for a large number of species. The pattern can be divided into two groups. The first group (Type I) has the stomata open most of the day, with a peak conductance before or near noon. The second group (Type II) has a peak conductance in the early morning, followed by a midday closure, and a second smaller peak conductance late in the afternoon.<sup>1</sup>

The Type I pattern has typically been found in plants growing in wet conditions with cool temperatures and a low  $\Delta W$ . For example, a Type I pattern was reported by Munro (1989) for two deciduous (*Alnus rugosa* and *Fraxinus nigra*) and one coniferous species (*Thuja occidentalis*) growing in a temperate wetland forest. A maximum early morning conductance steadily decreasing to a relatively constant value was also found in an apple orchard (*Malus pumila*) growing in the U.K. (Landsberg et al., 1975). In the subarctic, the Type I pattern has been found in *S. bebbiana*, *S. discolor*, *A. rugosa*, and *C. paleacea* growing in near-saturated soils (Lafleur, 1987). The Type I pattern has also been found in the High Arctic in *S. arctica* growing in constantly wet soils (Dawson and Bliss, 1989a).

---

<sup>1</sup> The Type I and Type II nomenclature have been created by the author and do not appear elsewhere in the literature.

The Type II pattern is characteristic of species adapted to external drought found in hot and dry regions. Roessler and Monson (1985) reported a pronounced midday depression of  $g$  in *Yucca glauca* growing in a Colorado short-grass prairie. This was primarily due to the large  $\Delta W$  and not due to water stress. Pereira et al. (1985) found a tendency to change from a Type I to a Type II pattern in *Eucalyptus globus* as the seasons changed from winter to spring and summer. This coincided with the changing climate regime of the Mediterranean region (Portugal) from mild and wet winters to hot and dry summers. Also in the Mediterranean region, the  $g$  of *Quercus ilex* changed from a Type I pattern between January and June to a Type II pattern during the summer drought period (Tenhunen et al., 1987). The change in patterns was not associated with an increase in internal water stress or soil moisture as plants grown in controlled environmental chambers under well-watered conditions still exhibited the Type II pattern. The seasonal dependent switch from a Type I to a Type II pattern has also been reported for *Jacquinia pugnans* and *Coccoloba liebmannii*, two deciduous shrubs growing in Mexico (Fanjul and Barradas, 1985).

Besides a seasonal change in the diurnal  $g$  pattern, species grown under the same environmental conditions may exhibit different patterns. Lange (1988) found that several well watered Mediterranean sclerophyllous shrub species grown in an environmental chamber simulating Mediterranean summer conditions displayed species-specific responses. Under identical conditions, some showed a pronounced Type II pattern while some showed a Type I pattern. Differences are thought to be a result of species-specific

sensitivities of stomata to atmospheric stress.

Two conclusions can be drawn from the above review. First, a Type II response appears to be due to external atmospheric controls in the form of high  $T_a$  and a large  $\Delta W$ . Second, the magnitude or even occurrence of the Type II response can vary between species found in the same area.

The diurnal patterns of  $g$  for each of the species found at this study site are shown in Figures 5.4a and 5.4b, with the daily averages given in Table 5.4. *S. planifolia* clearly displayed a Type II pattern on all measurement days. Maximum conductance was reached between 0500 and 0800 and quickly dropped to near 25% of  $g_{max}$  between 0800 and 1200. After the midday depression,  $g$  increased to approximately 50% of  $g_{max}$  value before gradually decreasing under the influence of failing irradiance. Overall, *S. planifolia* had the highest  $g$  of all species.

In contrast, *S. candida* displayed a diurnal pattern more similar to a Type I pattern. On June 29 and July 28,  $g_{max}$  was reached shortly after sunrise (0600) before steadily decreasing throughout the remainder the day. On July 16, however,  $g_{max}$  was reached at 1500, which corresponds to the time of the maximum  $\Delta W$ . On average, *S. candida* had the lowest conductance of all the species.

The shortest of the *Salix* species, *S. reticulata*, displayed a Type II pattern on all three days.  $g_{max}$  was reached between 0530 and 0730 followed by a midday depression to approximately 25% of  $g_{max}$  between 0930 and 1230. Conductance then reached a secondary peak of approximately 50% of  $g_{max}$  around 1400. Just prior to sunset, a

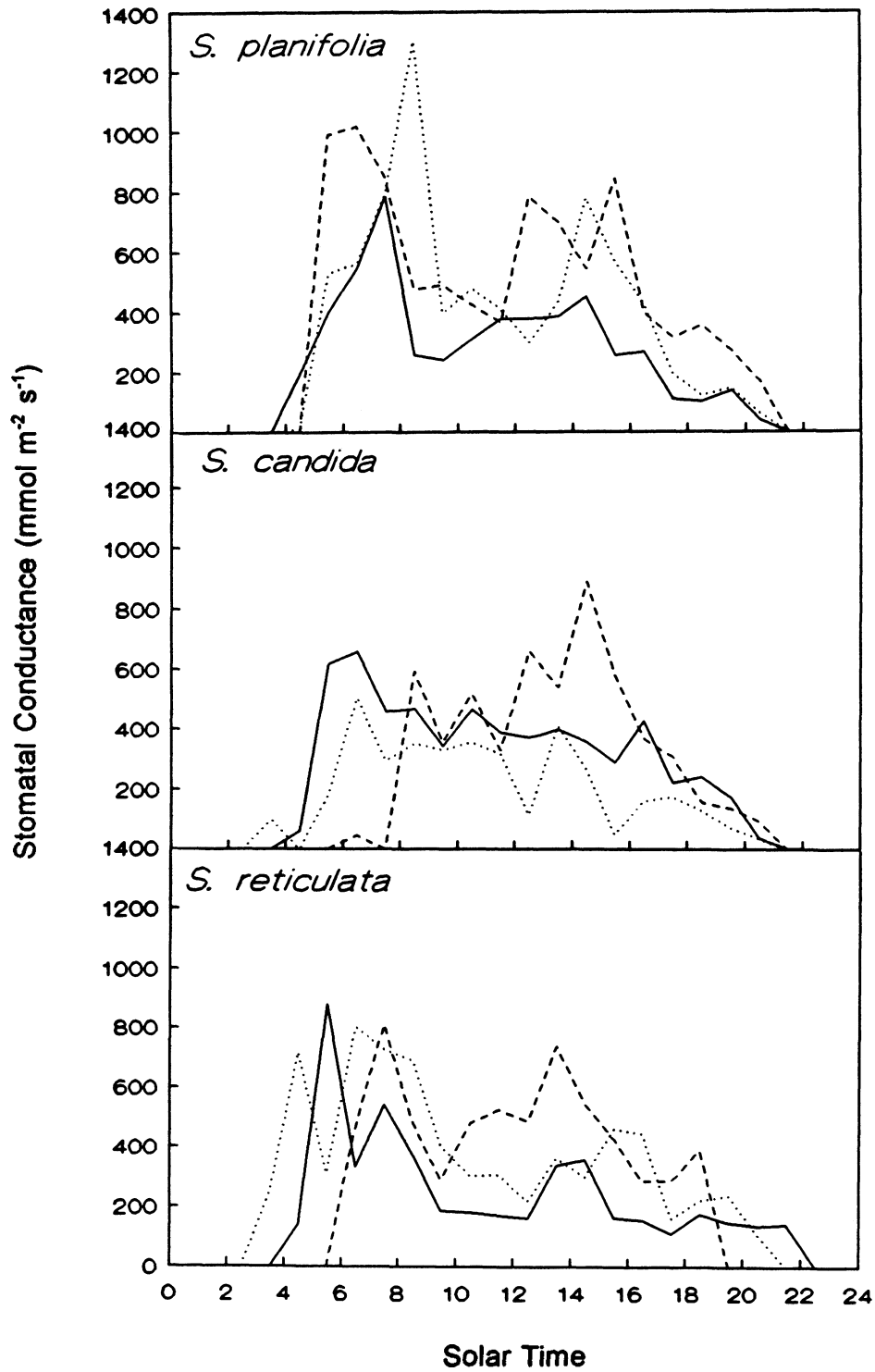


Figure 5.4a. Diurnal course of stomatal conductance. The solid line refers to June 29, the dashed line refers to July 16, and the dotted line refers to July 28.

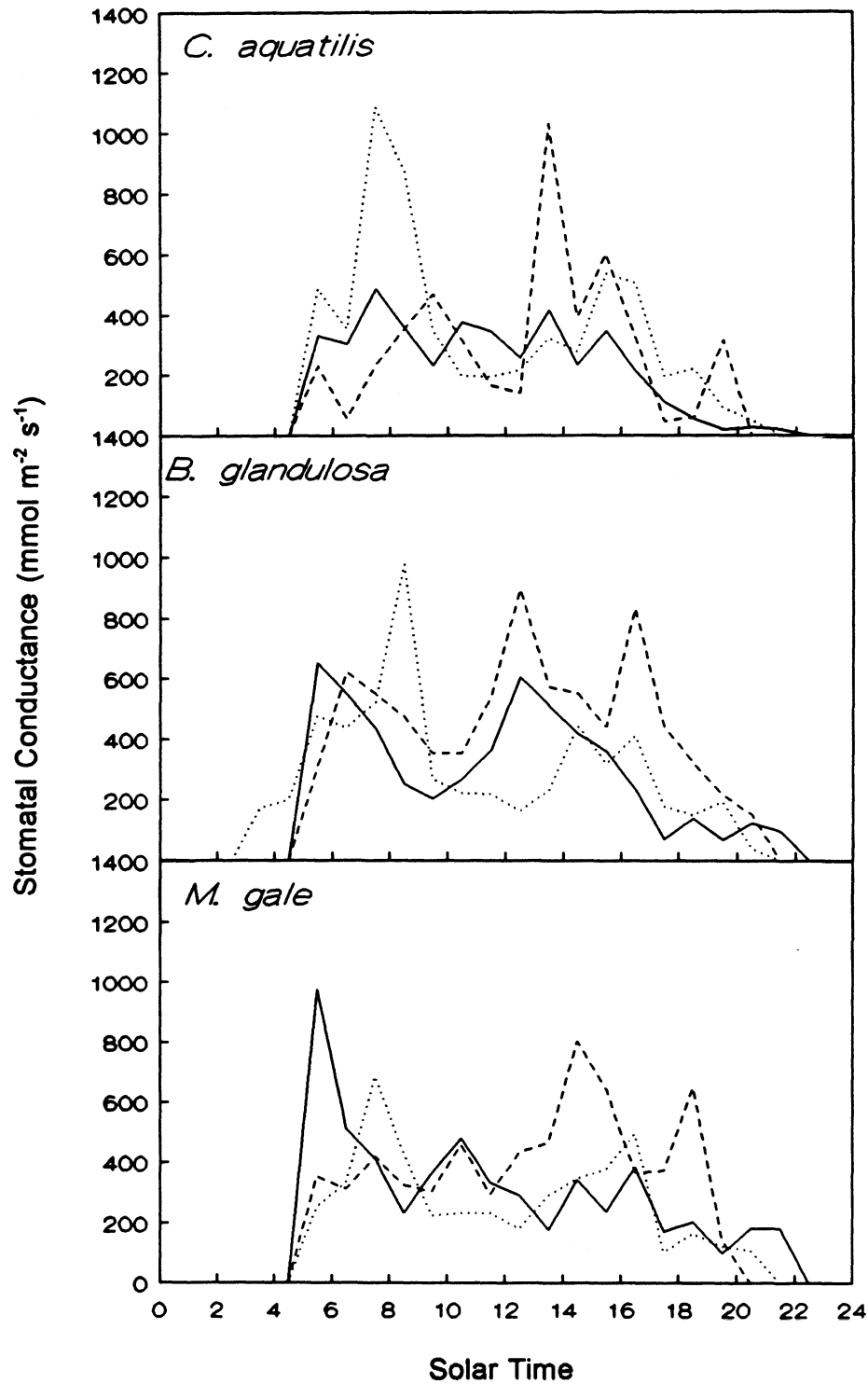


Figure 5.4b. Diurnal course of stomatal conductance. The solid line refers to June 29, the dashed line refers to July 16, and the dotted line refers to July 28.

Table 5.4. Average stomatal conductance ( $\text{mmol m}^{-2} \text{s}^{-1}$ ) for each species. Standard deviations are given in parenthesis.

Species	June 29	July 16	July 28	Average
<i>S. planifolia</i>	292 (186)	563 (257)	443 (309)	433
<i>S. reticulata</i>	260 (187)	478 (153)	391 (204)	376
<i>B. glandulosa</i>	315 (185)	479 (195)	315 (207)	370
<i>M. gale</i>	329 (198)	425 (161)	288 (151)	347
<i>C. aquatilis</i>	243 (144)	317 (244)	373 (269)	311
<i>S. candida</i>	332 (179)	372 (249)	213 (140)	306

tertiary peak can be discerned. Interestingly, the time between each peak in  $g$  is almost equal at 6 hrs, which may represent the length of time required for water to migrate from the soil into the roots and refill the xylem bundles.

*C. aquatilis* showed a Type I pattern on June 29, with a maximum conductance reached at 0730 before gradually decreasing for the remainder of the day. On July 16, the pattern was similar to that of *S. candida*, with a maximum conductance at 1500 coinciding to the maximum  $\Delta W$  reached during that day. A Type II pattern with a strong midday depression was displayed on July 28. Maximum conductance was reached at 0800, followed by a midday depression to approximately 20% of  $g_{max}$  value between 1000 and 1200. The secondary peak of approximately 50% of  $g_{max}$  was reached at 1600. The large  $\Delta W$  on July 28 appears to have elicited the Type II response.

On all three days, *B. glandulosa* displayed a Type II pattern.  $g_{max}$  was reached between 0500 and 0800 followed by a reduction to approximately 70% of  $g_{max}$  at 1000. On June 29 and July 16, the secondary peak was reached shortly after at 1300, while the secondary peak did not occur until 1500 on July 28. A tertiary peak at 1600 was displayed on July 16.

*M. gale* displayed a Type I pattern on June 29, while a strong Type II pattern was displayed on July 28. Again on July 16, a version of the Type I pattern was displayed, with a  $g_{max}$  at 1500 coinciding with the largest  $\Delta W$ .

In general, the species found at the site show three types of diurnal patterns. The first group are those which consistently show a Type II through a wide range of ambient

conditions. *S. planifolia*, *S. reticulata*, and *B. glandulosa* displayed this pattern, despite the cool temperatures and small  $\Delta W$  experienced on June 16. Presumably, these species are intolerable of even the slightest atmospheric moisture stress and are pushed into a Type II pattern even early in the growing season when soil moisture is plentiful.

The second group are those which change from a Type I to a Type II pattern as water stress becomes too great for the plant and midday stomatal closure is induced. *C. aquatilis* and *M. gale* change from a Type I on June 29 to a Type II pattern on July 28. Ambient conditions on June 29 were sufficient to maintain open stomata through most of the day, yet on July 28, midday stomatal closure was induced.

The third group comprises those plants which consistently show a Type I pattern. *S. candida* maintains a Type I pattern on all days, indicating that ambient conditions which could induce midday stomatal closure were not reached.

#### D.5. Diurnal Patterns of Xylem Pressure Potential

Measurements of xylem pressure potential have frequently been used in attempts to classify plant environments. Extensive measurements of  $\Psi$  over a wide range of habitats were made by Scholander et al., (1965). Values ranged from -0.5 to -8.0 MPa, and all species showed a large diurnal variation of from 1 to 2 MPa. Desert plants had the highest negative pressure, with a creosote bush and juniper displaying values of -8.0 and -6.0 MPa, respectively. Plants growing near salt water (halophytes) had the second highest negative pressures ranging from -6.0 to -3.5 MPa. Such a large negative pressure is

necessary to allow the diffusion of fresh water out of the salt water into the roots by reverse osmosis. Both understorey and overstorey forest plants had small values, ranging from -0.5 to -0.4 MPa. The smallest negative pressures were found in plants growing in or near fresh water. In freshwater habitats, values were never less than -2.0 MPa.

The plants in this study fit closest to Scholander's freshwater habitat (Table 5.5). Although it was hypothesized that higher (more negative)  $\Psi$  values may be displayed due to the proximity of the study site to the salt waters of Hudson Bay, values of  $\Psi$  similar to halophyte species were clearly not found. Although the soils are moderately saline, this was insufficient to evoke a large  $\Psi$ .

To help explain why plant species growing in the same environment under identical atmospheric conditions show different stomatal behaviour, measurements of  $\Psi$  are shown in Figures 5.5a and 5.5b.

As expected, the species showing a strong Type II pattern, also show the largest (most negative) values of  $\Psi$ . *S. planifolia*, *S. reticulata*, and to a lesser extent, *B. glandulosa* all indicated a relative large internal water stress even on July 16 when  $\Delta W$  was the smallest. If soil moisture did induce the midday stomatal closure, a coincidental plateau in  $\Psi$  would be expected (see, for example, Nobel, 1985). This phenomena has been observed in many species and seems to reflect moisture supply conditions and not species differences (Ritchie and Hinckley, 1975). Also, limiting soil moisture conditions should result in a failure of  $\Psi$  values at sunset to re-equilibrate with  $\Psi$  values at sunrise (Ritchie and Hinckley, 1975). Since the above behaviour did not occur for any of the

Table 5.5. Average xylem pressure potential (MPa) for each species. Standard deviations are given in parenthesis.

Species	June 29	July 16	July 28	Average
<i>S. reticulata</i>	-1.24 (0.47)	-0.98 (0.44)	-1.40 (0.63)	-1.21
<i>S. planifolia</i>	-0.88 (0.31)	-0.65 (0.24)	-1.38 (0.50)	-0.97
<i>B. glandulosa</i>	-0.83 (0.23)	-0.66 (0.20)	-0.97 (0.31)	-0.82
<i>S. candida</i>	-0.79 (0.21)	-0.63 (0.21)	-1.00 (0.42)	-0.81
<i>M. gale</i>	-0.73 (0.25)	-0.65(0.24)	-0.97(0.32)	-0.78
<i>C. aquatilis</i>	-	-	-	-

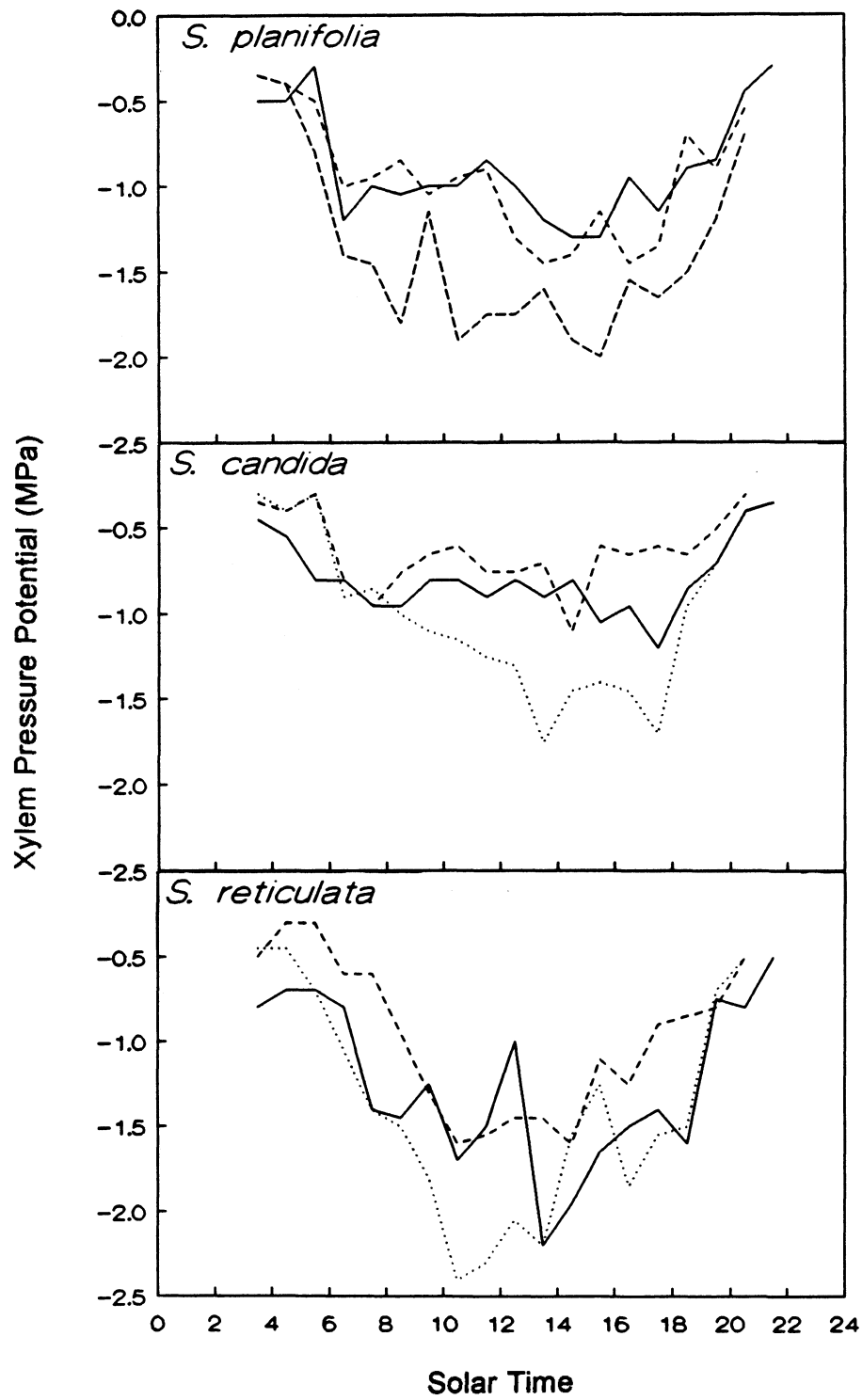


Figure 5.5a. Diurnal course of xylem pressure potential. The solid line refers to June 29, the dashed line refers to July 16, and the dotted line refers to July 28.

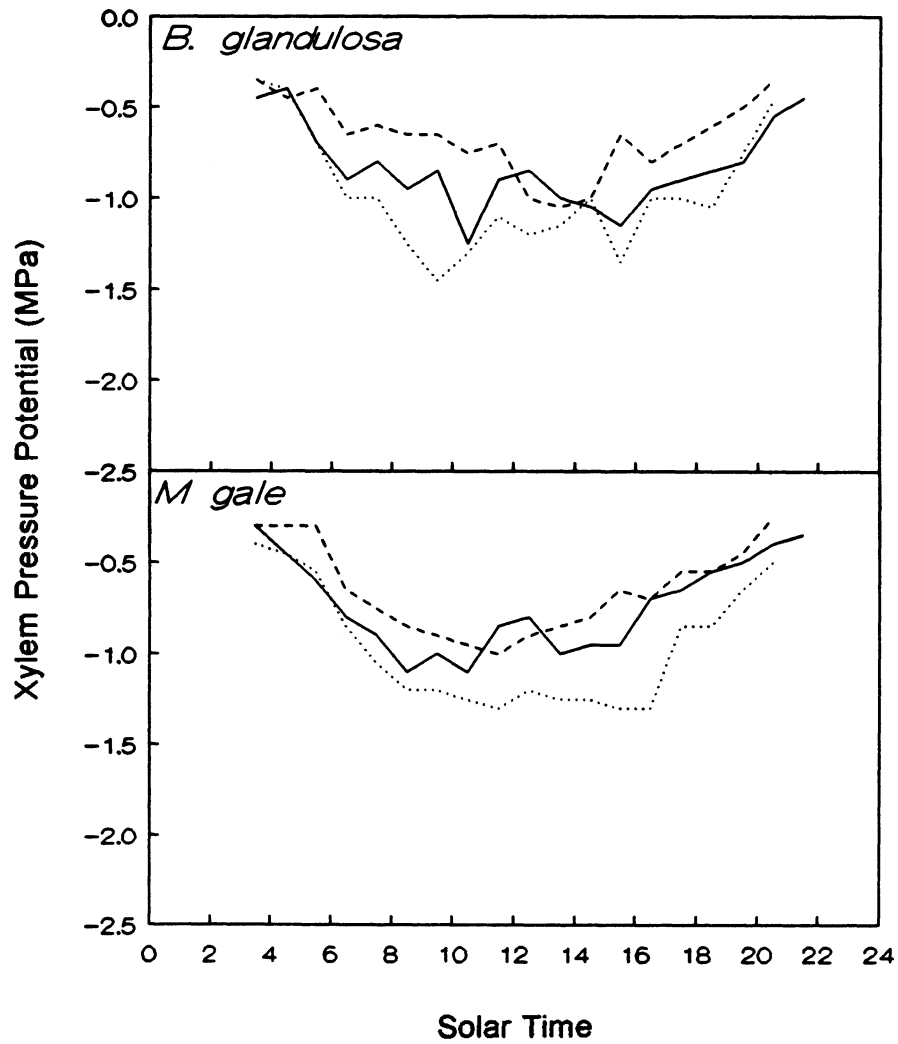


Figure 5.5b. Diurnal course of xylem pressure potential. The solid line refers to June 29, the dashed line refers to July 16, and the dotted line refers to July 28.

three species, it is felt that the Type II pattern was induced from the atmosphere and not by a soil moisture deficit.

Species which cross the stress threshold and change from a Type I to a Type II pattern (*C. aquatilis* and *M. gale*) should show a large increase in  $\Psi$  (more negative) when the Type II pattern is apparent. As explained previously, measurements on *C. aquatilis* were unavailable. *M. gale* does, however, show a larger internal water stress on July 28.

*S. candida*, which maintained a Type I pattern does not show the same bell shaped pattern as the other species, but rather displays a steadily increasing (more negative)  $\Psi$  as the day progresses. Apparently, the midday stomatal closure in the other species allows water to refill the internal plant vascular bundles. However, since a midday closure does not occur in *S. candida*, there is no "rest time" for the plant as is reflected in a progressively increasing internal water stress. Besides consistently having the lowest (least negative)  $\Psi$ , *S. candida* also showed the smallest standard deviation. The infilling of water during the resting period in the other species relieves water stress in a step function and causes  $\Psi$  to step back to smaller values. This results in a large standard deviation and a zig-zag temporal pattern. Since *S. candida* has no resting period,  $\Psi$  is not relieved and consistently increases throughout the day.

#### D.6. Root Resistance

Following Elfing et al. (1972), Landsberg et al. (1975) and Ritchie and Hinckley

(1975), the steady state flux of water through the plant is assumed to be directly proportional to the difference between the water potential in the soil and the leaves and inversely proportional to the sum of the resistances between the soil and the leaf. This relationship may be expressed as

$$Tr = \frac{\psi_{soil} - \psi}{r_{soil} + r_{plant}} \quad (5.2)$$

where  $T_r$  is taken represents the transpiration flux of water through the plant. Rearranging equation (5.2) gives

$$\psi = \psi_{soil} - Tr(r_{soil} + r_{plant}) \quad (5.3)$$

which is represented by the plot of  $\Psi$  against  $T_r$ , (Figure 5.6).

A linear relationship between  $\Psi$  and  $T_r$  was found on June 29. On July 16 and July 28, however, the relationship is better defined by a curvilinear logarithmic function. Both types of relationships have been reported in the past. Landsberg et al., (1975) found a linear relationship in apple trees when  $T_r$  did not exceeding  $2 \text{ mg m}^{-2} \text{ s}^{-1}$ , while Ritchie and Hinckley (1975) give a logarithmic relationship for orange trees with  $T_r$  in excess of  $2 \text{ mg m}^{-2} \text{ s}^{-1}$ .

If  $\Psi_{soil}$  is assumed to be relatively constant through the course of a day, then the only unknown variable in equation 5.3 is the resistance within the plant. This assumption is reasonable since ample soil moisture must have been available to supply the high transpiration flux. A linear relationship between  $\Psi$  and  $T_r$  indicates that the resistance

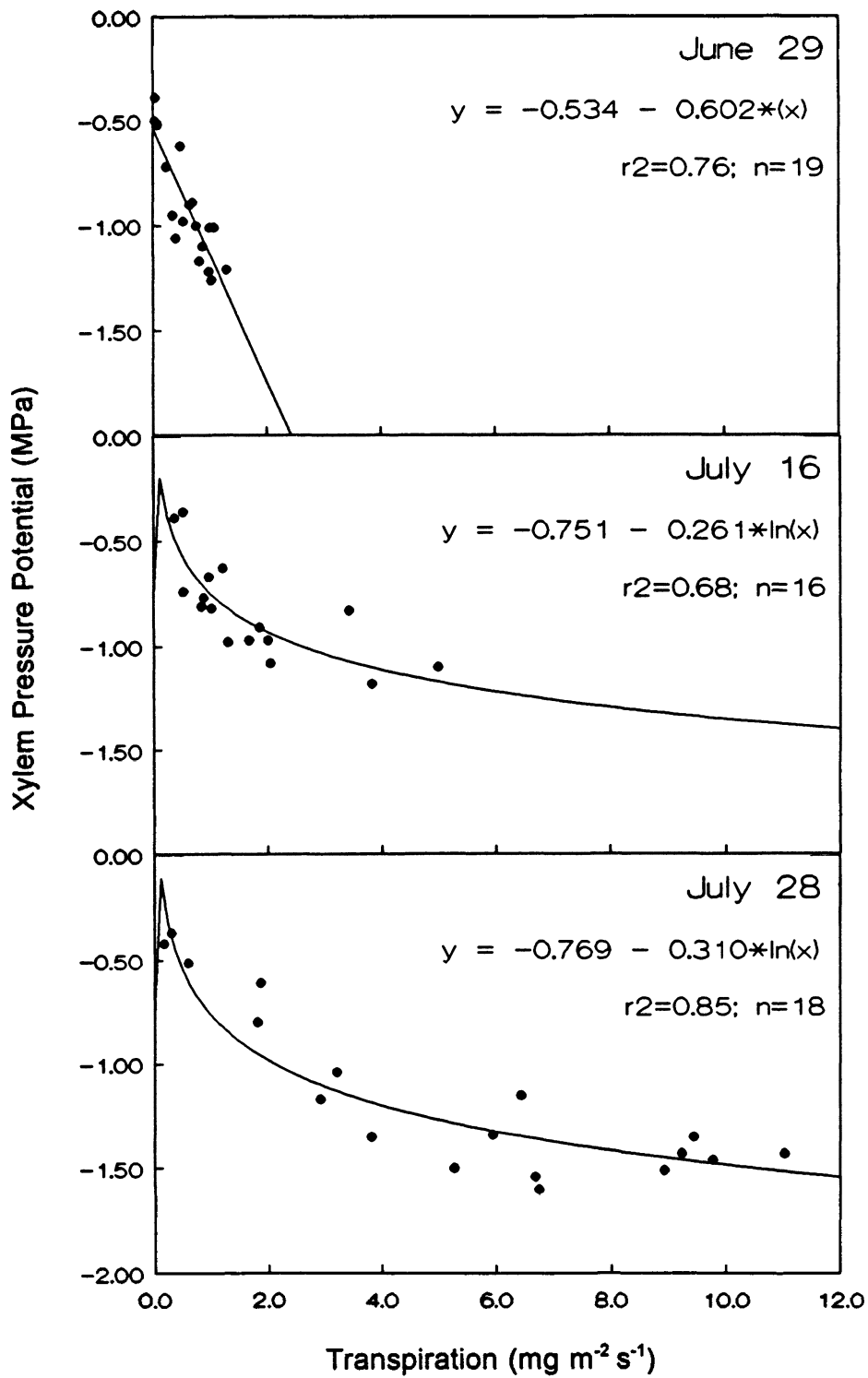


Figure 5.6. Relationship between canopy xylem pressure potential and canopy transpiration.

remains constant at  $0.60 \text{ MPa mg}^{-1} \text{ m}^2 \text{ s}$  when  $T_r < 2 \text{ mg m}^{-2} \text{ s}^{-1}$ . A curvilinear relationship indicates that the plant resistance is not constant and is a function of  $T_r$ . This occurs when  $T_r$  exceeds  $2 \text{ mg m}^{-2} \text{ s}^{-1}$ . The derivatives of the logarithmic equations shown in Figure 5.3 indicate that the plant resistance decreases to  $0.03 \text{ MPa mg}^{-1} \text{ m}^2 \text{ s}$  as  $T_r$  approaches  $12 \text{ mg m}^{-2} \text{ s}^{-1}$ .

The plant resistance as it appears in equation 5.3 is a composite of all individual resistances experienced within the plant. The resistance imparted by the roots, however, is the largest (Elfving et al., 1972; Jones, 1983). The curvilinearity, therefore, is likely explained by a decrease in the root resistance as  $T_r$  increases. This counter-intuitive relationship has been reported for many species (Elfving et al., 1972) and may be strategic adaptation of the willows to prevent severe water stress at a high transpirational flux (Jones, 1983).

## D.7. Environmental Controls on Stomatal Conductance

### *D.7.1. Introduction*

So far, the discussion on the internal plant water stress and the subsurface environment has given insight into the overall canopy behaviour, but has not considered the individual species differences in stomatal behaviour. The question as to why plants growing in the same environment under identical ambient conditions show different patterns of  $g$  needs to be addressed.

Investigations into the response of stomata to external environmental controls can

be separated into two groups. The first group relies on the use of laboratory environmental (growth) chambers. Usually, measurements of the environmental conditions are made in the field in order to obtain representative values of irradiance, air temperature, humidity, etc., which are then used to simulate the plants' natural environment in the environmental chamber. Then, in order to determine the stomatal response and sensitivity to environmental controls individually, each control is allowed to vary through its range of values observed under natural conditions, while all other controls are held constant. This method offers the advantage of allowing carefully controlled experiments to be performed, yet has the disadvantage of removing the plants from their natural environment, especially with respect to the subsurface conditions (for example, permafrost cannot easily be simulated and rooting networks are restricted).

The second group of investigation relies on measurements obtained in the field. Measurements of environmental controls are taken concurrently with  $g$  measurements. In order to isolate the effects of individual environmental controls,  $g$  is plotted against each control. Unfortunately, a large degree of scatter occurs because all the controls are influencing  $g$  in varying degrees at various times. In an attempt to analyze the influence of one control at a time, a boundary or upper-limit curve is plotted for each control. As first suggested by Jarvis (1976), the curve represents the ideal response of the stomata to each environmental control when all others are non-limiting. This boundary line analysis method has the disadvantage of not allowing controlled experiments to be performed, yet has the advantage of measuring stomatal response under natural conditions with

undisturbed plants.

The latter method is used in this study since time and equipment prevented the use of growth chambers. It would take years to produce ample quantities of genetically identical individual plants from each species. Also, a recreation of the Subarctic soil environment (for example, deep permafrost) would be impractical. All individual  $g$  measurements for each of the species have been pooled together and plotted as a scatter plot against each environmental control. The environmental controls considered in this study are  $K\downarrow$ ,  $\Delta W$ ,  $T_a$ , and  $\Psi$ .

#### D.7.2. Irradiance

The boundary curve describing the relationship between  $g$  and  $K\downarrow$  for each species was fitted by a hyperbolic function of the form

$$f(K\downarrow) = \frac{g_{max}K\downarrow}{(K_1 + K\downarrow)} \quad (5.4)$$

where  $g_{max}$  describes the asymptote of the curve and  $K_1$  is a parameter describing the slope of the curve. Parameters for all of the species are listed in Table 5.6. Figures 5.7a and 5.7b show that all species, with the exception of *S. reticulata* and *M. gale*, reached a saturation  $K\downarrow$  at approximately  $200 \text{ W m}^{-2}$ . Above this level of  $K\downarrow$ , additional light did not increase stomatal aperture. This saturation level corresponds roughly to 25% of the maximum summer  $K\downarrow$ , which is a common saturation level with most plant species (Jones, 1983).  $K\downarrow$  levels above  $200 \text{ W m}^{-2}$  were maintained between the hours of

Table 5.6. Parameters used to model stomatal conductance using boundary line analysis.  $K_1$  describes the slope of the irradiance curves (Figure 5.7a and 5.7b).  $K_2$  and  $K_3$  describe the y-intercept and slope, respectively, of the  $\Delta W$  curves (Figures 5.8a and 5.8b).  $K_4$ ,  $K_5$ , and  $K_6$  describe the parameters used to fit the  $T_a$  curves (Figure 5.11a and 5.11b).  $K_7$  and  $K_8$  describe the y-intercept and slope, respectively, of the  $\Psi$  curves (Figure 5.12a and 5.12b). Species are abbreviated as follows: SP = *S. planifolia*; CA = *C. aquatilis*; SC = *S. candida*; SR = *S. reticulata*; BG = *B. glandulosa* and; MG = *M. gale*.

K	SP	SC	SR	CA	BG	MG
$K_1$	75	75	15	75	75	15
$K_2$	1000.88	770.70	969.56	1312.42	1017.07	1083.60
$K_3$	-149.35	-157.80	-171.80	-237.62	-181.36	-198.47
$K_4$	-2077.85	-1637.97	-1121.76	-2399.18	-1736.63	-1357.87
$K_5$	337.48	257.37	188.52	335.20	284.73	212.73
$K_6$	-8.22	-6.47	-4.61	-8.05	-7.20	-5.13
$K_7$	1285.24	1088.84	1187.55	-	1380.16	1164.81
$K_8$	265.74	537.76	367.82	-	765.30	408.63

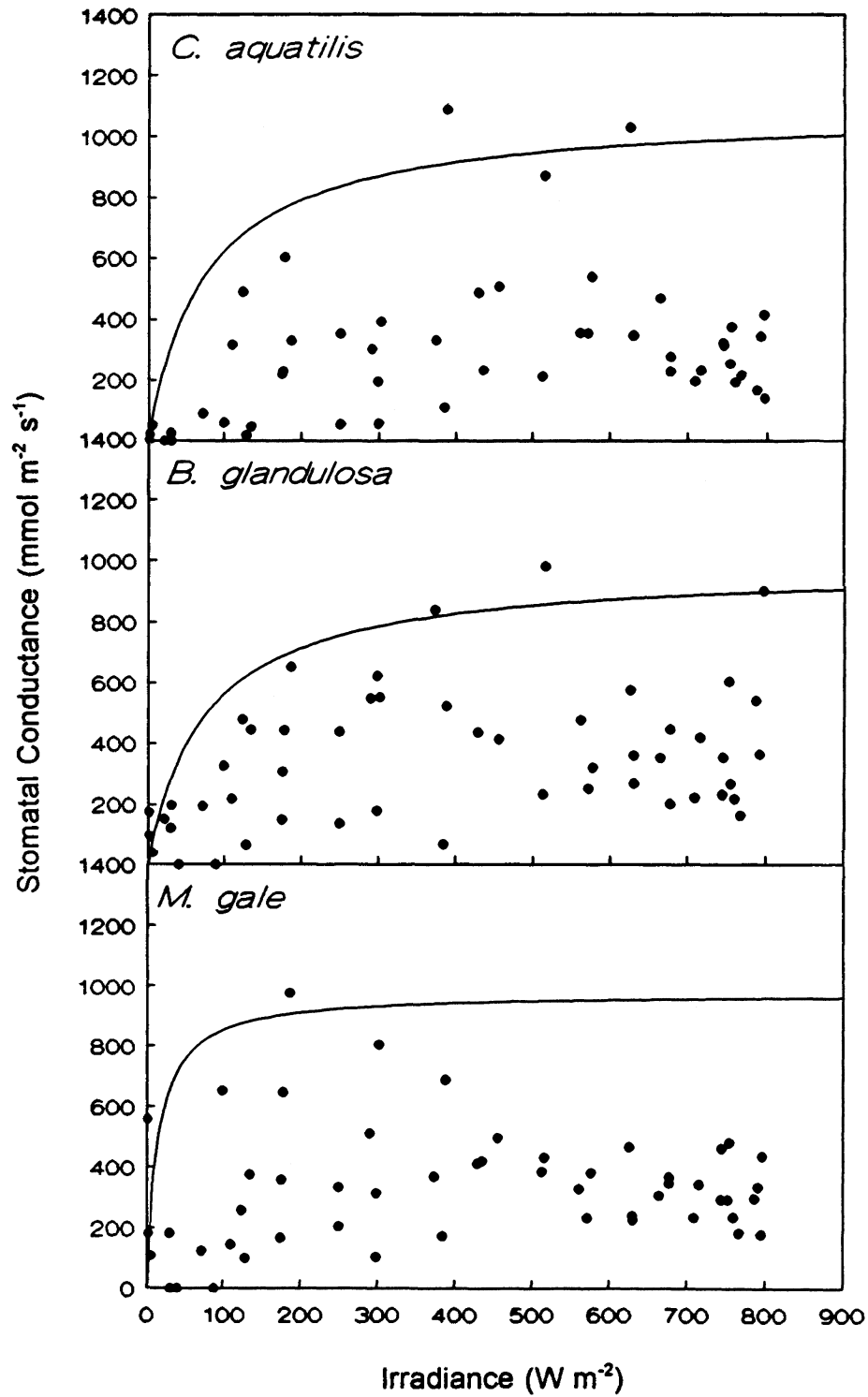


Figure 5.7a. Scatter diagram of stomatal conductance and irradiance. Solid lines indicate the probable upper limit of the observations.

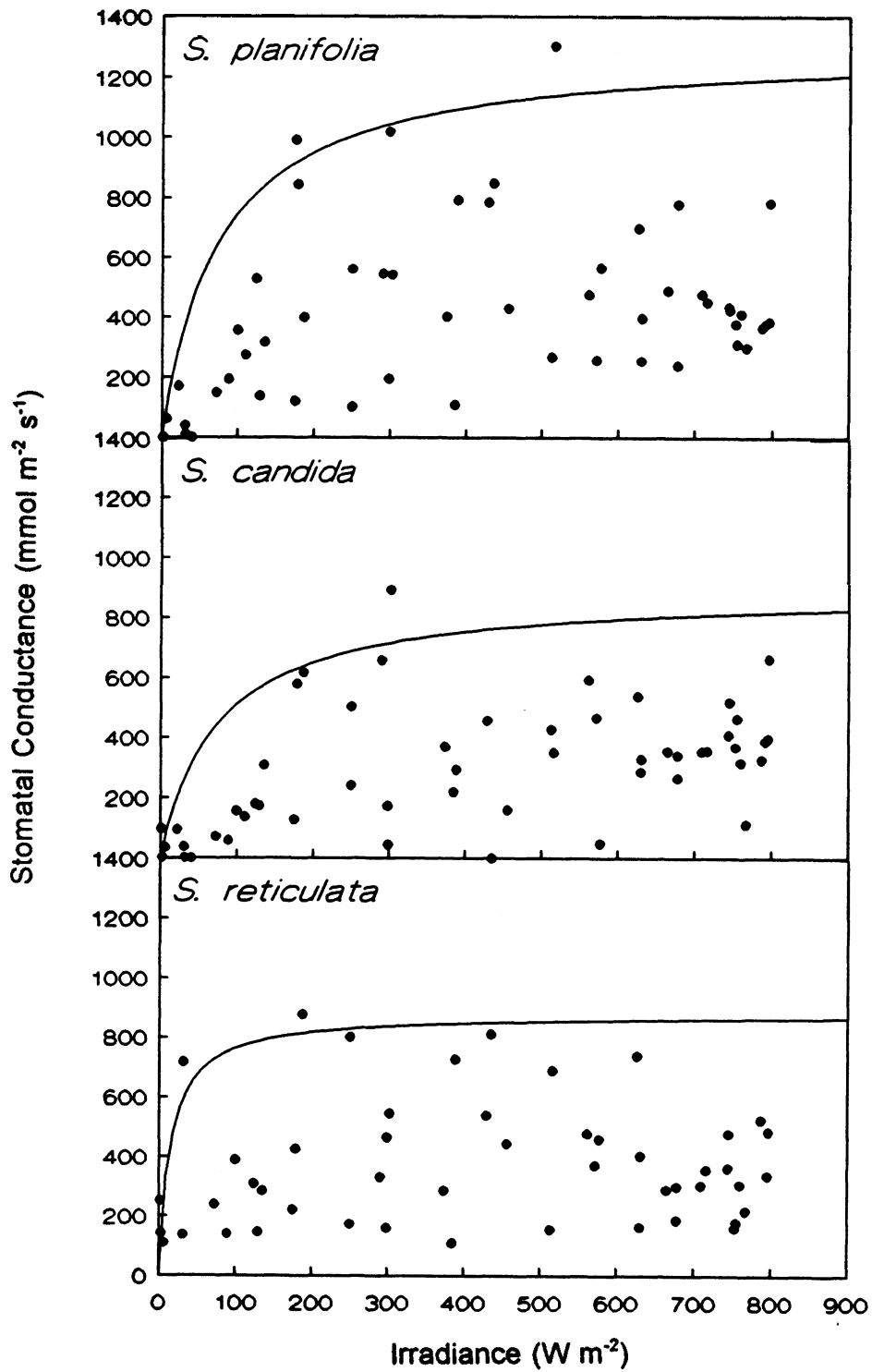


Figure 5.7b. Scatter diagram of stomatal conductance and irradiance. Solid lines indicate the probable upper limit of the observations.

approximately 0600 and 1800 on each measurement day (with the exception of late afternoon cloudy periods on July 28).

*S. reticulata* and *M. gale*, however, reach a saturation  $K\downarrow$  level at approximately  $100 \text{ W m}^{-2}$ . This lower saturation level is expected in these species since they are short (especially *S. reticulata*) and are grown beneath the taller species. Hence, they have adapted the lower radiation levels found beneath the upper canopy and are less strongly coupled to the radiation environment. They could be classified as shade-tolerant species. These results are similar to those found in other studies, which show lower saturation levels in shade-tolerant species (for example, see Jones, 1983; Massman and Kaufmann, 1991). Although *C. aquatilis* is also a short species, it is not found beneath the taller *Salix* species, but rather in open areas around small ponds. It therefore does not experience low radiation levels.

In summary, irradiance alone does not explain differences in stomatal behaviour between the species. The shade-tolerant species have evolved mechanisms to deal with the lower radiation levels, and the midday stomatal closure phenomena occurs when the  $K\downarrow$  saturation level has been surpassed.  $K\downarrow$  does, however, account for the rapid early morning increase and the late afternoon decrease in  $g$  in all species, since these are periods when  $\Delta W$  is low and  $K\downarrow$  levels fall below saturation levels.

#### D.7.3. Leaf-to-air Vapour Pressure Deficit

The role of  $\Delta W$  has received considerable attention, since it has been found that

it is one the most important environmental controls of  $g$ . Early experiments into the midday stomatal closure of *Prunus armeniaca* found that decreasing  $\Delta W$  was the main factor responsible for stomatal closure, while increasing  $T_a$  induced stomatal opening (Schulze et al., 1974). Lange et al., (1982) confirmed this finding with *Quercus ilex* and *Arbutus unedo*. Although the effects of  $T_a$  and  $\Delta W$  could not be separated, it was assumed that  $\Delta W$  played the dominant role in midday stomatal closure. However, a reopening of stomata after the midday depression during a period of high atmospheric stress could not be explained, and was suggested to be due to plant hormones. Aphalo and Jarvis (1991) found a linear stomatal response of *Hedera helix* to  $\Delta W$ , with  $g$  decreasing as  $\Delta W$  increased. Also, Bunce (1985) found  $g$  decreasing linearly with  $\Delta W$  for *Glycine max*, *Abutilon theophrasti*, and *Datura stramonium*. In *Yucca glauca*, Roessler and Monson (1985) reported that a decrease in photosynthesis was primarily due to a high leaf temperature, while a decrease in  $g$  was primarily due to a decrease in  $\Delta W$ .

In general, there have been a large number of studies finding that stomata close as  $\Delta W$  increases. According to L6sch and Tenhunen (1981), at least 70 vascular plants, including ferns, gymnosperms, dicotyledons, and monocotyledons have shown this stomatal response to  $\Delta W$ . Stomatal closure at a high  $\Delta W$  is thought to be an adaptation of plants to conserve water loss while maintain ample carbon gain. While it is assumed that this is accomplished by a uniform stomatal closure over the entire leaf surface, Beyschlag et al., (1992) found that *Arbutus unedo* and *Quercus suber* had patches of fully opened and fully close stomata during the midday depression period. The advantages of

this strategy are not known.

There are, however, some studies that find no stomatal response to  $\Delta W$ . For example, Rawson et al., (1977) found that in several dicotyledon and monocotyledons,  $T_s$  increased linearly with decreasing  $\Delta W$ , yet  $g$  in single leaves of any of the species showed no response. When an entire barley plant was exposed to a decreasing  $\Delta W$ , a reduction in  $g$  did occur. The authors suggest that this discrepancy in results is due to the ratio between leaf area and root volume. Similarly, other studies have found no stomatal response to  $\Delta W$  when only a small part of the plant (e.g. one leaf) is exposed to the measurement conditions. This finding may be especially relevant to Arctic and Subarctic plants where a small  $LAI$  and a small above-to-below ground plant volumes are common (Wielgolaski et al., 1981). In such plants, only a relatively small part of the plant is exposed to the atmospheric demand for water vapour, hence the stomata may show insensitivity to humidity.

Previously, it has been hypothesized that species related differences in stomatal behaviour may be due to differences in species sensitivity to  $\Delta W$ . As pointed out above, many vascular species show a strong response to humidity (expressed as  $\Delta W$  or  $D$ ), while some species show little or no response at all. The sensitivity of the plants found at the study site and the hypothesis about species specific  $\Delta W$  responses will be tested below through the use of a boundary line analysis.

Boundary lines describing the relationship between  $g$  and humidity have taken many forms. Some authors use  $D$  at some reference level in the atmosphere to describe

humidity, while others use  $\Delta W$  as the humidity gradient between the transpiring leaf surface and a reference level in the atmosphere. The latter is more common and is used in this study. The boundary line which was judged to fit the relationship between  $g$  and  $\Delta W$  took the form

$$f(\Delta W) = K_2 + K_3(\Delta W) \quad (5.5)$$

The plots of the  $\Delta W$  boundary line (Figures 5.8a and 5.8b) show that increasing  $\Delta W$  had the effect of lowering  $g$  with all species. Maximum conductances were always reached when  $\Delta W$  was the smallest, yet all species were capable of maintaining some level of  $g$  even during the exceptionally high  $\Delta W$  encountered on July 28. Three possible explanations for this are as follows. The first relates to the ratio of above-to-below ground plant volume. The small  $LAI$  together with the large portion of plant mass and moisture storage below the surface (Chapter 2, Sections C.8 and C.9) means that a large portion of the plant is not exposed to the large  $\Delta W$ . The second relates to the midday stomatal closure phenomena. During midday stomatal closure, water is allowed to refill the plant. The stomata then reopen when the internal stress is relieved, coincidentally when the  $\Delta W$  is large, and then again close when the stress becomes too great. Hence a brief period of high  $g$  occurs despite the large  $\Delta W$ . The third relates to atmospheric turbulence. As proposed by Idso et al. (1989) and Idso (1990), a short canopy will not respond to ambient humidity due to aerodynamic uncoupling between the short, closed canopy and the atmosphere above.

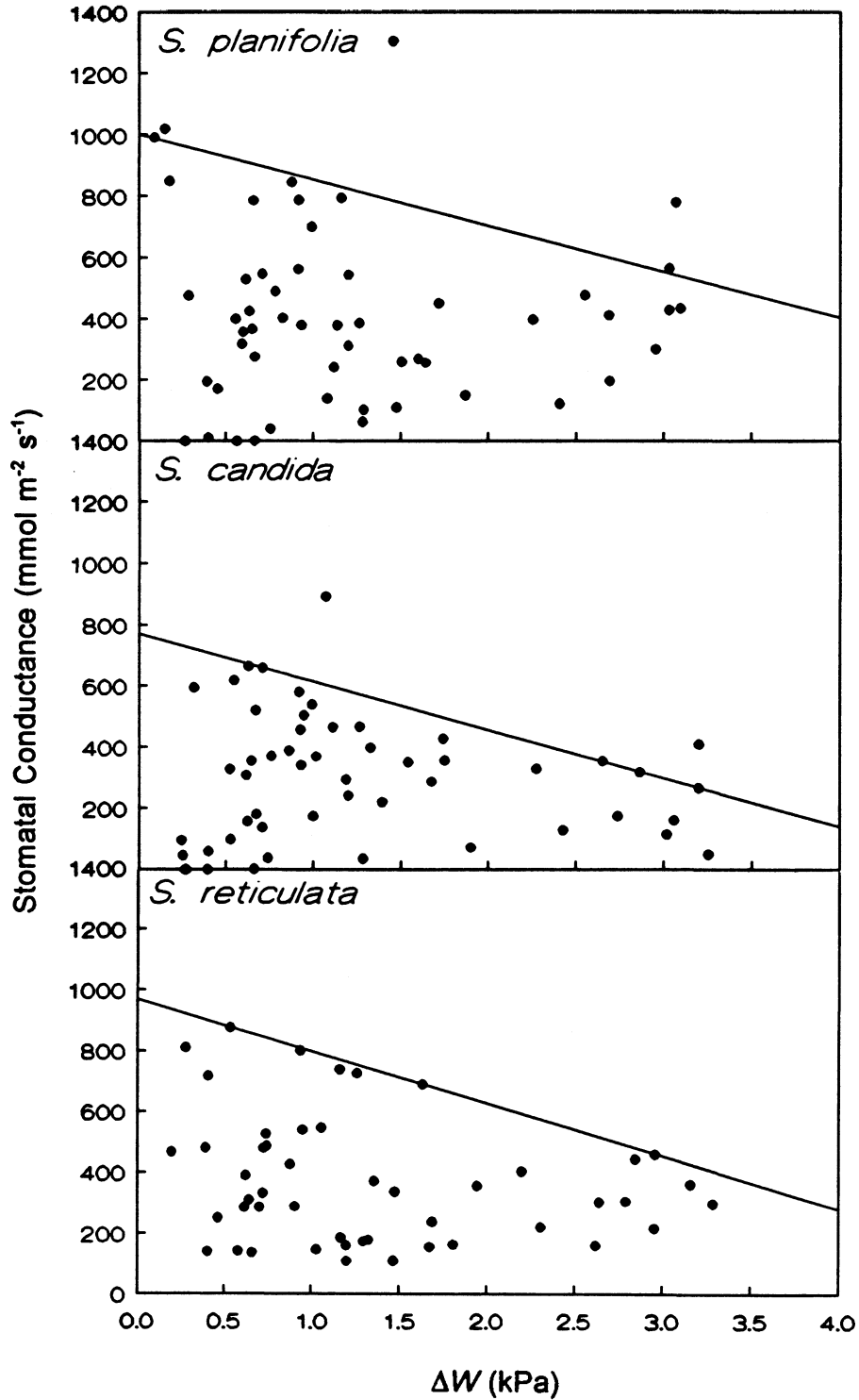


Figure 5.8a. Scatter diagram of stomatal conductance and the leaf-to-air vapour pressure deficit. Solid lines indicate the probable upper limit of the observations.

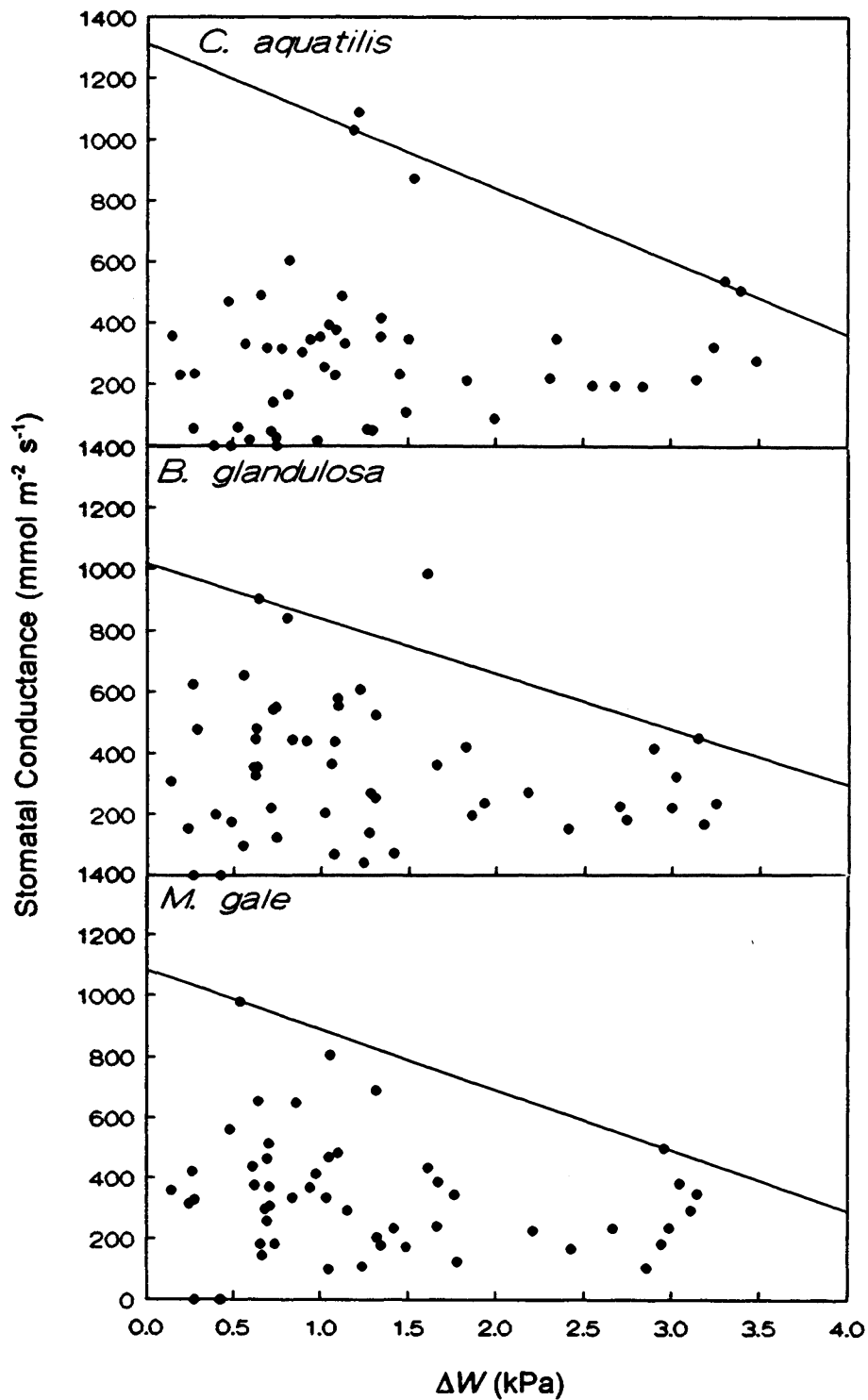


Figure 5.8b. Scatter diagram of stomatal conductance and the leaf-to-air vapour pressure deficit. Solid lines indicate the probable upper limit of the observations.

#### D.7.4. Threshold Values of the Leaf-to-air Vapour Pressure Deficit

If  $T_a$  and the associated  $\Delta W$  are responsible for a change in stomatal behaviour patterns, then there likely exists a threshold  $\Delta W$  which, when reached, would promote stomatal closure and result in a Type II pattern. Figure 5.9 illustrates the concept of a threshold  $\Delta W$  by plotting the theoretical relationship between  $g$  and  $\Delta W$ . The basic premise of the model is that below the threshold  $\Delta W$ ,  $g$  is a function of  $\Delta W$  since  $g$  decreases as  $\Delta W$  increases. Above the threshold  $\Delta W$ ,  $g$  is not a function of  $\Delta W$  since  $g$  remains at a constant low level due to stomatal closure.

The Type II species are intolerant of a large  $\Delta W$ , therefore the threshold  $\Delta W$  is small and the plants should be insensitive to  $\Delta W$ . The sensitivity of  $g$  to  $\Delta W$ , as represented by the slopes of the curves shown in Figure 5.8a and 5.8b, show that the Type II species (*S. planifolia*, *S. reticulata*, and *B. glandulosa*) are insensitive to  $\Delta W$  (Table 5.7). *S. planifolia*, which consistently displayed a strong Type II pattern, is, as the model predicts, the least sensitive to  $\Delta W$ .

The Type I species have a far greater tolerance to  $\Delta W$ , and therefore have a high threshold  $\Delta W$ . Since the range of  $\Delta W$  in which a Type I pattern can be maintained is very large,  $g$  does decrease as  $\Delta W$  increases, but the rate of change is very small. *S. candida*, which consistently displayed a Type I pattern, does show little sensitivity to  $\Delta W$ , as is predicted by the model.

When the threshold  $\Delta W$  is crossed, the model predicts a shift from a Type II to a Type I pattern. These species should show a high sensitivity to  $\Delta W$  if the observed  $\Delta W$

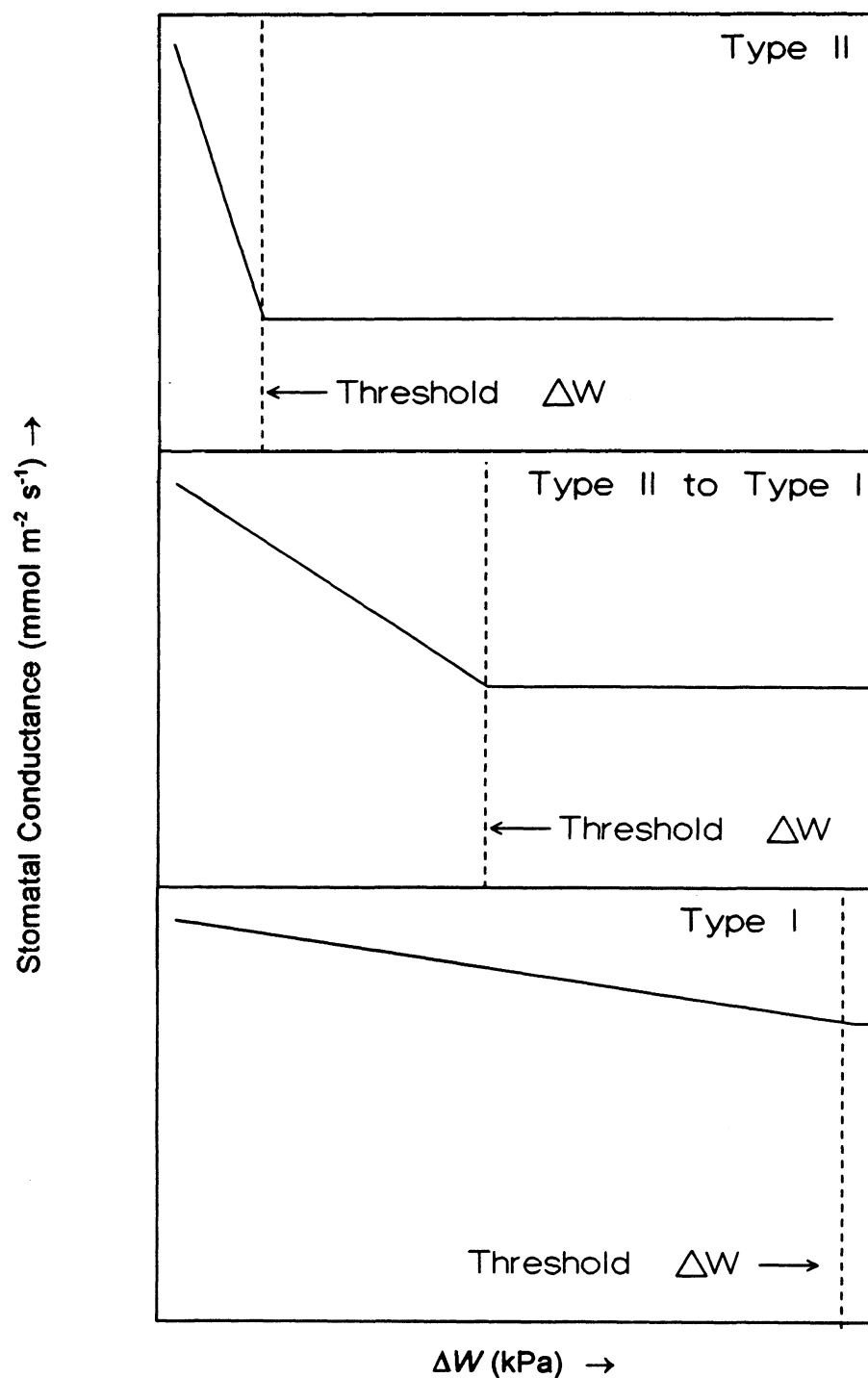


Figure 5.9. Theoretical relationship between stomatal conductance and the leaf-to-air vapour pressure deficit. Dashed line represents the threshold value of the leaf-to-air vapour pressure deficit that when reached would induce stomatal closure.

Table 5.7. Sensitivity of  $g$  to  $\Delta W$  for different stomatal behaviour patterns, as represented by the slope of the curves describing the relationships between  $g$  and  $\Delta W$  shown in Figures 5.8a and 5.8b.

Species	Type	Slope ( $\text{mmol m}^{-2} \text{s}^{-1} \text{kPa}^{-1}$ )
<i>S. planifolia</i>	II	-149
<i>S. reticulata</i>	II	-172
<i>B. glandulosa</i>	II	-181
<i>S. candida</i>	I	-158
<i>C. aquatilis</i>	I $\rightarrow$ II	-238
<i>M. gale</i>	I $\rightarrow$ II	-198

often lies near the threshold  $\Delta W$ . This occurs because a great deal of time would be spent around the threshold  $\Delta W$ , where the sensitivity of  $g$  to  $\Delta W$  is high. The species which showed a change between patterns (*C. aquatilis* and *M. gale*) did, as predicted by the model, show a high sensitivity to  $\Delta W$ .

The effect of a threshold  $\Delta W$  on the diurnal sensitivity of  $g$  to  $\Delta W$  is shown by Figure 5.10. On a cool day when  $\Delta W$  is small (typical with onshore winds), the threshold  $\Delta W$  for the Type II species may be reached shortly after sunrise and again shortly before sunset. Thus, during most of the daylight hours,  $g$  is insensitive to changes in  $\Delta W$ . For the remaining species, the threshold  $\Delta W$  is never reached, hence  $g$  remains insensitive to  $\Delta W$  throughout the day. On a hot day when  $\Delta W$  is large (typical with offshore winds), the threshold  $\Delta W$  for the Type II species is reached earlier in the morning and again later in the day than on a cool day. Hence, the period when  $g$  is insensitive to  $\Delta W$  occurs for a longer duration. Species whose threshold  $\Delta W$  occurs on the hot, dry day but not on the cool, damp day (*C. aquatilis* and *M. gale*) show an increasing sensitivity to  $\Delta W$  as the threshold  $\Delta W$  is reached twice during the day closer to noon. Species with a very large threshold  $\Delta W$  (*S. candida*) remain insensitive to  $\Delta W$  on the hot, dry day, since the threshold  $\Delta W$  is not reached.

In general, the sensitivity depends not only on the magnitude of the threshold  $\Delta W$ , but also on the period of time that experiences a  $\Delta W$  near the threshold  $\Delta W$ . A threshold  $\Delta W$  occurring near sunrise and sunset typical for the Type I species does not last long, since rapid changes in both temperature and  $\Delta W$  occur during these times. In contrast, a

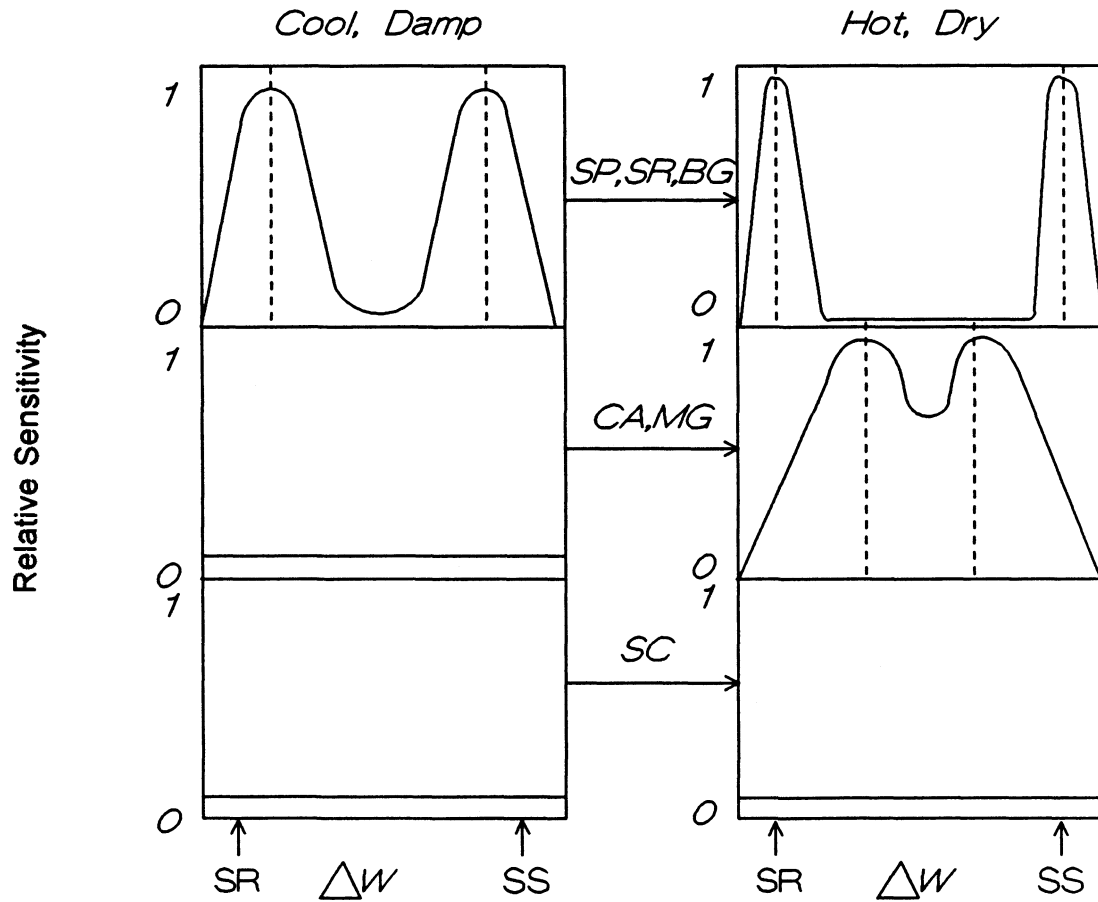


Figure 5.10. Theoretical diurnal course for the relative sensitivity of stomatal conductance to the leaf-to-air vapour pressure deficit during a cool, damp day and a hot, dry day. A value of 1 indicates a high sensitivity, and a value of 0 indicates a low sensitivity. The dashed line indicates the threshold leaf-to-air vapour pressure deficit that induces Type II behaviour. Symbols are defined as: *SP*-*S. planifolia*; *SR*-*S. reticulata*; *BG*-*B. glandulosa*; *CA*-*C. aquatilis*; *MG*-*M. gale*; *SC*-*S. candida*; SR-sunrise and; SS-sunset.

threshold  $\Delta W$  occurring closer to noon last for a longer duration since changes in temperature and  $\Delta W$  are not as rapid during these times.

Although this conceptual model explains the differences in stomatal behaviour amongst the species, it is unclear why there is a species-specific level of a threshold  $\Delta W$  when the plants are growing under identical conditions. Differences appear to be unrelated to preferred geographic location, above and below ground mass, and rooting network since two sharply contrasting species under all these categories (*S. planifolia* and *S. reticulata*) both consistently display a Type II pattern. Further investigation in this area is clearly required.

#### D.7.5. Air Temperature

The typical response of most plant species to  $T_a$  is for a maximum  $g$  to be reached at one temperature, with conductance decreasing both above and below this temperature. As noted by Turner (1991), the optimum  $T_a$  at which  $g$  peaks varies with the species, as temperate species have a lower optimum  $T_a$  than tropical species. The relationship is often described by a quadratic equation of the form

$$g(T_a) = K_4 + K_5(T_a) + K_6(T_a)^2 \quad (5.6)$$

Equation 5.6 was used to define the boundary line response of each species to  $T_a$  (Figures 5.11a and 5.11b). Taking the derivative of equation 5.6 and setting it equal to zero gives the optimal  $T_a$  for each species (Table 5.8). The optimal  $T_a$  for all species

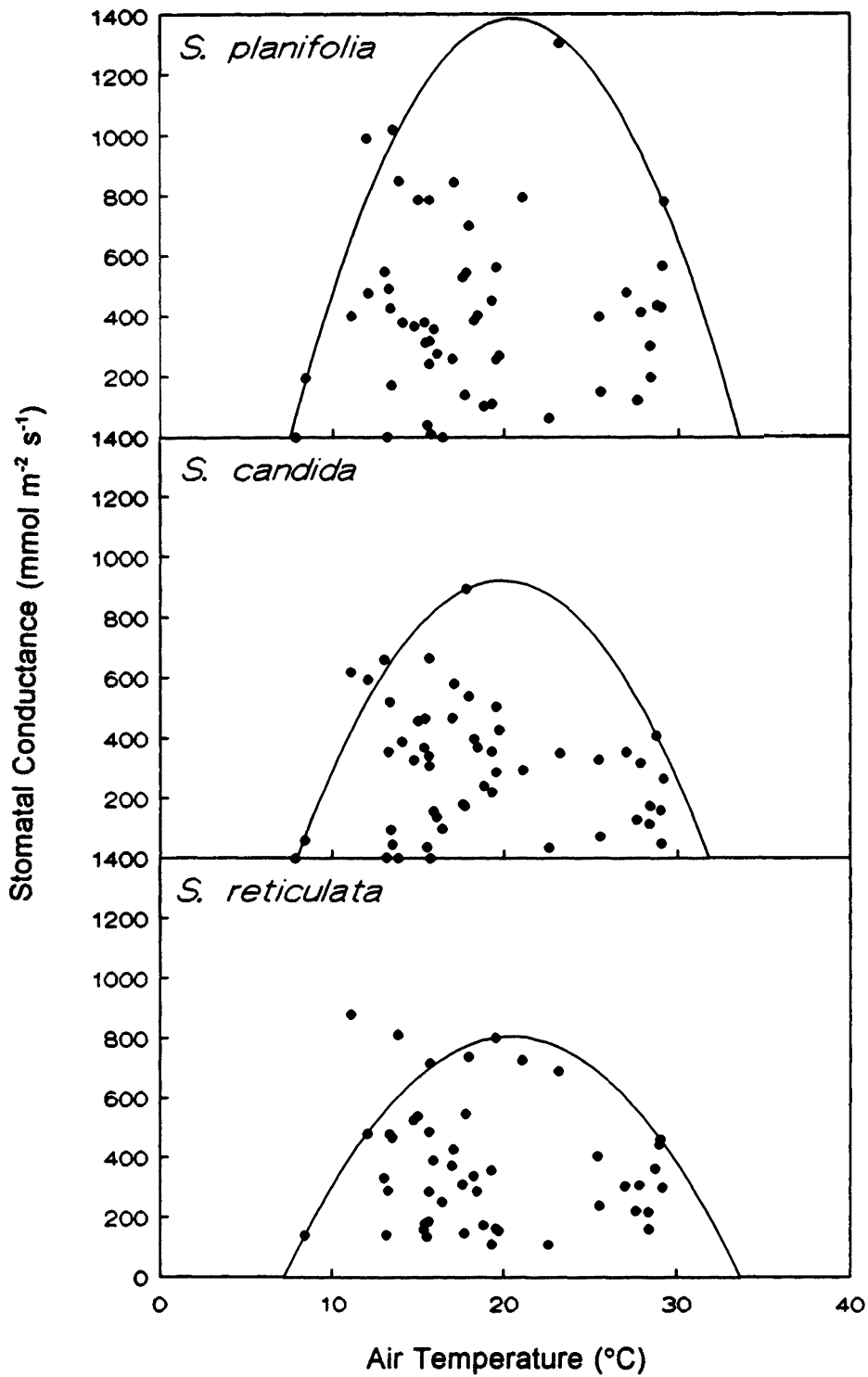


Figure 5.11a. Scatter diagram of stomatal conductance and air temperature. Solid lines indicate the probable upper limit of the observations.

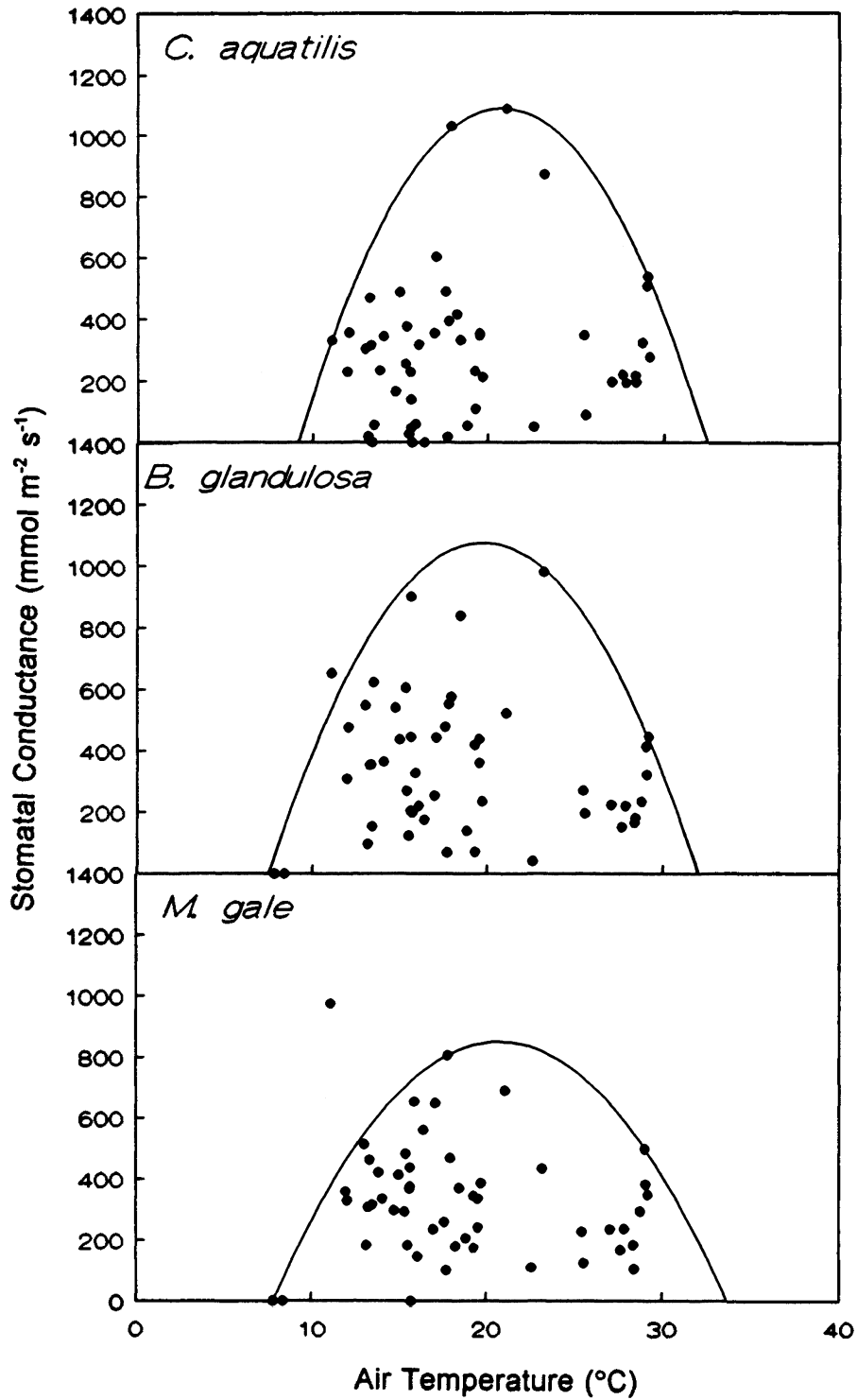


Figure 5.11b. Scatter diagram of stomatal conductance and air temperature. Solid lines indicate the probable upper limit of the observations.

Table 5.8. Optimum air temperatures for maximum stomatal conductance and the range of air temperatures for stomatal conductance for each species. Standard deviations are given in parentheses.

Species	Optimum $T_a$ (°C)	$T_a$ Range (°C)
<i>S. planifolia</i>	20.52	7.54 - 33.49
<i>S. candida</i>	19.89	7.96 - 31.82
<i>S. reticulata</i>	20.44	7.23 - 33.66
<i>C. aquatilis</i>	20.81	9.18 - 32.44
<i>B. glandulosa</i>	19.76	7.54 - 31.98
<i>M. gale</i>	20.74	7.88 - 33.60
Average	20.36 (0.40)	7.89 (0.63) - 32.83 (0.78)

averaged 20.36 °C, and the standard deviation about this mean was small (0.40 °C). Finding the mathematical roots of equation 5.6 gives the theoretical  $T_a$  where  $g$  would equal zero. Table 5.8 shows that with the possible exception of *C. aquatilis*, the  $T_a$  range for all species did not deviate far between the 8 to 33 °C range. *C. aquatilis* operates within a narrower  $T_a$  limit.

Overall, differences in stomatal behaviour do not appear to be the result of  $T_a$  since all species show a similar response. This species indifference seems to indicate that each species has evolved similar mechanisms to deal with the  $T_a$  range experienced.

#### D.7.6. Soil Temperature

Some researchers have found that soil temperature is an important environmental control on  $g$ . Although the exact mechanisms are not known, it has been suggested that cold soil temperatures limit  $g$  by increasing water viscosity and decreasing root permeability (Day et al., 1989; Turner, 1991). For example, Dawson and Bliss (1989a, 1989b) found that soil temperature had a significant effect on the  $g$  of *S. arctica*. The conductance of *S. arctica* in both alpine and arctic environments decreased as soil temperature decreased. Day et al. (1989) found that conifers (*Picea engelmannii* and *Pinus contorta*) had a lower  $g$  growing in cold soils (< 1°C) than those growing in warm soils (> 10 °C).

Despite these findings, no clear relationship between soil temperature at any depth in the rooting zone and  $g$  was found in this study. Soil temperatures were warmer than

those reported in the studies mentioned above (Table 5.1 and Figure 5.3) due to the absence of permafrost and snowcover near the roots during the growing season. Thus, soil temperatures at this site were warm enough not to limit  $g$ .

#### *D.7.7. Xylem Pressure Potential*

Although the relationship between  $g$  and  $\Psi$  can take many forms (see, for example, Fanjul and Barradas, 1985), stomata generally show a tendency to close as  $\Psi$  becomes more negative (Jarvis, 1976; Jones, 1983). For this study, the boundary line describing the relationship between  $\Psi$  and  $g$  took the linear form

$$g(\Psi) = K_7 + K_8(\Psi) \quad (5.7)$$

Graphically, the relationship between  $\Psi$  and  $g$  is difficult to interpret (Figures 5.12a and 5.12b). The Type II species would be expected to show a high sensitivity to  $\Psi$ , as indicated by the slope of the line (parameter  $K_8$ , Table 5.6). Furthermore, the Type I species would be expected to show little sensitivity to  $\Psi$ . Such patterns were not found and no clear relationship between  $\Psi$  and  $g$  could be discerned.

A possible explanation for this ambiguous result may lie in the direction of the relationship between  $\Psi$  and  $g$ . It is usually assumed that  $\Psi$  is a control on  $g$ , since the plant can sense if  $\Psi$  becomes too large and close the stomata (Section B.1). However, as noted by Jones (1983) and supported by Fanjul and Barradas (1985), well-watered plants sometimes do not close their stomata despite an increase in  $\Psi$  (becoming more negative).

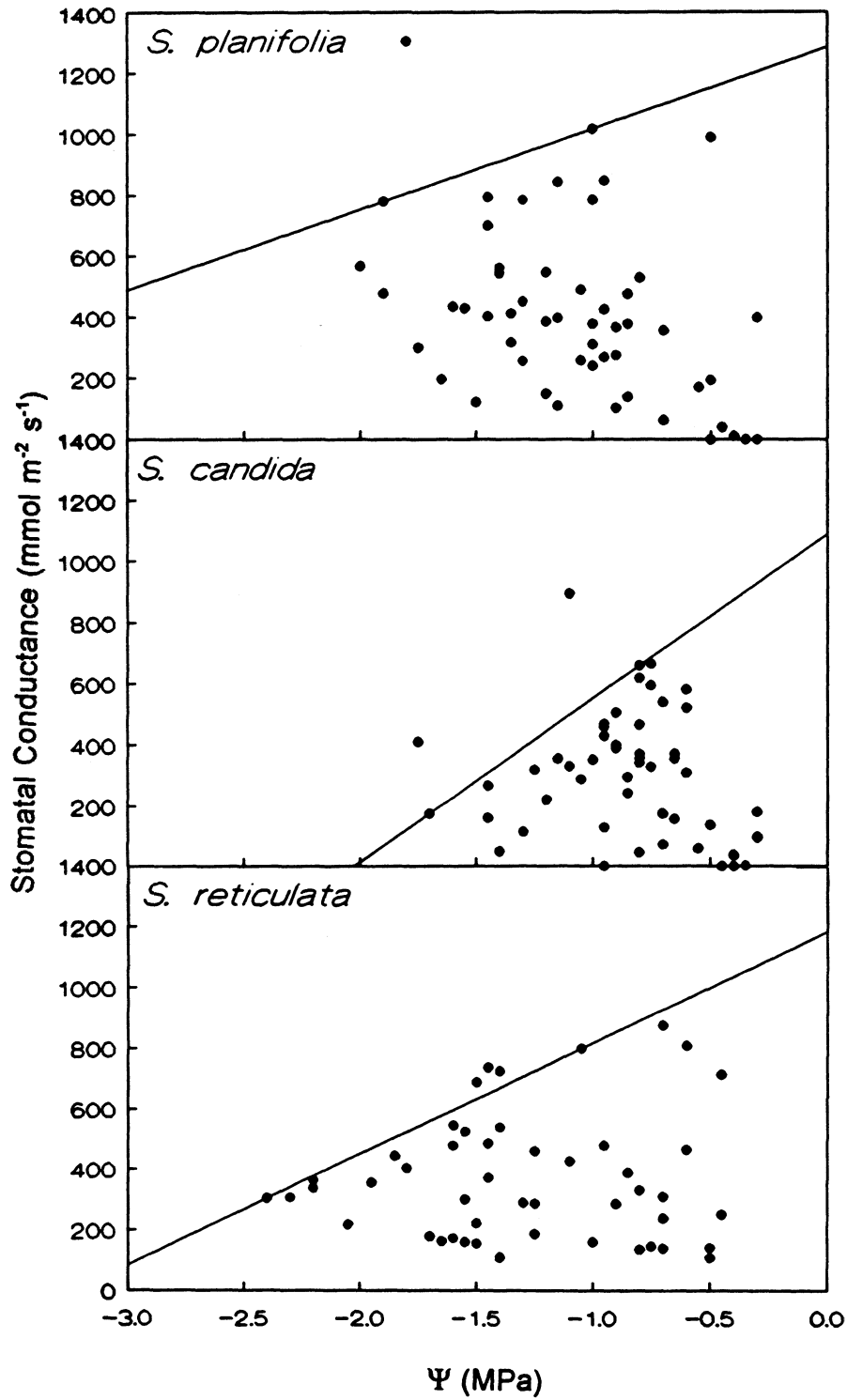


Figure 5.12a. Scatter diagram of stomatal conductance and xylem pressure potential. Solid lines indicate the probable upper limit of the observations.

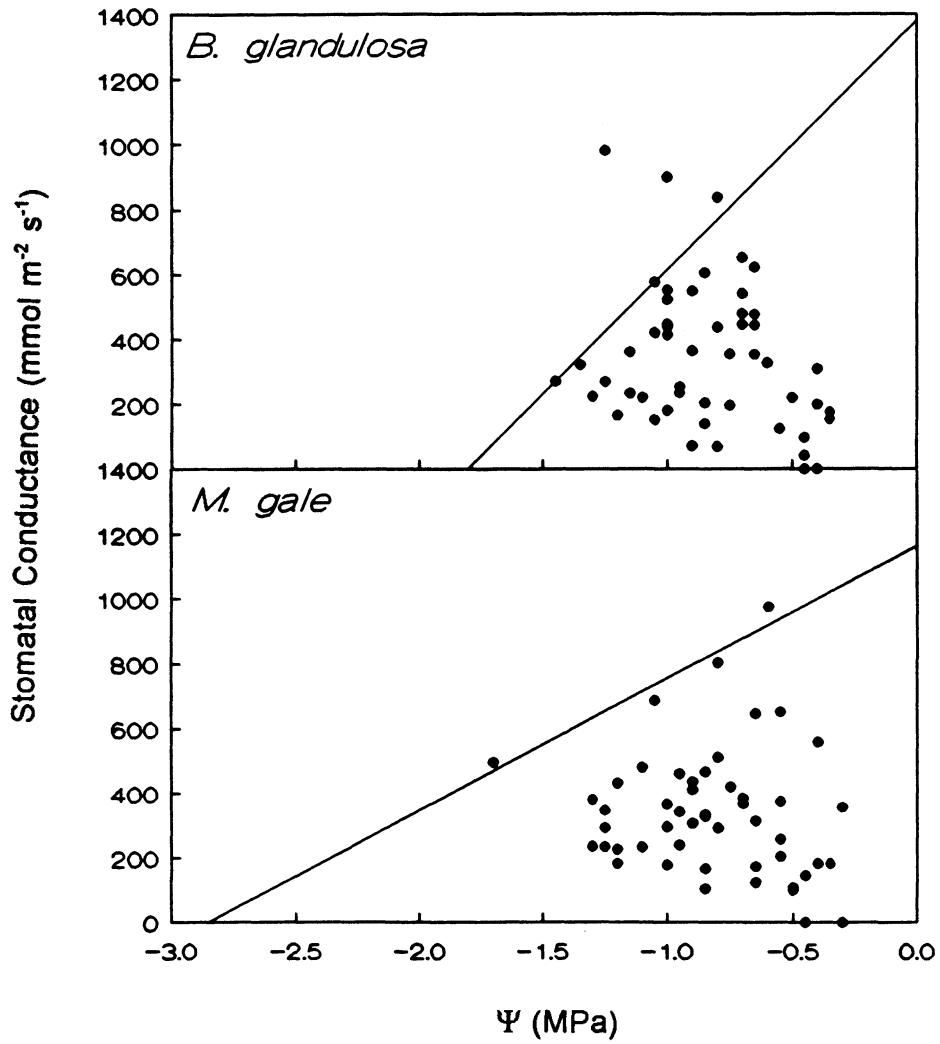


Figure 5.12b. Scatter diagram of stomatal conductance and xylem pressure potential. Solid lines indicate the probable upper limit of the observations.

In some cases,  $g$  will even increase as  $\Psi$  is falling. Jones (1983) proposes that this paradoxical result occurs because  $\Psi$  is falling in response to the increase in transpiration as the stomata open. In this case,  $g$  controls  $\Psi$ .

Figures 5.12a and 5.12b show that only *S. reticulata* has a strong tendency to decrease  $g$  as  $\Psi$  decreases, while all other species show weak results. This may indicate that in the case of *S. reticulata*,  $\Psi$  is a control on  $g$ . Because *S. reticulata* has a very shallow tap root depth and lateral root length (Chapter 2, Section C.7), any drying of the surface or lowering of the water table would first be felt by this plant. Hence,  $\Psi$  appears to be an important environmental control on the stomatal behaviour of *S. reticulata*.

For the remaining species, the deeper rooting depths and larger rooting networks may supply them with sufficient quantities of water making them less susceptible to diurnal drying of the soil in the rooting zone. In this case,  $\Psi$  is likely a result of  $g$ , since the plants are well-watered, and the falling of  $\Psi$  may be a response to water loss at the stomata.

The above discussion has made an important contribution in distinguishing the factors which lead to the differences in stomatal behaviour between the species. With the exception of *S. reticulata*, all species show little response to  $\Psi$ . Therefore  $\Psi$  does not play a role in initiating different types of stomatal behaviour. This result is confirmed by previous studies which show Type II patterns in well-watered conditions. In the case of *S. reticulata*, however,  $g$  does respond to  $\Psi$  due to the shallow rooting network.

As a consequence,  $\Psi$  is an environmental control on  $g$  and may be responsible for the Type II pattern displayed by *S. reticulata*.

#### D.8. Modelling Stomatal Conductance

Two basic approaches have in the past been used to model stomatal conductance (Jones, 1983). The first approach using multiple regression, regresses stomatal conductance against the independent environmental controls. This method assumes that all significant controls have been included. The major disadvantage of this approach is that it is purely empirical with no physical interpretation between  $g$  and each control. The second approach is to make use of the boundary line analysis equations described above. The relationships between  $g$  and all controls are fitted together non-linearly, with the assumption that there are no synergistic interactions between the controls. The major advantage of this approach is that it is physically based.

The form of the boundary line non-linear model is

$$g = g_{max} f(K\downarrow) f(\Delta W) f(T_a) f(\Psi) \dots \quad (5.8)$$

Each function in equation 5.8 is indexed to the maximum  $g$  observed for each boundary line (usually, but not always,  $0 < f < 1$ ). The species-specific equations for each variable have been given previously (Sections D.7.1 through D.7.7). Following an example given by Jarvis (1976), if  $K\downarrow$  limits  $g$  to 80% of  $g_{max}$ , and  $T_a$  limits  $g$  to 80% of  $g_{max}$ , and all other variables are non-limiting (i.e., 100%), then the resulting  $g$  would equal

$g_{max}(0.80)(0.80)(1)(1)$ . Therefore, the modelled  $g$  would equal 64% of  $g_{max}$ . This approach has had wide application with varying success (see Jarvis, 1976; Fanjul and Barradas, 1985; Lafleur, 1987; Adams et al., 1991; Balldocchi et al., 1991; Dickinson et al., 1991; Massman and Kaufmann, 1991; and others). Differences in the model's success lies with differences in the forms and goodness of fit in the equations used to fit the boundary line curve. More importantly, different species respond to different environmental controls, and data on all variables is often not available. Hence some models include variables that others do not (for example,  $CO_2$ ).

Modelling  $g$  has two purposes in this study. The first is to confirm if the environmental controls described above do indeed account for differences in stomatal behaviour. If the sensitivity and direction of the controls are correct, the modelling results should improve with each additional control put in place. A decrease or negligible increase in model performance would indicate little sensitivity of  $g$  to that control. The second purpose is to assess the accuracy of this modelling approach to reliably predict  $g$ . Successful modelling of  $g$  would allow simulation studies on the sensitivity of a subarctic willow ecosystem to climate change.

Model performance will not be quantified by the conventional  $r$  or  $r^2$ , since these values are often misleading and unrelated to the sizes of the differences between the observed mean ( $O$ ) and the predicted mean ( $P$ ) (Willmott, 1982). Alternatively, model performance will be assessed using an "index of agreement" proposed by Willmott and Wicks (1980) of the form

$$D_i = 1 - \left( \frac{\sum_{i=1}^N (P_i - O_i)^2}{\sum_{i=1}^N (|P_i - \bar{O}| + |O_i - \bar{O}|)^2} \right) \quad (5.9)$$

where  $D_i$  varies between 0 (poor agreement) and 1 (good agreement). Bias is described by the mean bias error ( $MBE$ ) calculated as

$$MBE = N^{-1} \sum_{i=1}^N (P_i - O_i) \quad (5.10)$$

while the variability of ( $P-O$ ) about the  $MBE$  is described by the root mean square error ( $RMSE$ ) calculated as

$$RMSE = \sqrt{N^{-1} \sum_{i=1}^N (P_i - O_i)^2} \quad (5.11)$$

Tables 5.9a and 5.9b show that for all species, modelling  $g$  as only a function of  $K\downarrow$  gave moderately good results, indicating that  $K\downarrow$  is an important variable. The shade tolerant species (*S. reticulata* and *M. gale*) displayed the lowest  $D_i$  values indicating their relative insensitivity to irradiance. *C. aquatilis* also displayed relatively poor modelling results with only  $K\downarrow$  as a variable, which indicates that this species also may show some tolerance of low irradiance levels.

The addition of the  $\Delta W$  to the model resulted in a large improvement in model performance for all species. Largest improvement were experienced by the taller species, while the shorter species (for example, *S. reticulata*, *M. gale*, and *C. aquatilis*) showed

Table 5.9a. Results of boundary line analysis with individual species responding to solar irradiance ( $K\downarrow$ ), leaf-to-air vapour pressure deficit ( $\Delta W$ ), air temperature ( $T_a$ ), and xylem pressure potential ( $\Psi$ ). Symbols are defined as follows:  $n$  = number of observations;  $O$  = observed mean;  $P$  = predicted mean;  $MBE$  = mean bias error;  $RMSE$  = root mean square error and ;  $D_i$  = index of agreement.

<i>S. planifolia</i>	$n$	$O$	$P$	$MBE$	$RMSE$	$D_i$
$f(K\downarrow)$	53	411.06	953.39	542.32	617.25	0.46
$f(K\downarrow)f(\Delta W)$	"	"	584.08	173.02	292.35	0.67
$f(K\downarrow)f(\Delta W)f(T_a)$	"	"	492.70	81.64	277.49	0.67
$f(K\downarrow)f(\Delta W)f(T_a)f(\Psi)$	"	"	369.59	-41.48	267.46	0.59
<i>S. candida</i>	$n$	$O$	$P$	$MBE$	$RMSE$	$D_i$
$f(K\downarrow)$	52	296.10	653.64	357.54	409.39	0.50
$f(K\downarrow)f(\Delta W)$	"	"	404.64	108.54	198.85	0.72
$f(K\downarrow)f(\Delta W)f(T_a)$	"	"	329.63	33.53	178.45	0.76
$f(K\downarrow)f(\Delta W)f(T_a)f(\Psi)$	"	"	236.33	-59.77	190.53	0.65
<i>S. reticulata</i>	$n$	$O$	$P$	$MBE$	$RMSE$	$D_i$
$f(K\downarrow)$	48	369.94	784.58	414.64	475.94	0.41
$f(K\downarrow)f(\Delta W)$	"	"	651.30	281.36	355.20	0.52
$f(K\downarrow)f(\Delta W)f(T_a)$	"	"	488.73	118.79	257.62	0.57
$f(K\downarrow)f(\Delta W)f(T_a)f(\Psi)$	"	"	396.26	26.32	226.81	0.59

Table 5.9b. Results of boundary line analysis with individual species responding to solar irradiance ( $K\downarrow$ ), leaf-to-air vapour pressure deficit ( $\Delta W$ ), air temperature ( $T_a$ ), and xylem pressure potential ( $\Psi$ ). Symbols are defined as follows:  $n$  = number of observations;  $O$  = observed mean;  $P$  = predicted mean;  $MBE$  = mean bias error;  $RMSE$  = root mean square error and;  $D_i$  = index of agreement.

<i>C. aquatilis</i>	$n$	$O$	$P$	$MBE$	$RMSE$	$D_i$
$f(K\downarrow)$	51	291.41	807.33	515.92	575.55	0.41
$f(K\downarrow)f(\Delta W)$	"	"	722.61	431.20	515.52	0.42
$f(K\downarrow)f(\Delta W)f(T_a)$	"	"	551.11	259.70	368.42	0.55
$f(K\downarrow)f(\Delta W)f(T_a)f(\Psi)$	"	"	-	-	-	-
<i>B. glandulosa</i>	$n$	$O$	$P$	$MBE$	$RMSE$	$D_i$
$f(K\downarrow)$	51	345.58	710.72	365.15	435.65	0.50
$f(K\downarrow)f(\Delta W)$	"	"	391.01	45.44	200.38	0.70
$f(K\downarrow)f(\Delta W)f(T_a)$	"	"	342.31	-3.27	197.33	0.73
$f(K\downarrow)f(\Delta W)f(T_a)f(\Psi)$	"	"	251.46	-94.11	223.11	0.61
<i>M. gale</i>	$n$	$O$	$P$	$MBE$	$RMSE$	$D_i$
$f(K\downarrow)$	52	329.51	871.76	542.25	595.59	0.32
$f(K\downarrow)f(\Delta W)$	"	"	732.67	403.16	473.78	0.39
$f(K\downarrow)f(\Delta W)f(T_a)$	"	"	494.64	165.14	287.75	0.51
$f(K\downarrow)f(\Delta W)f(T_a)f(\Psi)$	"	"	380.79	51.28	255.92	0.49

only moderate improvement. As suggested previously, this may be the result of the poor atmospheric coupling between the short vegetation and the atmosphere.

When the  $T_a$  function is added to the model, performance again improves for all species. The better performance, however, is small which indicates that this variable seems to be of minimal importance. *M. gale* showed the greatest improvement in performance, while *S. planifolia* showed no change in performance at all.

The addition of  $\Psi$  showed a decrease in model performance in all species except *S. reticulata*. This decrease reinforces the idea that  $\Psi$  is a result of  $g$ , not a control on  $g$ , in the plants that do not experience any water stress. The increase in model performance for *S. reticulata*, however, indicates that  $\Psi$  is in fact a control on  $g$ , and its inclusion as such increases model performance.

Comparison between the observed diurnal  $g$  and the predicted diurnal  $g$  using variables in the model which gave the best results for each species are shown in Figures 5.13a through 5.13f. For all species, a Type II pattern was predicted by the model on July 28 owing primarily to the large  $\Delta W$  observed during that day. This result agrees with the observed trends, with the exception of *S. candida*. On July 16, the model predicts the midday stomatal closure of *S. reticulata*, yet fails to predict the Type II pattern for *S. planifolia* and *B. glandulosa*. This occurs because the midday stomatal closure is due to  $\Psi$ , a variable which is included in the model. The model, however, failed to predict the Type II pattern found in *S. planifolia*, *S. reticulata*, and *B. glandulosa* on June 29. Overall,  $g$  is modelled reasonably well for all species even on this fine time resolution of

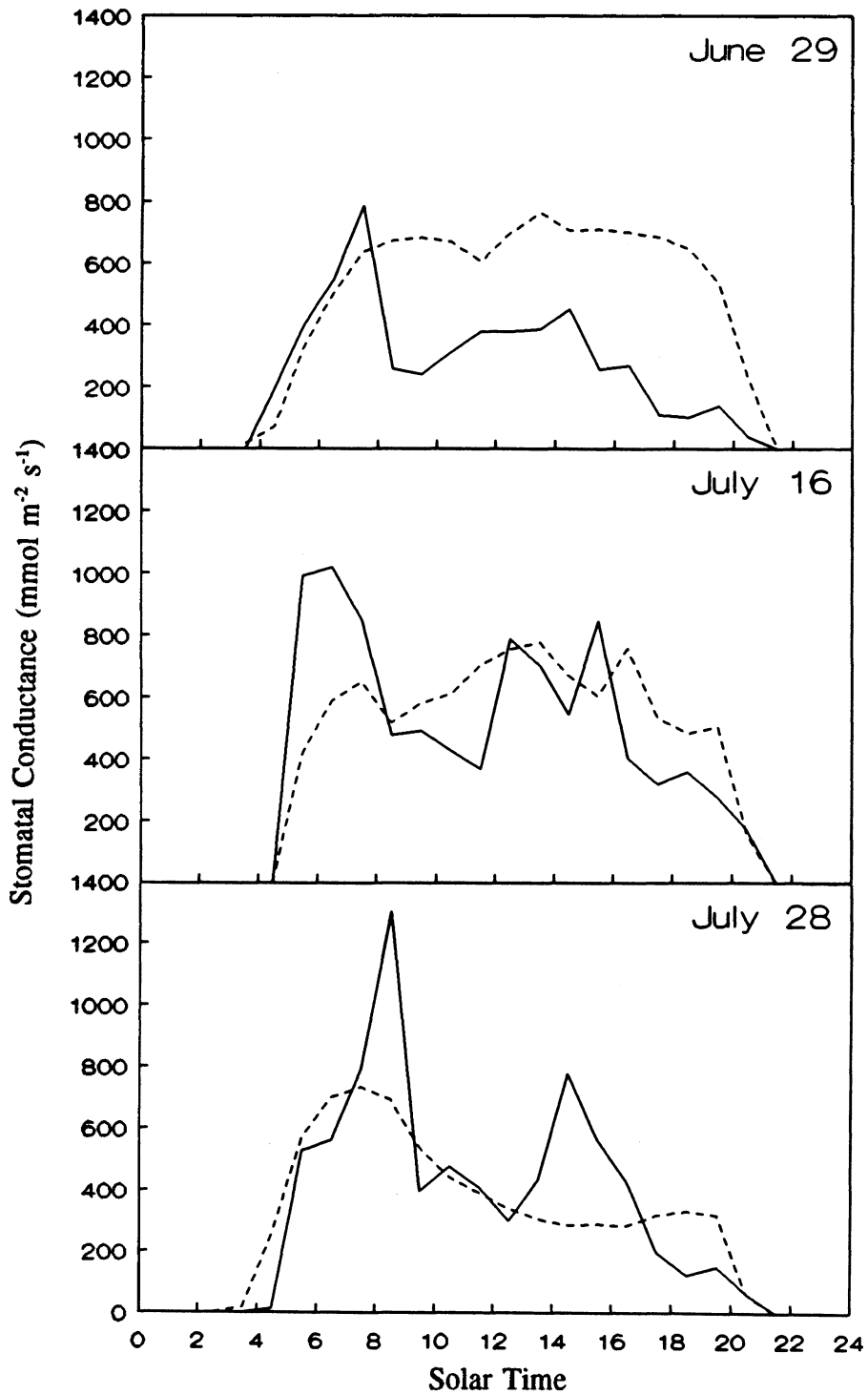


Figure 5.13a. Diurnal course of the stomatal conductance of *S. planifolia* (solid line plotted with the best boundary line non-linear modelling estimate (dashed line)).

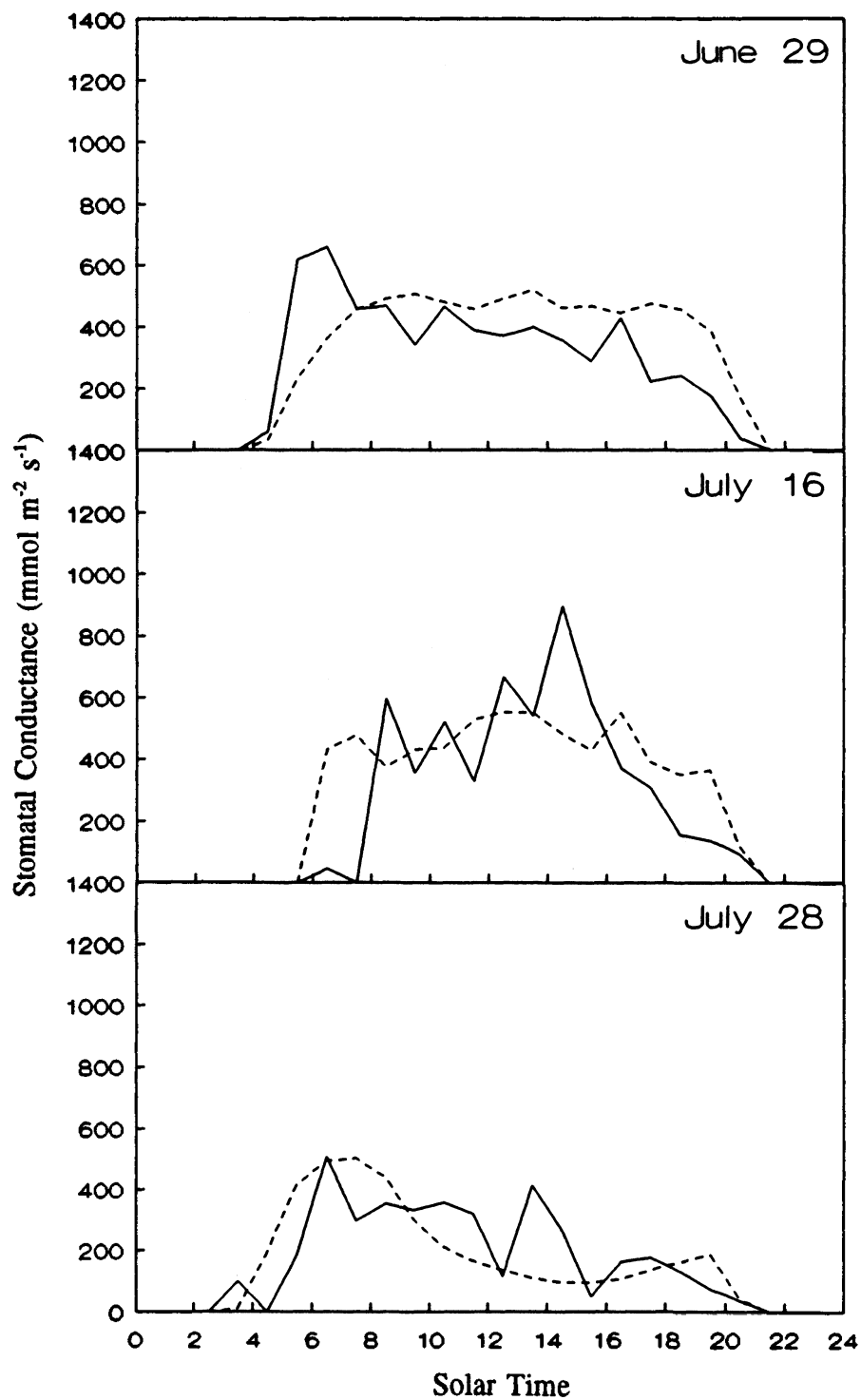


Figure 5.13b. Diurnal course of the stomatal conductance of *S. candida* (solid line) plotted with the best boundary line non-linear modelling estimate (dashed line).

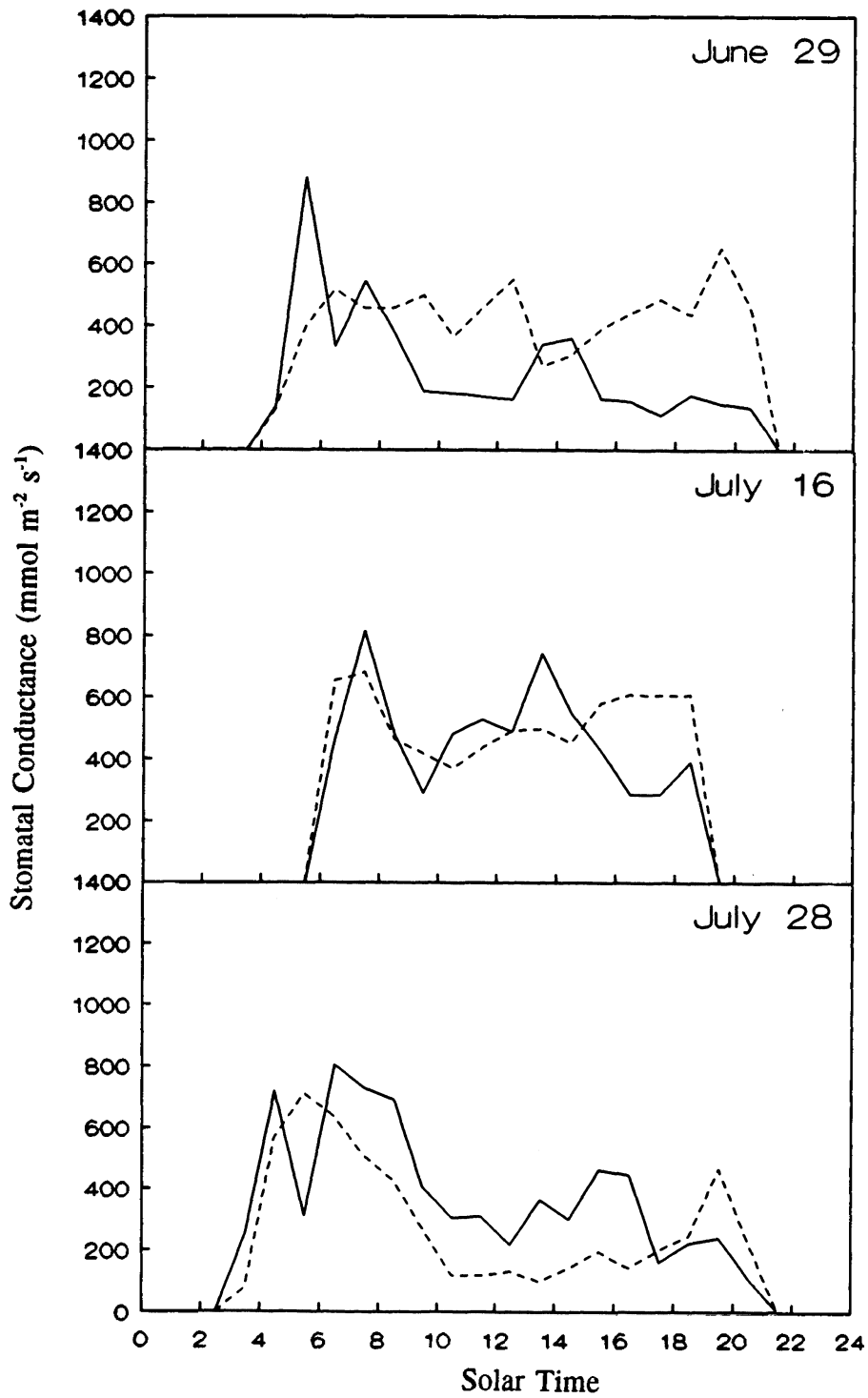


Figure 5.13c. Diurnal course of the stomatal conductance of *S. reticulata* (solid line) plotted with the best boundary line non-linear modelling estimate (dashed line).

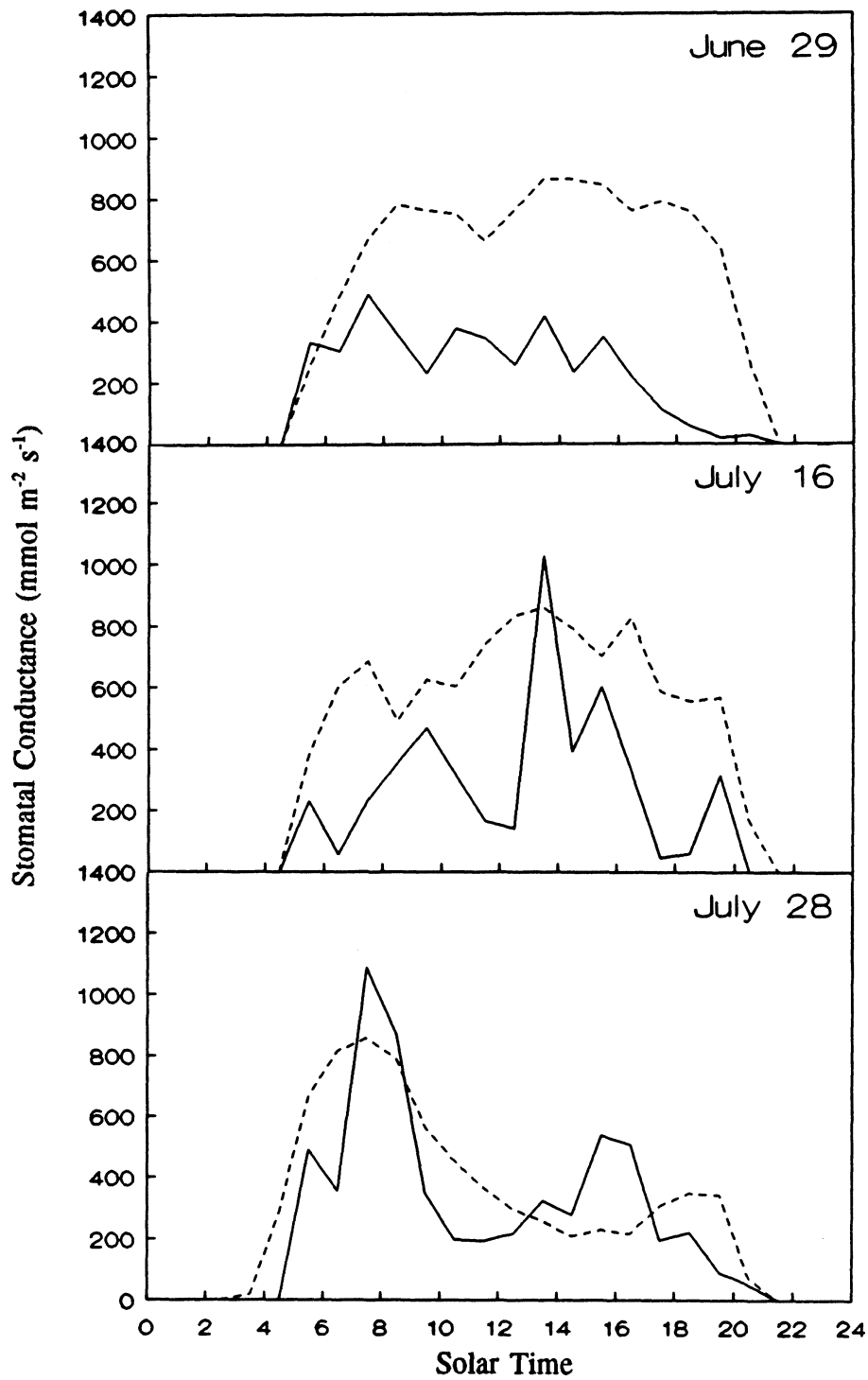


Figure 5.13d. Diurnal course of the stomatal conductance of *C. aquatilis* (solid line) plotted with the best boundary line non-linear modelling estimate (dashed line).

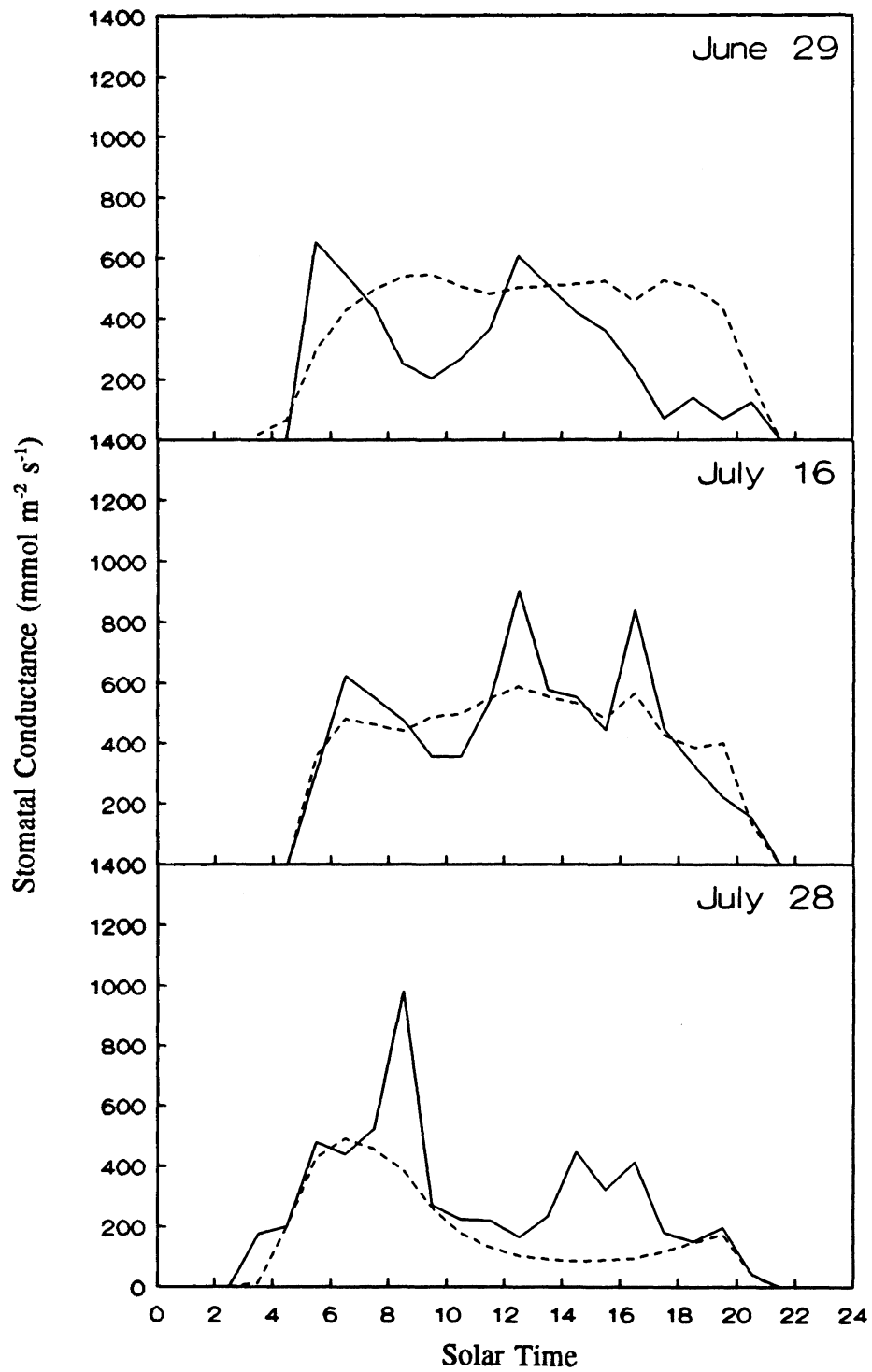


Figure 5.13e. Diurnal course of the stomatal conductance of *B. glandulosa* (solid line) plotted with the best boundary line non-linear modelling estimate (dashed line).

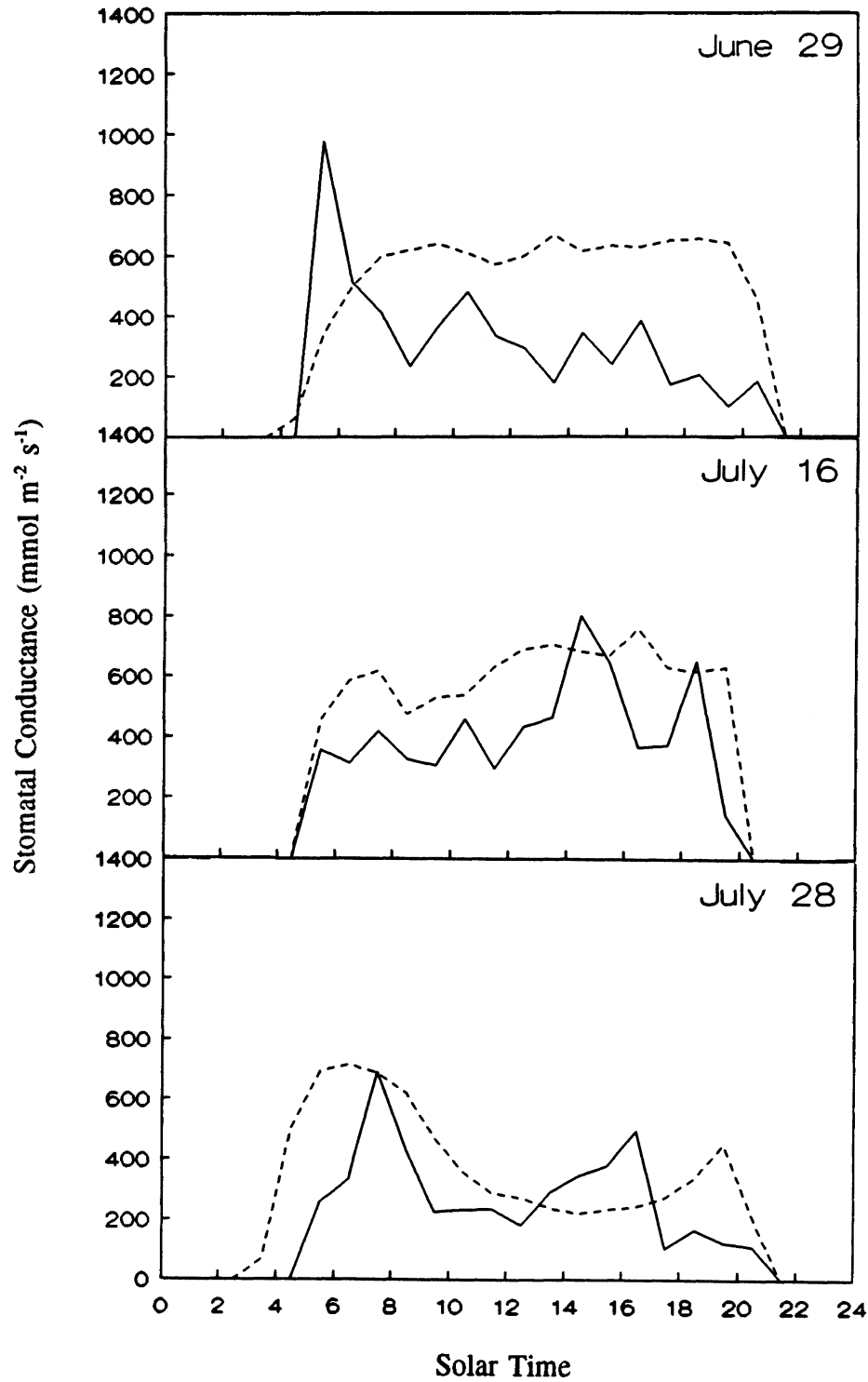


Figure 5.13f. Diurnal course of the stomatal conductance of *M. gale* (solid line) plotted with the best boundary line non-linear modelling estimate (dashed line).

1 hour. By simply calculating daily averages, for example, model performance would improve substantially.

Possible sources of error in this modelling approach will now briefly be examined. First, although all possible precautions were taken (as per LI-COR, 1989; McDermitt, 1990) porometer error may account for some of the anomalous peaks observed in  $g$ . Tyree and Wilmot (1990) maintain that the thermocouple in the LI-1600 porometer may underestimate leaf temperatures and therefore overestimate  $g$  by as large of a factor of 2. It is also possible the boundary layer conductance has been overestimated. Extrapolation of the wind profile to the mean canopy height is not always valid, since neutral conditions were assumed and species like *S. reticulata* clearly fall far below the mean canopy height. Also, the aerodynamic influence of one leaf on another has not been accounted for. For example, it has been found that coniferous needles crowded together (a dense shoot) mutually decrease the boundary layer conductance. This sheltering effect can, for example, reduce the boundary layer conductance of a typical shoot to half that of an individual needle (Jarvis et al., 1976).

Although the above sources of error could easily bias the results, the magnitude of such bias would likely be small. A large discrepancy between  $P$  and  $O$  is more likely the result of a missing control on  $g$ . The missing control is probably changes in  $\text{CO}_2$  concentration due to photosynthesis. The mechanism between  $\text{CO}_2$  uptake and  $g$  is explained as follows. It is assumed that plants attempt to maximize the amount of  $\text{CO}_2$  intake while minimizing water loss through transpiration. It has been hypothesized that

the ratio of the flux of CO<sub>2</sub> to the flux of water vapour remains constant through various feedback and feedforward mechanisms (Cowen, 1977; Cowen and Farquhar, 1977; Nobel, 1991). Hence, the maximum amount of CO<sub>2</sub> is fixed with a minimum loss of water. On days such as June 29, it is possible that the maintenance of a constant water use efficiency (water use efficiency = mass CO<sub>2</sub> fixed/mass H<sub>2</sub>O transpired; Nobel, 1991) has lowered *g* and caused a Type II pattern to appear in some species in order to maintain sufficient CO<sub>2</sub> fixation levels. Since CO<sub>2</sub> levels were not measured in this study, this hypothesis is left for further research.

## E. CONCLUSIONS

This discussion in the physiology of water movement through the shrub species found in the willow-birch forest has led to a number of important findings. All species are amphistomatous, with a stomatal conductance that is large relative to other species found in similar habitats. Some species show a pronounced midday stomatal closure, while others do not. The diurnal pattern of stomatal conductance is not a response to soil moisture. To prevent excessive stress during high transpiration, root resistance increases as transpiration increases.

A non-linear boundary line analysis indicates that *S. reticulata* and *M. gale* are shade-tolerant. All species display a similar optimal temperature for stomatal conductance. *S. planifolia*, *S. reticulata* and, *B. glandulosa* have a low tolerance to vapour pressure

deficit, while *S. candida* has a high tolerance. The tolerance of *C. aquatilis* and *M. gale* lies somewhere in between. A conceptual model describing the species-specific response to the vapour pressure deficit was developed to explain these differences. Xylem pressure potential is a response rather than control of stomatal conductance for all species except *S. reticulata*. Xylem pressure potential partially controls stomatal conductance in *S. reticulata* as a response to the shallow rooting depth.

Step-wise modelling of stomatal conductance confirms the boundary-line analysis results and indicates that individual species modelling of stomatal conductance using a 1/2 hr time step can be performed reasonably.

## CHAPTER 6

### MODELLING EVAPORATION

#### A. INTRODUCTION

Besides giving valuable insight into the processes involved in evaporation, a physically based modelling approach allows the possible impacts of climate change scenarios to be investigated. This chapter investigates not only how atmospheric forcing may alter the climate, but also how vegetation changes may affect climate through changes in stomatal conductance and *LAI*. The modelling approach used in this chapter establishes the dynamic link between the vegetation and the atmosphere, a link that has not been established in the past.

#### B. EXPERIMENTAL PROCEDURE

Because the vegetation cover at the study site does not provide 100% ground cover,  $Q_E$  must be separated into transpiration  $Q_E(Tr)$  and evaporation  $Q_E(Water)$  components where

$$Q_E = Q_E(Tr) + Q_E(Water) \quad (6.1)$$

$Q_E(T_r)$  is predicted using the Penman-Monteith combination model

$$Q_E(T_r) = \frac{S(Q^* - Q_G) + \rho C_p D g_a}{S + \gamma(1 + g_d/g_c)} \quad (6.2)$$

in which the aerodynamic conductance,  $g_a$  is calculated as

$$g_a = \frac{k^2 u}{[\ln((z-d)/z_o)]^2} \quad (6.3)$$

and the canopy conductance,  $g_c$  is calculated as

$$g_c = \sum_{i=1}^n g_i(LAI)(COV_i) \quad (6.4)$$

where  $n$  is the number of species  $i$ , and  $COV$  is the surface cover of species  $i$ .

Stomatal conductance is modelled using the species-specific responses of each species to the environmental controls discussed in Chapter 5, Section E.8. For all species,  $g_i$  is predicted as

$$g_i = g_{\max(i)} f_i(K^{\downarrow}) f_i(\Delta W) f_i(T_a) \quad (6.5)$$

except for *S. reticulata*, where

$$g = g_{\max} f(K^{\downarrow}) f(\Delta W) f(T_a) f(\Psi) \quad (6.6)$$

The  $\Psi$  function is included since  $\Psi$  is a control on the stomatal conductance of *S. reticulata*, but is a response to  $g$  in the other species. The individual functions describing the relationships between  $g$  and the environmental controls are given as

$$f_i(K_1) = \frac{(g_{\max(i)})(K_1)}{(K_{1i} + K_1)} \quad (6.7)$$

$$f_i(\Delta W) = K_{2i} + K_{3i}(\Delta W) \quad (6.8)$$

$$f_i(T_a) = K_{4i} + K_{5i}(T_a) + K_{6i}(T_a)^2 \quad (6.9)$$

$$f_i(\Psi) = K_{7i} + K_{8i}(\Psi) \quad (6.10)$$

where the derivation of equations 6.7 through 6.10 are described fully in Chapter 5, Section D.7. The parameters  $K_1$  through  $K_8$  are unique for each species and are summarized in Chapter 5, Table 5.6.

To predict  $Q_E(\text{Water})$ , the canopy conductance term in equation 6.2 is allowed to approach  $\infty$  so that

$$Q_E(\text{Water}) = \left( \frac{S(Q^* - Q_G) + \rho C_p D g_c}{S + \gamma} \right) COV_{(\text{Water})} \quad (6.11)$$

In order to include important physiological factors such as the midday stomatal closure, modelling was performed on a time scale of 1/2 hour for each day of measurement. The period of vegetation growth (June 16-July 12) was excluded. Values were then averaged for each day.

## C. RESULTS AND DISCUSSION

### C.1. Model Performance

The seasonal trends of modelled and measured  $Q_E$  are shown in Figure 6.1. Early in the season,  $Q_E$  is underestimated due to the immature canopy (small  $LAI$ ). After July 13 when the canopy has matured, the modelled  $Q_E$  closely follows the measured  $Q_E$ . Tables 6.1 shows that  $Q_E$  can be modelled very reasonably after canopy maturation is reached, as indicated by the high  $Di$  and  $r^2$ . The model has a tendency to underestimate, rather than overestimate  $Q_E$ , (Figure 6.2).

### C.2. The Role of Transpiration

Since evaporation from open water and transpiration have been explicitly calculated, the relative role of the vegetation in the overall  $Q_E$  is shown in Figure 6.3. The transpiration stream accounts for the majority of  $Q_E$  ( $Q_E(T_r)/Q_E=0.80$ ) through most of the measurement period. The seasonal effect of the vegetation on  $Q_E$  is indicated in Figure 6.4. Early in the season, the canopy plays a minor role. The fast (15 day) development to full leaf dramatically increases the magnitude of transpiration until it comprises 80% of all evaporation, a level which is maintained for the majority of the season. Decreases in relative transpiration occurs on days when the water table is at or above the surface (Figure 2.2c). On these days, stomatal closure has occurred due to cold temperatures and low irradiance levels (e.g. July 18 and July 23). At the end of the

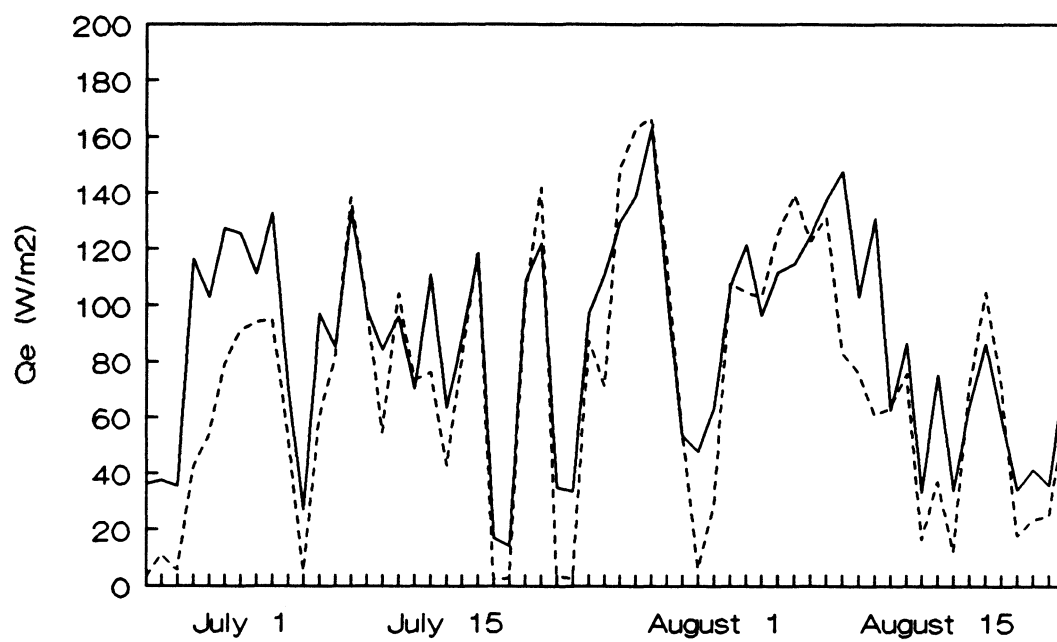


Figure 6.1. Seasonal course of measured  $Q_E$  (solid line) and modelled  $Q_E$  (dashed line).

Table 6.1. Comparison of measured  $Q_E$  to modelled  $Q_E$  for the fully developed canopy. All units are in  $W m^{-2}$ , except  $Di$  and  $r^2$ , which are dimensionless.

	Measured $Q_E$	Modelled $Q_E$	Performance	
Average	79	71	<i>MBE</i>	-8.5
Std. Error	5.7	7.2	<i>RMSE</i>	19.5
Maximum	163	167	<i>Di</i>	0.95
Minimum	14	3	$r^2$	0.89
n	44	44	Std. Err. Y Est.	16.1

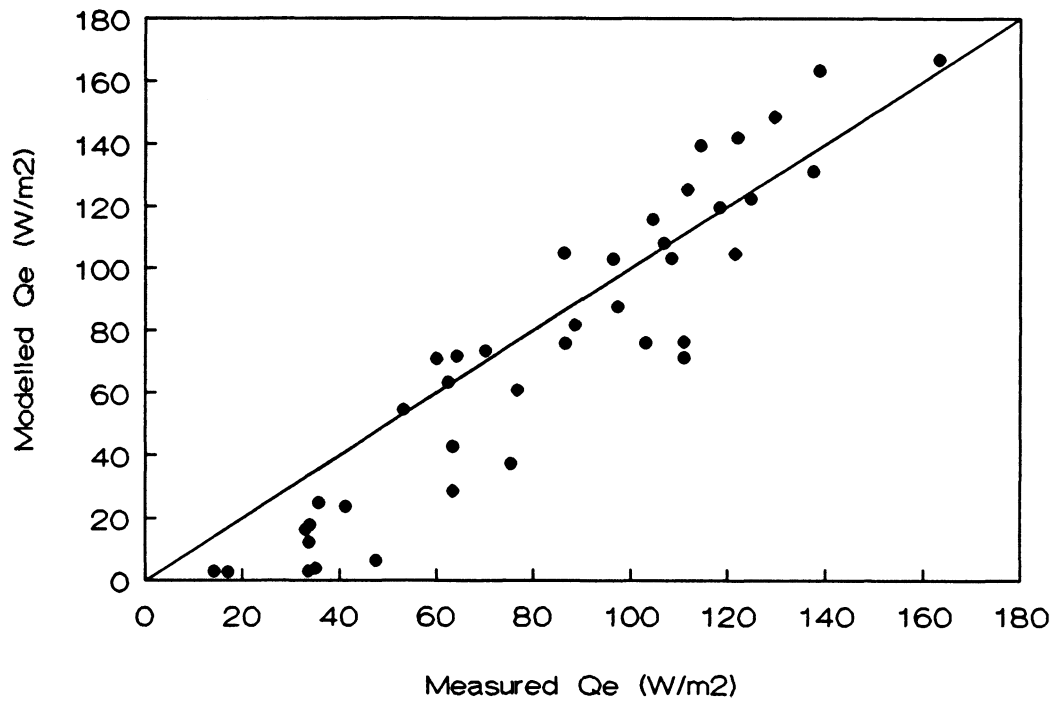


Figure 6.2. Relationship between measured  $Q_E$  and modelled  $Q_E$ . Solid line is the 1:1 line.

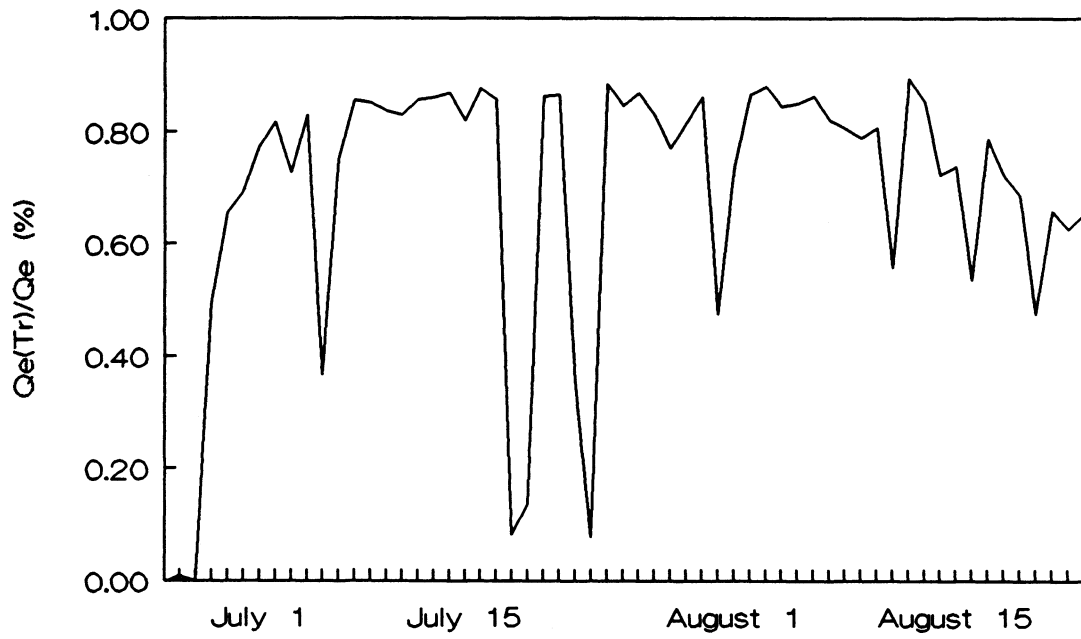


Figure 6.3. Seasonal course of the relative role of transpiration in the overall evaporation.

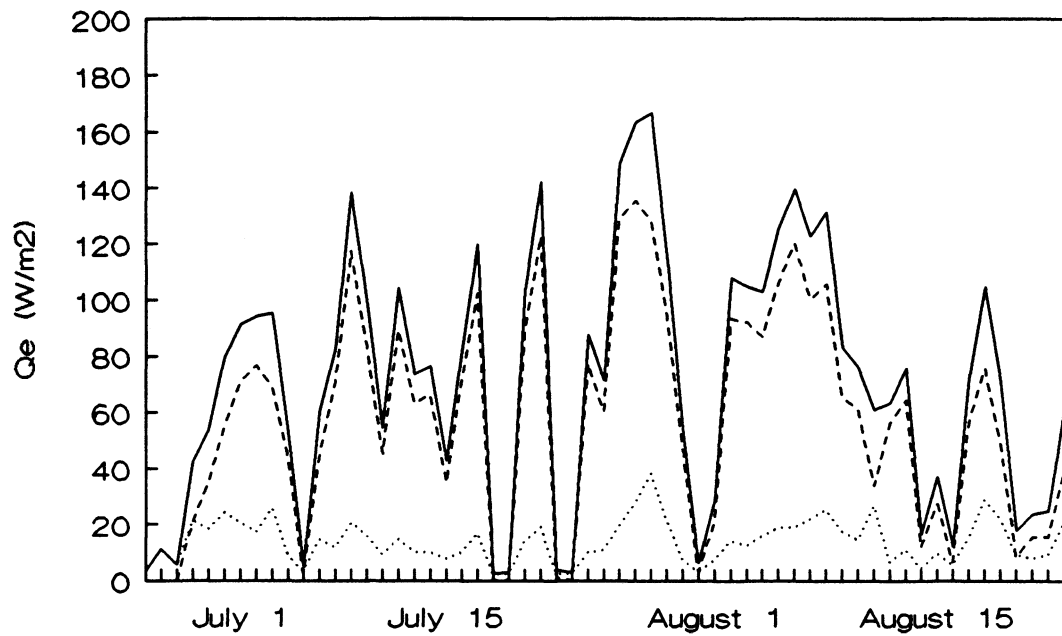


Figure 6.4. Seasonal course of the overall evaporation (solid line), transpiration (dashed line) and pond evaporation (dotted line).

season,  $Q_E(T_r)/Q_E$  has decreased by approximately 20% from its mid-season high due to senescence and decreased stomatal activity.

### C.3. Climate Change Scenarios

The potential impact of a changing ecosystem on  $Q_E$ , is assessed for three vegetation scenarios using a model which employs the present  $T_a$  and  $LAI$ . The first (referred to as the *DRY* scenario) represents the impact of a surface drying due, for example, to rapid isostatic rebound or to lowering of the water table because of less precipitation or an increase in permafrost melting. With surface drying, it is hypothesized that *B. glandulosa* would dominate, since this species is presently found in the drier locations of the study site. It is assumed that the water table would not rise above the surface so that standing water is never present.

The second vegetation change (*WET* scenario) represents a situation where surface wetness would increase if, for example, precipitation increases or the permafrost active layer decreases. Under these conditions, it is likely that *C. aquatilis* would dominate the surface, since this species is presently found in very wet areas of the study site. For this scenario, it is hypothesized that there would be an increase in standing water to cover 10% of the surface.

The third vegetation change (*DOM* scenario) provides for the domination of one species. Since *S. planifolia* is presently the dominant species, the scenario where *S. planifolia* dominates the surface accompanied by a 10% surface cover of standing water

is simulated. This situation could occur if *S. planifolia* would continue to dominate the surface cover and eventually out-compete all other species.

To investigate the impact of a CO<sub>2</sub> enriched atmosphere (2 x CO<sub>2</sub>), the three vegetation change scenarios were simulated with a 20% increase in  $T_a$  and a doubling of  $LAI$ . The effects of the  $T_a$  and  $LAI$  on the present day vegetation cover and composition were also investigated (*Present* scenario). An increase in  $T_a$  of 20% is equivalent to an increase of 2.8°C above the 1991 growing season average of 14.2°C, and lies within the 2 to 4°C increase in  $T_a$  range given for the Churchill region for a doubling of CO<sub>2</sub> (Rouse et al., 1992). It is assumed that this increase in  $T_a$  would double  $LAI$  from the present maximum of 0.81 to 1.62 m<sup>2</sup> m<sup>-2</sup>, a modest increase compared to present day  $LAI$  of 1.98, 2.45 and 4.98 m<sup>2</sup> m<sup>-2</sup> for two coastal *Carex* marshes and a shrub woodland, respectively, found near southern James Bay (Lafleur, 1988).

The results of the simulations are shown in Table 6.2. Under the current conditions (1 x CO<sub>2</sub>), the *DRY* scenario would elicit a 16% decrease in  $Q_E$ . The large decrease in  $Q_E$  due to the disappearance of standing water offsets the slight increase in transpiration from *B. glandulosa*. For both the *WET* and *DOM* scenarios, the increase in standing water is responsible for the majority of the increase in  $Q_E$ . Despite having identical proportions of the surface covered by vegetation, *C. aquatilis* increases transpiration by 5%, yet *S. planifolia* has almost no effect on transpiration. This occurs because of the unique response of each species to the leaf-to-air vapour pressure deficit ( $\Delta W$ ). *S. planifolia* displays a Type II diurnal stomatal conductance pattern with pronounced midday stomatal

Table 6.2. Changes in  $Q_E$  from the present  $Q_E$  expressed as a percentage. 1 x CO<sub>2</sub> refers to no changes in  $T_a$  or  $LAI$ ; 2 x CO<sub>2</sub> refers to a 20% increase in  $T_a$  and a doubling of  $LAI$ . Scenarios are defined as follows: *Present* - no change in species composition or surface cover; *Dry* - *B. glandulosa* only with no standing water; *Wet* - *C. aquatilis* only with 10% standing water and; *Dom* - *S. planifolia* only with 10% standing water.

Scenario		$Q_E(Tr)$	$Q_E(Water)$	$Q_E$
1 x CO <sub>2</sub>	<i>Present</i>	-	-	-
	<i>Dry</i>	4	-20	-16
	<i>Wet</i>	5	14	19
	<i>Dom</i>	< 1	14	14
2 x CO <sub>2</sub>	<i>Present</i>	48	8	56
	<i>Dry</i>	48	-20	28
	<i>Wet</i>	52	27	79
	<i>Dom</i>	49	27	76

closure. This species is intolerant of a large  $\Delta W$ . In contrast, *C. aquatilis* shifts from a Type I (no midday stomatal closure) to a Type II pattern. Because this species is more tolerant of a high  $\Delta W$ , midday stomatal closure does not occur as often as with *S. planifolia*, therefore allowing larger transpiration.

Given the postulated increases in  $T_a$  and  $LAI$  for a doubling of  $CO_2$ , all vegetation scenario simulations predict increases in  $Q_E$ . Given the present vegetation composition and standing water area,  $Q_E$  would increase by 56% with the majority of this increase originating from the canopy. Evaporation would increase under the *DRY* scenario, with the loss in pond evaporation being offset by the large increase in transpiration from the *B. gladiosa* canopy. Large increases in  $Q_E$  would occur under the *WET* and *DOM* scenarios, with approximately 1/3 of the increase due to the increase in standing water. The increase in air temperature and water vapour in the atmosphere would reduce  $\Delta W$ . This reduction in  $\Delta W$  decreases the occurrence of midday stomatal closure in *S. planifolia*, thereby allowing stomatal conductance (and transpiration) from this species to approach that of *C. aquatilis*.

#### D. CONCLUSIONS

Modelling evaporation on a 1/2 hour basis over the growing season can be performed accurately using a modified version of the Penman-Monteith combination model coupled with a submodel of stomatal conductance. Vegetation plays a crucial role

in the overall evaporation, as 80% of the evaporation originates from the plants (transpiration). Simulating various vegetation change scenarios shows that species composition, through differences in stomatal behaviour, has a marked effect on evaporation. Increases in evaporation due to "greenhouse warming" would be largest if surface wetness were to increase and sedge species were to dominate.

## CHAPTER 7

### CONCLUSIONS

The purpose of this study was to investigate the surface-atmosphere interaction over a dwarf willow-birch forest located in the Hudson Bay Lowland. The role of the vegetation has been emphasized because climatology has, until recently, failed to adequately treat the vegetation as an active component in the surface climate. This study shows that the willow-birch vegetation plays a major role in the surface energy balance. Despite a small leaf area index, rapid leaf growth results in a marked increase in the surface albedo. The energy balances both before vegetation maturation and after senescence are almost identical. However, the actively transpiring vegetation during the mature phase results in a dramatic increase in evaporation relative to available energy. Evaporation is most sensitive to the canopy resistance to transpiration.

The analysis of the surface-atmosphere interaction has also led to a number of findings concerning the stomatal conductance. Species-specific sensitivities to a threshold level of the leaf-to-air vapour pressure deficit causes some species to show a pronounced midday stomatal closure, while others show no midday closure. Some species show no midday stomatal closure on cool, damp days, yet show midday closure on hot, dry days. Soil moisture appears to have little affect on stomatal conductance.

A model was developed that predicts the stomatal conductance for each species. Coupling the vegetation's response to the atmosphere to a model of evaporation indicates that transpiration is responsible for 80% of the evaporation, despite a small leaf area index. Simulating various climate change scenarios indicates that the species composition may affect overall evaporation through species-specific responses to atmospheric controls.

The findings are significant for a number of reasons. The dynamic role the vegetation plays in the energy balance suggests that it is not adequate to use simplistic parametrizations for vegetation-atmosphere interactions. It is expected that the influence of the vegetation on the climate in a Subarctic region would be minimal. In this region, however, where the vegetation has a small leaf area index and grows under harsh conditions, a strong vegetation-atmosphere interaction was found. The impact of climate change may be especially large in the Subarctic Hudson Bay Lowland not only due to the strengthening of the temperature-albedo feedback and reduction in the cooling effect from winds originating over Hudson Bay, but also due to the strong linkage between the vegetation and the atmosphere.

# APPENDIX A

## CALCULATING STOMATAL CONDUCTANCE AND TRANSPIRATION

### A. Stomatal Conductance

Leaf conductance,  $g_l$  was measured with an automatic null-balance steady state porometer (LI-1600M, LI-COR, Lincoln, Nebraska, U.S.A).  $g_l$  on one side of a leaf is measured by enclosing the leaf in a chamber (cuvette). Once inside the cuvette, the transpiring leaf begins to increase humidity above the pre-set ambient value. Dry air is pumped into the cuvette at a sufficient rate to bring humidity back to the ambient humidity (LI-COR, 1989; McDermitt, 1990). Following LI-COR (1989), the volumetric flow rate  $F$  of dry air into the cuvette is calculated as

$$F = \left( \frac{T_c}{273.15} + 1 \right) \left( \frac{101.3}{P} \right) M \quad (\text{A.1})$$

where  $T_c$  is the cuvette temperature,  $P$  is the ambient barometric pressure (set at 101.3 kPa for all measurements), and  $M$  is the volumetric flow rate of dry air into the cuvette as measured by the LI-1600M mass flow meter.

The leaf transpiration rate within the cuvette,  $E$  is calculated as

$$E = (\rho_c - \rho_a) \frac{F}{A} \quad (\text{A.2})$$

where  $\rho_c$  and  $\rho_a$  are the water vapour densities in the cuvette and dry air stream entering the cuvette, respectively, and  $A$  is the exposed leaf area in the cuvette (set at 0.60 cm<sup>2</sup>). Saturation vapour pressure density at the cuvette temperature is determined from a table stored in the LI-1600M memory. The saturation vapour density is then multiplied by the cuvette relative humidity (RH/100) to give  $\rho_c$  (cuvette RH is measured by a Vaisala HUMICAP).  $\rho_a$  is calculated as the saturation vapour density multiplied by the dry air stream RH/100 (a constant dry air stream RH of 2 % is assumed).

After  $E$  is converted from  $\mu\text{g cm}^{-2} \text{s}^{-1}$  to  $\text{mmol m}^{-2} \text{s}^{-1}$  (using a molecular weight of water equal to 18.016 g mol<sup>-1</sup>),  $g_l$  ( $\text{mmol m}^{-2} \text{s}^{-1}$ ) can be expressed as

$$g_l = E \left( \frac{P}{e_l - e_c} \right) \quad (\text{A.3})$$

where  $e_l$  and  $e_c$  are the vapour pressures at the leaf and cuvette, respectively.  $E$  expressed in molecular units (i.e.  $\text{mmol m}^{-2} \text{s}^{-1}$ ) is preferred over velocity units since molecular units depend less on temperature and pressure and are more thermodynamically correct (McDermitt, 1990). Equations expressing saturation vapour pressure as a function of temperature (e.g. Buck, 1981; Lowe, 1977) can be used to calculate the saturation vapour pressures at leaf and cuvette temperatures. The saturation vapour pressures are then

multiplied by RH/100 to give vapour pressures. In the case of  $e_p$ , it is assumed that the RH in the substomatal cavity is 100%, therefore the leaf saturation vapour pressure equals the vapour pressure. As stated previously, cuvette RH is measured by a Vaisala HUMICAP.

Once a leaf is placed in the cuvette, the exposed leaf is subject to a constant air flow produced by the cuvette mixing fan. Thus, a laminar boundary layer develops over the leaf which remains constant due to the fixed exposed leaf area and constant fan speed. Therefore,  $g_i$  as measured by the LI-1600M is a composite of both the true stomatal conductance ( $g_s$ ) and the boundary layer conductance created in the cuvette ( $g_{bc}$ ). In order to obtain  $g_s$ ,  $g_{bc}$  must be subtracted. In terms of resistances, this can be expressed as a series circuit

$$r_i = r_s + r_{bc} \Rightarrow r_s = r_i - r_{bc} \quad (\text{A.4})$$

where  $r_i$  is the leaf resistance,  $r_s$  is the stomatal resistance, and  $r_{bc}$  is the cuvette boundary layer resistance. Expressing  $r_s$  in terms of conductance gives

$$g_s = \frac{g_{bc}g_i}{g_{bc} - g_i} \quad (\text{A.5})$$

where  $g_s$  is the true stomatal conductance with the cuvette boundary layer conductance removed.

To determine  $g_{bc}$  with the 0.60 cm<sup>2</sup> porometer aperture, a wet piece of filter paper was placed in the cuvette. It is assumed that  $g_i$  measured by the LI-1600M is equal to  $g_{bc}$

since  $g_s$  equals zero. Using this technique, it was found that  $g_{bc}=2140 \text{ mmol m}^{-2} \text{ s}^{-1}$  ( $\pm 91$ ;  $n=20$ ). This value, however, is likely an overestimate since the leaf thermocouple might underestimate the temperature of the filter paper thus giving too small a vapour pressure gradient (D. McDermitt, pers. comm., 1992).

Since the LI-1600M measures  $g_i$  on one side of the leaf only, for an amphistomatous leaf, the resistances for each side of the leaf act as a parallel circuit and can be expressed as

$$\frac{1}{r_{2l}} = \frac{1}{r_{sad}} + \frac{1}{r_{sab}} \quad (\text{A.6})$$

where  $r_{2l}$  is the total leaf resistance from both sides of the leaf, and  $r_{sad}$  and  $r_{sab}$  are the stomatal resistances on the adaxial and abaxial surfaces of the leaf, respectively. Expressing equation A.6 in terms of conductances gives

$$g_{2l} = g_{sad} + g_{sab} \quad (\text{A.7})$$

where  $g_{2l}$  is the leaf conductance for a amphistomatous leaf, and  $g_{sad}$  and  $g_{sab}$  are the adaxial and abaxial stomatal conductances, respectively. Since equation A.5 must first be used to correct for the cuvette boundary layer conductance on each side of the leaf, combining equations A.5 and A.6 gives

$$g_{2s} = \frac{g_{bc}g_{sadc}}{g_{bc} - g_{sadc}} + \frac{g_{bc}g_{sabc}}{g_{bc} - g_{sadc}} \quad (\text{A.8})$$

where  $g_{2s}$  is the intrinsic stomatal conductance for an amphistomatous leaf corrected for

boundary layer conductance developed within the cuvette,  $g_{sadc}$  and  $g_{sabc}$  are the adaxial and abaxial stomatal conductances, respectively corrected for the cuvette boundary layer conductance.

## B. Transpiration

Given an accurate measurement of  $g$ , it is possible to estimate the transpiration rate under field conditions ( $E_f$ ). The most obvious and erroneous method is to use the value of  $E$  as given by the porometer (equation A.2). This is wrong since conditions in the cuvette rarely represent ambient field conditions. For example, in this study, cuvette temperatures were significantly greater than the ambient  $T_a$ . Thus,  $E_f$  would be underestimated due an underestimation of the vapour pressure gradient. Also, the boundary layer conductance in the ambient air will be different than that in the cuvette due to changing wind speeds and different leaf shapes.

Before  $E_f$  can be calculated, the boundary layer conductance under ambient field conditions,  $g_{bf}$  must be determined. This must be added to  $g_{2s}$ , not  $g_{2b}$ , since  $g_{2l}$  has not been corrected for the cuvette boundary layer conductance.  $g_{bf}$  can be calculated as a function of leaf shape and wind speed at the leaf surface. For a flat leaf, the average thickness of the boundary layer,  $bl$  can be expressed as

$$bl=4.0\sqrt{\frac{l}{u_l}} \quad (\text{A.9})$$

where  $l$  is the mean length of the leaf in the downward wind direction, and  $u_l$  is the wind speed near the leaf (Nobel, 1991).

Under neutral atmospheric conditions, the wind speed near the leaf can be calculated using equation 3.12 with  $z$  representing the mean canopy height.  $g_{bf}$  can then be calculated as

$$g_{bf}=\frac{D_w}{bl} \quad (\text{A.10})$$

where  $D_w$  is the diffusion coefficient of water vapour.  $g_{bf}$  can then be converted from velocity units to molecular units using the general equation

$$g_m=\frac{P}{R(T_l+271.15)}g_v \quad (\text{A.11})$$

where  $g_m$  is the conductance in molar units  $R$  is the ideal gas constant ( $8.314 \text{ Pa m}^3 \text{ mol}^{-1} \text{ K}^{-1}$ ) and  $g_v$  is the conductance in velocity units.

In terms of resistances, the resistance experienced by water vapour moving from the substomatal cavity through the laminar boundary layer and into the atmosphere ( $r_{sf}$ ) can be expressed as

$$r_{sf}=r_s+r_{bf} \quad (\text{A.12})$$

In terms of conductances, equation A.12 becomes

$$g_{sf} = \frac{g_b g_s}{g_{bf} + g_s} \quad (\text{A.13})$$

where  $g_{sf}$  is the stomatal conductance under field conditions on one side of a leaf surface.

For an amphistomatous leaf, and assuming  $g_b$  is the same on both the adaxial and abaxial leaf surfaces, the stomatal conductance under field conditions can be expressed as

$$g_{2sf} = \frac{g_{bf} g_{sadc}}{g_{bf} + g_{sadc}} + \frac{g_{bf} g_{sabc}}{g_{bf} + g_{sabc}} \quad (\text{A.14})$$

where  $g_{2sf}$  is the amphistomatous leaf conductance adjusted for the field boundary layer conductance.

Since vegetated surfaces are rarely composed of just one species,  $g_{2sf}$  must be measured for each species individually. Given measurements of  $LAI$  for the entire vegetated area, and the percentage surface cover of each species,  $COV$  (%), the canopy conductance  $g_c$  can be calculated as

$$g_c = \sum_{i=1}^n g_{2sf} LAI \left( \frac{COV_i}{100} \right) \quad (\text{A.15})$$

where  $n$  is the number of species  $i$ .

The transpiration rate under field conditions  $E_f$  for, vegetated areas comprising several species can then be calculated as

$$E_f = g_c \Delta W = g_c \left( \frac{e_s(T_c) - e_a}{P} \right) \quad (\text{A.16})$$

where  $\Delta W$  is the leaf-to-air water vapour mole fraction gradient,  $e_s(T_l)$  is the saturation vapour pressure evaluated at the average canopy leaf temperature  $T_c$  and  $e_a$  is the ambient vapour pressure.

## APPENDIX B

### SYMBOLS

#### A. UPPER CASE ROMAN

<i>A</i>	exposed leaf area in the cuvette (0.60 cm <sup>2</sup> )
<i>COV<sub>i</sub></i>	surface cover of species <i>i</i> (%)
<i>C<sub>p</sub></i>	specific heat of dry air at constant temperature and pressure (1010 J Kg <sup>-1</sup> K <sup>-1</sup> )
<i>D</i>	atmospheric vapour pressure deficit (kPa)
<i>D<sub>w</sub></i>	diffusion coefficient of water vapour (m <sup>2</sup> s <sup>-1</sup> )
<i>DAI</i>	dead area index (m <sup>2</sup> m <sup>-2</sup> )
<i>E</i>	leaf transpiration rate within the cuvette (μg cm <sup>-2</sup> s <sup>-1</sup> )
<i>E<sub>f</sub></i>	transpiration under field conditions (mmol m <sup>-2</sup> s <sup>-1</sup> )
<i>F</i>	volumetric flow rate of dry air into cuvette (cm <sup>3</sup> s <sup>-1</sup> )
<i>FAI</i>	foliage area index (m <sup>2</sup> m <sup>-2</sup> )
<i>G</i>	acceleration due to gravity (9.81 m <sup>2</sup> s <sup>-1</sup> )
<i>JD</i>	Julian day
<i>K*</i>	net shortwave radiation (W m <sup>-2</sup> )
<i>K<sub>H</sub></i>	turbulent transfer coefficient for heat (m <sup>2</sup> s <sup>-1</sup> )
<i>K<sub>M</sub></i>	turbulent transfer coefficient for momentum (m <sup>2</sup> s <sup>-1</sup> )
<i>K<sub>w</sub></i>	turbulent transfer coefficient for water vapour (m <sup>2</sup> s <sup>-1</sup> )
<i>K<sub>1-8</sub></i>	parameters used in the stomatal conductance boundary line analysis
<i>K↓</i>	incoming shortwave radiation (W m <sup>-2</sup> )

$K\uparrow$	reflected shortwave radiation ( $\text{W m}^{-2}$ )
$L^*$	net longwave radiation ( $\text{W m}^{-2}$ )
$LAI$	leaf area index ( $\text{m}^2 \text{m}^{-2}$ )
$L_v$	latent heat of vapourization ( $\text{J kg}^{-1}$ )
$L\downarrow$	incoming longwave radiation ( $\text{W m}^{-2}$ )
$L\uparrow$	emitted longwave radiation ( $\text{W m}^{-2}$ )
$M$	volumetric flow rate of dry air into cuvette (measured by the mass flow meter) ( $\text{cm}^3 \text{s}^{-1}$ )
$P$	ambient barometric air pressure (101.3 kPa)
$Q^*$	net radiation ( $\text{W m}^{-2}$ )
$Q_E$	latent heat flux ( $\text{W m}^{-2}$ )
$Q_G$	ground heat flux ( $\text{W m}^{-2}$ )
$Q_H$	sensible heat flux ( $\text{W m}^{-2}$ )
$R$	ideal gas constant ( $8.314 \text{ Pa m}^3 \text{ mol}^{-1} \text{ K}^{-1}$ )
$RH$	relative humidity (%)
$RS(Q^*)$	relative sensitivity of evaporation to net radiation (dimensionless)
$RS(r_a)$	relative sensitivity of evaporation to aerodynamic resistance (dimensionless)
$RS(r_c)$	relative sensitivity of evaporation to canopy resistance (dimensionless)
$Ri$	Richardson number (dimensionless)
$S$	slope of the saturation vapour pressure versus temperature curve ( $\text{kPa } ^\circ\text{C}^{-1}$ )
$T_a$	air temperature ( $^\circ\text{C}$ )
$T_c$	canopy temperature ( $^\circ\text{C}$ )
$T_l$	leaf temperature ( $^\circ\text{C}$ )
$T_o$	surface temperature ( $^\circ\text{C}$ )

$T_r$	transpiration ( $\text{W m}^{-2}$ )
$T_{root}$	rooting zone temperature ( $^{\circ}\text{C}$ )
$T_w$	wet bulb temperature ( $^{\circ}\text{C}$ )
$WAI$	wood area index ( $\text{m}^2 \text{m}^{-2}$ )
$\Delta W$	leaf-to-air vapour pressure deficit (kPa)

## B. LOWER CASE ROMAN

$bl$	leaf boundary layer thickness (mm)
$d$	zero plane displacement (m)
$e_a$	atmospheric vapour pressure (kPa)
$e_c$	cuvette vapour pressure (kPa)
$e_l$	leaf vapour pressure (kPa)
$e_s$	saturation vapour pressure (kPa)
$g$	stomatal conductance ( $\text{mmol m}^{-2} \text{s}^{-1}$ , $\text{m s}^{-1}$ )
$g_{2l}$	amphistomatous leaf conductance ( $\text{mmol m}^{-2} \text{s}^{-1}$ )
$g_{2s}$	intrinsic stomatal conductance for an amphistomatous leaf ( $\text{mmol m}^{-2} \text{s}^{-1}$ )
$g_{2sf}$	amphistomatous leaf stomatal conductance under field conditions ( $\text{mmol m}^{-2} \text{s}^{-1}$ )
$g_{bc}$	boundary layer conductance ( $\text{mmol m}^{-2} \text{s}^{-1}$ )
$g_{bf}$	boundary layer conductance under field conditions ( $\text{mmol m}^{-2} \text{s}^{-1}$ )
$g_l$	leaf stomatal conductance ( $\text{mmol m}^{-2} \text{s}^{-1}$ )
$g_m$	conductance in molar units ( $\text{mmol m}^{-2} \text{s}^{-1}$ )
$g_s$	cuvette stomatal conductance ( $\text{mmol m}^{-2} \text{s}^{-1}$ )
$g_{sab}$	abaxial stomatal conductance ( $\text{mmol m}^{-2} \text{s}^{-1}$ )

$g_{sabc}$	abaxial stomatal conductance corrected for boundary layer conductance (mmol m <sup>-2</sup> s <sup>-1</sup> )
$g_{sad}$	adaxial stomatal conductance (mmol m <sup>-2</sup> s <sup>-1</sup> )
$g_{sadc}$	adaxial stomatal conductance corrected for boundary layer conductance (mmol m <sup>-2</sup> s <sup>-1</sup> )
$g_{sf}$	stomatal conductance under field conditions on one side of a leaf (mmol m <sup>-2</sup> s <sup>-1</sup> )
$g_v$	conductance in velocity units (m s <sup>-1</sup> )
$k$	von Karman's constant (0.4) (dimensionless)
$l$	mean leaf length (m)
$r_{2l}$	total leaf resistance (s m <sup>-1</sup> )
$r_a$	aerodynamic resistance (s m <sup>-1</sup> )
$r_{bc}$	cuvette boundary layer resistance (s m <sup>-1</sup> )
$r_c$	canopy resistance (s m <sup>-1</sup> )
$r_l$	leaf resistance (s m <sup>-1</sup> )
$r_s$	stomatal resistance (s m <sup>-1</sup> )
$r_{sab}$	abaxial stomatal resistance (s m <sup>-1</sup> )
$r_{sad}$	adaxial stomatal resistance (s m <sup>-1</sup> )
$r_{sf}$	resistance between the substomatal cavity and the atmosphere (s m <sup>-1</sup> )
$u$	horizontal wind speed (m s <sup>-1</sup> )
$u^*$	friction velocity (m s <sup>-1</sup> )
$u_i$	wind speed near the leaf (m s <sup>-1</sup> )
$z$	height (m)
$z_o$	roughness length (m)

## C. GREEK

$\alpha$	surface albedo (dimensionless)
$\beta$	Bowen ratio (dimensionless)
$\gamma$	psychrometer constant ( $\text{kPa K}^{-1}$ )
$\varepsilon$	surface emissivity (dimensionless)
$\varepsilon'$	apparent atmospheric emissivity (dimensionless)
$\rho$	density of air ( $\text{kg m}^{-3}$ )
$\rho_a$	dry air stream water vapour density ( $\mu\text{g cm}^{-3}$ )
$\rho_c$	cuvette water vapour density ( $\mu\text{g cm}^{-3}$ )
$\sigma$	Stephan-Boltzmann constant ( $\text{W m}^{-2} \text{K}^{-4}$ )
$\tau$	momentum flux density ( $\text{N m}^{-2}$ )
$\Phi_H$	stability function for heat (dimensionless)
$\Phi_M$	stability function for momentum (dimensionless)
$\Phi_w$	stability function for water vapour (dimensionless)

## REFERENCES

- Adams, R.S., Black, T.A. and Fleming, R.L., 1991. Evapotranspiration and surface conductance in a high elevation, grass-covered forest clearcut. *Agricultural and Forest Meteorology*, 56: 173-193.
- Aphalo, P.J. and Jarvis, P.G., 1991. Do stomata respond to humidity?. *Plant, Cell and Environment*, 14: 127-132.
- Arms, K. and Camp, P.S., 1982. *Biology, Second Edition*. Saunders, Philadelphia, 942 pp.
- Baldocchi, D.D., Luxmoore, R.J. and Hatfield, J.L., 1991. Discerning the forest from the trees: an essay on scaling canopy stomatal conductance. *Agricultural and Forest Meteorology*, 54: 197-226.
- Beven, K., 1979. A sensitivity analysis of the Penman-Monteith actual evapotranspiration estimates. *Journal of Hydrology*, 44: 169-190.
- Beyschlag, W., Pfanz, H. and Ryel, J., 1992. Stomatal patchiness in Mediterranean evergreen Sclerophylls. *Planta*, 187: 546-553.
- Binns, W.W., Blunden, G., 1980. Comparative leaf anatomy of *Salix* species and hybrids. *Botanical Journal of the Linnean Society*, 81: 205-214.
- Brutsaert, W., 1982. *Evaporation into the Atmosphere*. Reidel, Dordrecht, 299 pp.
- Buck, A.L., 1981. New equations for computing vapor pressure and enhancement factor. *Journal of Applied Meteorology*, 20: 1527-1532.
- Bunce, J.A., 1985. Effect of boundary layer conductance on the response of stomata to humidity. *Plant, Cell and Environment*, 8: 55-57.
- Chapin, F.S. and Shaver, G.R., 1985. Arctic. In B.F. Chabot and H.A. Mooney (eds.) *Physiological Ecology of North American Plant Communities*. Chapman and Hall, New York, pp. 16-40.

- Chen, J.M., Black, T.A. and, Adams, R.S., 1991. Evaluation of hemispherical photography for determining plant area index and geometry of a forest stand. *Agricultural and Forest Meteorology*, 56: 129-143.
- Clarke, K.E., Martini, I.P. and Glooschenko, W.A., 1982. Sedimentary characteristics of the coastal environment of North Point, Ontario. *Le Naturaliste Canadien*, 109: 385-397.
- Cowan, I.R., 1977. Stomatal behaviour and environment. In R.D. Preston and H.W. Woolhouse (eds.) *Advances in Botanical Research*. Academic Press, London. pp. 117-228.
- Cowan, I.R. and Farquhar, G.D., 1977. Stomatal function in relation to leaf metabolism and environment. In D.H. Jennings (ed.) *Integration of Activity in the Higher Plant, Society for Experimental Biology Symposium No. 31*. Cambridge University Press, Cambridge. pp. 471-505.
- Dawson, T. E. and Bliss, L. C., 1989a. Intraspecific variation in the water relations of *Salix Arctica*, an arctic-alpine dwarf Willow. *Oecologia*, 79: 322-331.
- Dawson, T.E. and Bliss, L.C., 1989b. Course of water use and the tissue water relations in the dioecious shrub, *Salix Arctica*: The physiological basis for habitat partitioning between the sexes. *Oecologia*, 79: 332-343.
- Day, T.A., DeLucia, E.H. and Smith, W.K., 1989. Influence of cold soil and snowcover on photosynthesis and leaf conductance in two Rocky Mountain conifers. *Oecologia*, 80: 546-552.
- Dickinson, R.E., Henderson-Sellers, A., Rosenzweig, C., and Sellers, P.J., 1991. Evapotranspiration models with canopy resistance for use in climate models, A review. *Agricultural and Forest Meteorology*, 54: 373-388.
- Dyer, A.J., 1974. A review of flux-profile relationships. *Boundary-Layer Meteorology*, 7: 363-372.
- Dyke, L., 1988. Permafrost aggradation along an emergent coast, Churchill, Manitoba. In *Proceedings of the Fifth International Conference on Permafrost*. Trondheim, Norway, pp. 138-142.

- Ecoregions Working Group, 1989. *Ecoclimatic Regions of Canada, First Approximation*. Ecoregions Working Group of the Canada Committee on Ecological Land Classification. Ecological Land Classification Series No. 23, Sustainable Development Branch, Canadian Wildlife Service, Conservation and Protection, Environment Canada, Ottawa, 119 pp.
- Elfving, D.C., Kaufmann, M.R., and Hall, A.E., 1972. Interpreting leaf water potential measurements with a model of the soil-plant-atmosphere continuum. *Physiological Plant*, 27: 161-169.
- Energy, Mines, and Resources, 1981. Canada - Growing Degree Days. *National Atlas of Canada, Fifth Edition*. Environment Canada, Ottawa.
- Fanjul, L. and Barradas, V.L., 1985. Stomatal behaviour of two heliophile understory species of a tropical deciduous forest in Mexico. *Journal of Applied Ecology*, 22: 943-954.
- FitzPatrick, E.A., 1986. *An Introduction to Soil Science*. Longman, Hong Kong, 225 pp.
- Goudley, J.S., Dale, M. and Hoddinott, J., 1985. The effects of oil spill chemicals on transpiration, CO<sub>2</sub> exchange, and cuticular structure in *Salix interior*. *Canadian Journal of Botany*, 63: 2340-2344.
- Halliwell, D.H., 1989. *A Numerical Model of the Surface Energy Balance and Ground Thermal Regime in Organic Permafrost Terrain*. Ph.D. Thesis, McMaster University, Hamilton, 195 pp.
- Halliwell, D.H. and Rouse, W.R., 1987. Soil heat flux in permafrost: Characteristics and accuracy of measurement. *Journal of Climatology*, 7: 571-584.
- Halliwell, D.H. and Rouse, W.R., 1989. A comparison of sensible and latent heat flux calculations using the Bowen ratio and aerodynamic methods. *Journal of Atmospheric and Oceanic Technology*, 6: 563-574.
- Hansell, R.I.C., Scott, P.A., Staniforth, R., and Svoboda, J., 1983. Permafrost development in the intertidal zone at Churchill, Manitoba: A possible mechanism for accelerated beach uplift. *Arctic*, 36: 198-203.
- Hutchinson, B.A., Matt, D.R., McMillen, R.T., Gross, L.J., Tajchman, S.J. and Norman, J.M., 1986. The architecture of a deciduous forest canopy in Eastern Tennessee, U.S.A. *Journal of Ecology*, 74: 635-646.

- Idso, S.B., 1990. Stomatal response to humidity as inferred by porometer and infrared thermometry. *Agricultural and Forest Meteorology*, 49: 169-172.
- Idso, S.B., Allen, S.G. and Choudhury, B.J., 1988. Problems with porometry: measuring stomatal conductance of potentially transpiring plants. *Agricultural and Forest Meteorology*, 43: 49-58.
- Idso, S.B., Jackson, R.D., Ehrler, W.L. and Mitchell, S.T., 1969. A method of determination of infrared emittance of leaves. *Ecology*, 50: 899-902.
- Ingram, W.J., Wilson, C.A., and Mitchell, J.F.B., 1989. Modeling climate change: An assessment of sea ice and surface albedo feedbacks. *Journal of Geophysical Research*, 94: 8609-8622.
- Jacobs, C.M.J. and DeBruin, H.A.R., 1992. The sensitivity of regional transpiration to land-surface characteristic: Significance of feedback. *Journal of Climate*, 5: 683-698.
- Jarvis, P.G., 1976. The Interpretation of the variations in leaf water potential and stomatal conductance found in canopies in the field. *Philosophical Transactions of the Royal Society of London*, 273: 593-610.
- Johnson, K.L., 1987. *Wildflowers of Churchill and the Hudson Bay Region*. Manitoba Museum of Man and Nature, Winnipeg, 400 pp.
- Jones, H.G., 1983. *Plants and Microclimate*. Cambridge University Press, Cambridge, 323 pp.
- Körner, C.H., Scheel, J.A., and Bauer, H., 1978. Maximum leaf diffusive conductance in vascular plants. *Photosynthetica*, 13: 45-82.
- Larsson, S., 1980. Influence of intercepted water on transpiration and evaporation of *Salix*. *Agricultural Meteorology*, 23: 331-338.
- Lafleur, P.M., 1987. Leaf conductance of four species growing in a subarctic marsh. *Canadian Journal of Botany*, 66: 1367-1375.
- Lafleur, P.M., 1988. *The Surface Cover and Air Mass Controls on Evaporation from a Subarctic Marsh*. Ph.D. Thesis. McMaster University, Hamilton. 165 pp.

- Lafleur, P.M., Rouse, W.R., and Carlson, D.W., 1992. Energy balance differences and hydrologic impacts across the northern treeline. *International Journal of Climatology*, 12: 193-203.
- Landsberg, J.J., Beadle, C.L., Biscoe, P.V., Bulter, D.R., Davidson, B., Incoll, L.D., James, G.B., Jarvis, P.G., Martin, P.J., Neilson, R.E., Powell, D.B.B., Slack, E.M., Thorpe, M.R., Turner, N.C., Warrit, B., and Watts, W.R., 1975. Diurnal energy, water and CO<sub>2</sub> exchanges in an Apple (*Malus Pumila*) orchard. *Journal of Applied Ecology*, 12: 659-684.
- Lange, O.L., 1988. Ecophysiology of photosynthesis: Performance of poikilohydric lichens and homoiohydric mediterranean Sclerophylls. *Journal of Ecology*, 76: 915-937.
- Lange, O.L., Tenhunen, J.D., and Braun, M., 1982. Midday stomatal closure in Mediterranean type Sclerophylls under simulated habitat conditions in an environmental chamber. *Flora*, 172: 563-579.
- Lettau, H.H., 1957. Computation of Richardson Numbers, Classification of Wind Profiles, and Determination of Roughness Parameters. In *Exploring the Atmosphere's First Mile. Volume I. Instrumentation and Data Evaluation*. Pergamon Press, London, pp. 328-336.
- LI-COR, 1989. *LI-1600 Steady State Porometer Instruction Manual*. LI-COR Inc., Lincoln, 76 pp.
- LI-COR, 1992. *LAI-2000 Plant Canopy Analyzer Operating Manual*. LI-COR Inc., Lincoln, 182 pp.
- Lösch, R. and Tenhunen, J.D., 1981. Stomatal Response to Humidity - Phenomena and Mechanisms. In P.G. Jarvis and T.A. Mansfield (eds.) *Stomatal Physiology*. Cambridge University Press, Cambridge, pp. 137-161.
- Lowe, P.R., 1977. An approximating polynomial for the computation of saturation vapor pressure. *Journal of Applied Meteorology*, 16: 100-103.
- Massman, W.J., and Kaufmann, M.R., 1991. Stomatal response to certain environmental factors: A comparison of models for subalpine trees in the Rocky Mountains. *Agricultural and Forest Meteorology*, 54: 155-167.

- McCuen, R.H., 1974. A sensitivity and error analysis of procedures used for estimating evaporation. *Water Resources Bulletin*, 10: 486-497.
- McDermitt, D.K., 1990. Sources of error in the estimation of stomatal conductance and transpiration from porometer data. *Hortscience*, 25: 1538-1548.
- McDermitt, D.K., 1992. Personal Communication, Applications Scientist, LI-COR Inc., Lincoln, Nebraska, U.S.A.
- Monteith, J.L., 1965. Evaporation and Environment. In G.E. Fogg (ed.) *The State and Movement of Water in Living Organisms, Symposium of the Society of Experimental Biology, Volume 19*. Cambridge University Press, London, pp. 205-234.
- Munro, D.S., 1989. Stomatal conductances and surface conductance modelling in a mixed wetland forest. *Agricultural and Forest Meteorology*, 48: 235-249.
- Neumann, H.H., Den Hartog, G., 1989. Leaf area index measurements based on hemispheric photographs and leaf-litter collection in a deciduous forest during autumn leaf-fall. *Agricultural and Forest Meteorology*, 45: 325-345.
- Nobel, P.S., 1985. Desert Succulents. In B.F. Chabot and H.A. Mooney (eds.) *Physiological Ecology of North American Plant Communities*. Chapman and Hall, New York, pp. 181-197.
- Nobel, P.S., 1991. *Physiochemical and Environmental Plant Physiology*. Academic Press, San Diego, 635 pp.
- Ohmura, A., 1982. Objective criteria for rejecting data for Bowen ratio flux calculations. *Journal of Applied Meteorology*, 21: 595-598.
- Oke, T.R., 1987. *Boundary Layer Climates, Second Edition*. Methuen, New York, 435 pp.
- Penman, H.L., 1948. Natural evaporation from open water, bare soil, and grass. *Proceedings of the Royal Society of London, Series A*, 193: 120-146.
- Pereira, J.S., Tenhunen, J.D., Lange, O.L., Beyschlag, W., Meyer, A., and David, M.M., 1985. Seasonal and diurnal patterns in leaf gas exchange of *Eucalyptus globulus* trees growing in Portugal. *Canadian Journal of Forest Research*, 16: 177-184.

- Petzold, D.E. and Rencz, A.N., 1975. The albedo of selected subarctic surfaces. *Arctic and Alpine Research*, 7: 393:398.
- Phillips, D., 1990. *The Climates of Canada*. Ministry of Supply and Services Canada, Ottawa, 176 pp.
- Porsild, A.E. and Cody, W.J., 1980. *Vascular Plants of the Continental Northwest Territories, Canada*. National Museum of Natural Sciences, National Museum of Canada, Ottawa, 667 pp.
- Price, J.S., Woo, M.K., and Rouse, W.R., 1992. Damming James Bay: II. Impacts on coastal marshes. *The Canadian Geographer*, 36: 8-13.
- Rauner, J.L., 1976. Deciduous Forest. In J.L. Monteith (ed.) *Vegetation and the Atmosphere, Volume 2. Case Studies*. Academic Press, London, pp. 241-264.
- Raven, P.H., Evert, R.F., and Curtis, H., 1981. *Biology of Plants, Third Edition*. Worth, New York, 686 pp.
- Rawson, H.M., Begg, J.E., and Woodward, R.G., 1977. The effect of atmospheric humidity on photosynthesis, transpiration and water use efficiency of leaves of several plant species. *Planta*, 134: 5-10.
- Riley, J.L., 1990. *The Vascular Plants of the Hudson Bay Lowland and their Postglacial Origins*. Ontario Ministry of Natural Resources. Parks and Recreational Areas Section, Central Region, Richmond Hill, 222 pp.
- Ritchie, G.A. and Hinckley, T.M., 1975. The Pressure Chamber as an Instrument for Ecological Research. In A. MacFadyen (ed.) *Advances in Ecological Research*. Academic Press, London, pp. 166-254.
- Rizzo, B. and Wilken, E., 1992. Assessing the sensitivity of Canada's ecosystems to climatic change. *Climatic Change*, 21: 37-55.
- Roessler, P.G. and Monson, R.K., 1985. Midday depression in net photosynthesis and stomatal conductance in *Yucca glauca*. *Oecologia*, 67: 380-387.
- Roots, E.F., 1989. Climate change: High-latitude regions. *Climatic Change*, 15: 223-253.

- Rost, T.L., Barbour, M.G., Thornton, R.M., Weier, T.E., and Stocking, C.R., 1979. *Botany, A Brief Introduction to Plant Biology*. John Wiley and Sons, New York, 411 pp.
- Rouse, W.R., 1984a. Microclimate at arctic tree line 1. Radiation balance of tundra and forest. *Water Resources Research*, 20: 57-66.
- Rouse, W.R., 1984b. Microclimate at arctic tree line 2. Soil microclimate of tundra and forest. *Water Resources Research*, 20: 67-73.
- Rouse, W.R., 1991. Impacts of Hudson Bay on the terrestrial climate of the Hudson Bay Lowlands. *Arctic and Alpine Research*, 23: 24-30.
- Rouse, W.R., Carlson, D.W., and Weick, E.J., 1992. Impacts of summer warming on the energy and water balance of wetland tundra. *Climatic Change*, (in press).
- Rowntree, P.R., 1991. Atmospheric Parameterization Schemes for Evaporation over Land: Basic Concepts and Modeling Aspects. In T. J. Schmugge and André, J. (eds.) *Land Surface Evaporation: Measurement and Parameterization*. Springer-Verlag, New York, pp. 5-29.
- Scholander, P.F., Hammel, H.T., Bradstreet, E.D., and Hemmingsen, E.A., 1965. Sap pressure in vascular plants. *Science*, 148: 339-346.
- Scholander, P.F., Hammel, H.T., Hemmingsen, E.A., and Bradstreet, E.D., 1964. Hydrostatic pressure and osmotic potential in leaves of Mangroves and some other plants. *Proceedings of the National Academy of Science*, 52: 119-125.
- Scott, P.A., 1991. *The Flora of Churchill Manitoba, Seventh Edition*. Department of Zoology, University of Toronto, Toronto, 28 pp.
- Shulze, E.D., Lange, O.L., Evenari, M., Kappen, L., and Buschbom, U., 1974. The role of air humidity and leaf temperature in controlling stomatal resistance of *Prunus armeniaca* L. under desert conditions. I. A simulation of the daily course of stomatal resistance. *Oecologia*, 17: 159-170.
- Standley, L.A., 1986. Variation of stomatal distribution in *Carex Aquatilis* (Cyperaceae). *American Journal of Botany*, 73: 1393-1399.
- Tanner, C.B., 1963. *Basic Instrumentation and Measurements for Plant Environment and Micrometeorology*. Soils Bulletin 6. University of Wisconsin, Wisconsin, 602 pp.

- Tenhunen, J.D., Pearcy, R.W., and Lange, O.L., 1987. Diurnal Variations in Leaf Conductance and Gas Exchange in Natural Environments. In E. Zeiger (ed.) *Stomatal Function*. Stanford University Press, Stanford, pp. 323-351.
- Thom, A.S., 1975. Momentum, Mass and Heat Exchange of Plant Communities. In J.L. Monteith (ed.) *Vegetation and the Atmosphere. Volume 1. Principles*. Academic Press, London, pp. 57-109.
- Turner, N.C., 1991. Measurement and influence of environmental and plant factors on stomatal conductance in the field. *Agricultural and Forest Meteorology*, 54: 137-154.
- Tyree, M.T. and Wilmot, T.R., 1990. Errors in the calculation of evaporation and leaf conductance in steady-state porometry: the importance of accurate measurement of leaf temperature. *Canadian Journal of Forestry Research*, 20: 1031-1035.
- Weatherald, R.T. and Manabe, S., 1981. Influence of seasonal variation upon the sensitivity of a climate model. *Journal of Geophysical Research*, 86: 1194-1204.
- Welles, J.M. and Norman, J.M., 1991. Instrument for indirect measurement of canopy architecture. *Agronomy Journal*, 83: 818-825.
- Wetlands Working Group, 1981. *The Canadian Wetland Classification System*. Series No. 21, Lands Conservation Branch, Canadian Wildlife Service, Ottawa, 18 pp.
- Wielgolaski, F.E., Bliss, L.C., Svoboda, J., and Doyle, G., 1981. Primary Production of Tundra. In L.C. Bliss, O.W. Heal and J.J. Moore (eds.) *Tundra Ecosystems: A Comparative Analysis*. Cambridge University Press, Cambridge, pp. 187-225.
- Willmott, C.J., 1982. Some performances on the evaluation of model performance. *Bulletin of the American Meteorological Society*, 63: 1309-1313.
- Willmott, C.J. and Wicks, D.E., 1980. An empirical method for the spatial interpolation of monthly precipitation within California. *Physical Geography*, 1: 59-73.